Improving Recovery from Mature Oil Fields in the West Texas Permian Basin

by

Ali Jamali, M.Sc.

A Dissertation

In

Petroleum Engineering

Submitted to the Graduate Faculty
of Texas Tech University in
Partial Fulfillment of
the Requirements for
the Degree of

DOCTOR OF PHILOSOPHY

IN

PETROLEUM ENGINEERING

Approved

Amin Ettehadtavakkol
Chair of Committee

Marshall C. Watson

Sheldon Gorell

Denny Bullard

Mark Sheridan
Dean of the Graduate School

May, 2018

Copyright 2018, Ali Jamali

ACKNOWLEDGMENTS

I am deeply indebted to my supervisor and chair of committee, Dr. Amin Ettehadtavakkol, for his valuable guidance and discussion throughout this research. The completion of this dissertation would not have been possible without his continuing encouragement and instructions which conceptualized the framework of this research from the beginning. I thank him for his valuable inputs, constant accessibility, and patience.

This research was initiated by Apache Corporation which provided the production and injection data for the Slaughter field. Furthermore, the Whitacre College of Engineering and the Bob L. Herd Department of Petroleum Engineering at Texas Tech University provided the financial support for my graduate studies. Computer Modeling Group's reservoir simulation package (CMG IMEX, GEM, and WINPROP) was used throughout this research. I thank Texas Tech University for their financial support and Computer Modeling Group for academic access to their reservoir simulator.

I appreciate our discussions with my committee members, Dr. Sheldon Gorell, Dr. Marshall Watson, and Mr. Denny Bullard. I also would like to thank faculty, secretaries, and fellow students of Bob L. Herd Department of Petroleum Engineering for their understanding and help during the course of my graduate studies. Assistance given by my colleagues, Dr. Elias Pirayesh, Dr. Fahd Siddiqui, and Mr. Chad Kronkosky are greatly acknowledged and appreciated.

Last but not least, I want to thank my wife, Laura, for her never-ending love and support throughout the course of my graduate studies. She lived, endured, and survived this experience with me, and never denied her support.

TABLE OF CONTENTS

ACKNOWLEDGMENTS ..... **ii**

ABSTRACT ..... **v**

LIST OF TABLES ..... **vi**

LIST OF FIGURES ..... **viii**

I. INTRODUCTION **1**

1.1. Motivation Behind this Study 1
1.2. Application of Capacitance Resistance Models 3
1.3. Maximized Workover Benefits through Stimulation of Better Producers 4
1.4. CO_2 Enhanced Oil Recovery in the Residual Oil Zone 5
1.5. Scope and Organization of this Dissertation 6

II. APPLICATION OF CAPACITANCE RESISTANCE MODELS **8**

2.1. Problem Definition 9
2.2. Procedure 13
2.2.1. Discrete Producer Model 14
2.2.2. Flowing Bottomhole Pressure 16
2.2.3. Effect of Flowing Bottomhole Pressure Variations 17
2.2.4. Estimation of the CRMP Parameters 20
2.2.5. Global and Local Minima 21
2.2.6. Solution Time and Convergence Rate 24
2.2.7. The Gradient of the CRMP Objective Function 24
2.2.8. Analytical Derivation of the Gradient Vector of the CRMP Objective Function 24
2.2.9. The Hessian of the CRMP Objective Function 26
2.2.10. Analytical Derivation of the Hessian Matrix of CRMP Objective Function 27
2.2.11. Improvements from the use of Analytical Gradient and Hessian 30
2.2.12. Scaling the Fitting Parameters 31
2.3. Analysis of Mature Oil Fields 32
2.3.1. Radius of Influence of the Injectors (ri) 32
2.4. Results: Application to Large-Scale Mature Oil Fields 33
2.4.1. Example 1: Validation of CRMP Results 34
2.4.2. Example 2: Determining Current Water Injectors Suited for CO_2 Injection 37
2.4.3. Example 3: Determining Current CO_2 Injectors Not Suited for CO_2 Injection 37
2.5. Discussion 39

III. MAXIMIZED WORKOVER BENEFITS: STIMULATION OF BETTER PRODUCERS **41**

3.1. Problem Definition 42
3.2. Solution Method 46
3.3. Results 47
3.3.1. Literature Data 47

3.3.2. Analysis of Field Data 49
3.4. Application to Stimulation Well Screening 54
3.5. Reservoir Simulation Model 56
3.6. Results 61
3.7. Discussion 65

IV. CO_2 ENHANCED OIL RECOVERY IN THE RESIDUAL OIL ZONE..... 66

4.1. Problem Definition 67
4.2. Permian Basin San Andres Reservoir Model 70
4.3. Reservoir Model Description 75
4.4. Results and Discussion 81
4.4.1. ROZ History Matching and Model Verification 81
4.4.2. Primary Recovery and Secondary Waterflood 88
4.4.3. CO_2-EOR and Storage Potential of the MPZ-ROZ 89
4.4.4. CO_2 Storage in the ROZ: Opportunities and Challenges 99

V. CONCLUSIONS AND RECOMMENDATIONS FOR FUTURE WORK ... 103

5.1. Application of Capacitance Resistance Models 104
5.2. Maximizing Stimulation Benefits Using Data Analytics 105
5.3. CO_2-EOR in the Residual Oil Zone 106
5.4. Recommendations for Future Work 107
5.4.1. Future Work for the CRM Study 107
5.4.2. Future Work for the Candidate Selection Study 107
5.4.3. Future Work for the ROZ Study 108

BIBLIOGRAPHY 110

A. DISCUSSION ON HUBBERT'S TILT FORMULA 123

5.1. Potentiometric Surface 123
5.2. Parameters Affecting the Tilt of Oil Water Contact During Hydrodynamic Flushing 129

VITA 131

ABSTRACT

We undertake reservoir characterization, reservoir simulation, and data analytics to investigate various pathways for improving oil production from mature oil fields. This study focuses on the oil fields located in the West Texas Permian Basin. We provide guidelines for optimizing waterflood and CO_2-Enhanced Oil Recovery (CO_2-EOR), maximizing the benefits of well stimulation, and determining the best development strategies for Residual Oil Zone (ROZ).

We offer several improvements to the numerical solution of Capacitance Resistance Models to facilitate their application to large-scale mature oil fields. We put forward an evidence-based analysis to show that good wells make better stimulation candidates and evaluate the applicability of this idea in improving well intervention candidate selection. We review and evaluate the origin and resource potential of ROZs in the Permian Basin and assess the effect of various design variables and reservoir properties on the performance of CO_2-EOR and storage in ROZs.

Mature oil fields amount to more than 70% of current worldwide oil production and play a prominent role in energy supply. Using our proposed approach which combines both proactive and reactive mature fields solutions, the operators can mitigate the problem of declining oil production from three different angles depending on the characteristics of the reservoir, the investment budget, and the required implementation timeline.

LIST OF TABLES

2.1 Effect of bottomhole pressure variations on the value of connectivities inferred from CRMP. 20

2.2 CRMP connectivity results (f_{ij}) for CTI01, I38 and I23; BRI: Beyond the Radius of Influence, C: Connected, NC: Not Connected. Refer to Figure 6b for the well locations. 38

3.1 Selected publications on well stimulation optimization with focus on candidate selection. 44

3.2 Selected publications supporting stimulation of good producers. 46

3.3 Results of regression analysis for Mallet Unite, East Mallet Unit, W. A. Coons, and F. L. Woodley leases in the Slaughter field. 53

3.4 Reservoir model description for the anticlinal model used to evaluate the proposed candidate selection scheme 56

3.5 Reservoir and injected gas fluid composition (Ettehadtavakkol, 2013). 61

4.1 Several basins with documented effect of hydrodynamics on oil and gas entrapment. 70

4.2 MPZ and ROZ fluid composition (Honarpour et al., 2010). Oil biodegradation can affect reservoir oil attributes in several ways, including raising the oil viscosity and reducing the oil API gravity both resulting from significant com-position difference between MPZ and ROZ oil. 80

4.3 PVT data of the MPZ-ROZ simulation model based on the oil composition in Table 4.2. The bubble point pressure and minimum miscibility pressure are 1400 psi and 1350 psi respectively. These results consistently match the experimental data (Honarpour et al., 2010). 80

4.4 Major reservoir properties of the MPZ-ROZ simulation model (Honarpour et al., 2010) 81

4.5 Sensitivity analysis scenarios performed to determine the sensitivity of the saturation profile to key parameters, including vertical to horizontal permeability ratio and the potentiometric gradient. 86

4.6 Development strategy and reservoir performance of cases 1 through 6. The results show that cases 3 and 6 should be prioritized over cases 4 and 5. 94

A.1 List of sensitivity analysis scenarios performed on the effects of heterogeneity, capillary pressure, vertical to horizontal permeability ratio, and potentiometric gradient. 129

LIST OF FIGURES

1.1 The onset of maturity in a mature field (Mallet Unit lease in the Slaughter field). 1

1.2 General mature field solution and the three methods investigated in this study. 3

1.3 Fields analyzed in this study. Data from the Slaughter field is analyzed in Chapter II and Chapter III and data from the Seminole field is analyzed in Chapter IV. 6

2.1 (a) Variations in number of active producers in four leases located in Slaughter field, West Texas (top) and (b) Variations in number of active injectors. Normalized number of producers is the ratio of active lease producers to the largest number of active lease producers (bottom). 12

2.2 (a) Schematic of the base CRM (top). The total production response, *Q*, is a function of the total injection signal, *I*, control volume properties and the operating conditions (b) Schematic of CRMP. Each producer is assumed to be receiving a certain fraction of each injector's fluid (bottom). 16

2.3 The permeability map of the 8P-6I model. This model is used to investigate the effect of bottomhole pressure variations on CRMP connectivity maps. 18

2.4 Flowing bottomhole pressure variations for some of the producers, normalized to the initial flowing bottomhole pressure. 19

2.5 Distribution of start points used for the global optimization solver. 23

2.6 CRMP runtime for small- to large-scale problems. 31

2.7 Normalized history match error as a function of radius of influence for four leases located in Slaughter field, West Texas. 33

2.8 The study area: the Slaughter field in West Texas. 34

2.9 East Mallet Unit. The circles show the radius of influence (approximately 2000 feet for this lease). 35

2.10 (a) CTI01 CO_2 injection signal and P04 and P05 CO_2 production response (top), and (b) P04 and P05 oil production response (bottom). 36

2.11 Application of CRMP to predicting future performance of Mallet Unit lease. The model underestimates the fluid production rates in the presence of major workover operations starting in 2011. 39

3.1 Two-year stimulation incremental oil production. 47

3.2 Incremental recovery from well stimulation reported by numerous studies (Afolabi et al., 2008; Brand, 2010; Burgos et al., 2005; Ghauri, 1960; Harris et al., 1966; Kartoatmodjo et al., 2007; Kumar et al., 2005; Meehan, 1995; Sencenbaugh et al., 2001; Strong et al., 1997; Trebbau et al., 1999). 48

3.3 Combined plot of incremental recovery from well stimulation reported by numerous studies (Afolabi et al., 2008; Brand, 2010; Burgos et al., 2005; Ghauri, 1960; Harris et al., 1966; Kartoatmodjo et al., 2007; Kumar et al., 2005; Meehan, 1995; Sencenbaugh et al., 2001; Strong et al., 1997; Trebbau et al., 1999). 49

3.4 Locations of (a) Slaughter field (modified after Behm and Ebanks Jr., 1984, 1984) (top) and (b) the four leases investigated in this study (modified after Watson, 2005) (bottom)..... 50

3.5 Stimulation campaign started in 2004 and slowed down production decline in Mallet Unit..... 51

3.6 Stimulation incremental oil recovery for the four leases of the Slaughter field. 52

3.7 Combined plot of stimulation incremental oil recovery for the four leases of the Slaughter field. 53

3.8 Results of spatial grouping for Mallet Unit, (a) grouping map (○: unstimulated, ●: stimulated), (top) and (b) stimulation response for each region (bottom) (pre-stimulation and incremental oil rates are average values for each region.) 55

3.9 Well locations and permeability map of the reservoir simulation model. 57

3.10 Average horizontal permeability of each layer. The low, medium, and high sequence of permeabilities represent different depositional regimes throughout geologic time. 58

3.11 Relative permeability curves for (a) water-wet oil-water system (top), (b) water-wet gas-liquid system (second from top), (c) intermediate-wet oil-water system (second from bottom), and (d) intermediate-wet gas-liquid system (bottom). 59

3.12 Post waterflood stimulated and unstimulated oil production performance for the reservoir model. 63

3.13 Performance of various candidate selection schemes (a) as a function of the fraction of wells stimulated (top), and (b) when half of producers are stimulated (bottom). 64

4.1 The concept of lateral pressure gradient or potentiometric surface. Regional flow of water through sand from higher to lower outcrop results in continuous drop in potential. This figure is adopted from Hubbert (1954). 69

4.2 Location of San Andres, Grayburg, and Canyon & Cisco oil fields with proved (Cowden S, Goldsmith, Hanford, Kelly-Snyder, Means, Salt Creek, Seminole, Vacuum, Wasson) and/or predicted (others) ROZs. Data compiled from Koperna et al. (2013) and West (2014). Other map details are constructed based the maps presented in Ward et al. (1986). 71

4.3 Idealized oil saturation profile under the capillary, gravitational and hydrodynamic equilibrium. The average oil saturation in the ROZ is slightly greater than the residual oil saturation to waterflood. Recoverable ROZ trapped oil is shaded..... 73

4.4 Logarithm of horizontal permeability with an average of 15 md. Model dimensions are 10000 ft × 600 ft. Data adapted from Wang et al. (1998). 75

4.5 Major rock and rock-fluid properties of the MPZ-ROZ simulation model (a) Experimental data for vertical to horizontal permeability correlation (Honarpour et al., 2010) used to generate the joint probability distribution of vertical-horizontal permeability (top), and (b) Experimental permeability-porosity correlation (Honarpour et al., 2010) used to generate the joint distribution of permeability-porosity (bottom). 76

4.6 Major rock and rock-fluid properties of the MPZ-ROZ simulation model: Water-oil imbibition relative permeability curves (Honarpour et al., 2010) 78

4.7 Major rock and rock-fluid properties of the MPZ-ROZ simulation model: Drainage and imbibition capillary pressure curves (Brown, 2001; Killough, 1976). Related concepts adopted from Abdallah et al. (2007) 79

4.8 Effect of AHFF on lateral pressure variation. A potentiometric surface slope of 7.5 feet per mile corresponding to a lateral pressure gradient of 3.3 psi per mile is introduced

to the system. The solid lines are the isobar contour lines under hydrodynamic conditions. The dashed lines are the isobar contour lines under hydrostatic condition and are shown only for comparison. 82

4.9 Fieldwide oil saturation distribution at 0.03×10^5 (top), 0.50×10^5 (middle), and 1.00×10^5 (bottom) years. Local variations are affected by layering particularly in the low permeable east side of the reservoir; however, the general OWC slope corresponds to both field observations and Hubbert's tilt formula. 84

4.10 Oil saturation profile in the middle of the reservoir at the end of the AHFF process. 85

4.11 Oil saturation profile under various potentiometric slopes (PS) and vertical to horizontal permeability ratios: (1) Kv/Kh = 0.01, PS = 7.5 feet per mile, (2) Kv/Kh = 0.1, PS = 7.5 feet per mile, (3) Kv/Kh = 0.5, PS = 7.5 feet per mile, (4) Kv/Kh = 1.0, PS = 7.5 feet per mile, (5) Kv/Kh = 0.5, PS = 20 feet per mile, (6) Kv/Kh = 0.5, PS = 50 feet per mile. 87

4.12 Location of the wells with an average 1300 ft well spacing. Only the MPZ is developed during the primary and secondary recovery stages. From west to east, the wells are completed at continuously lower depths to ensure that the injected fluids remain confined to the intended zone and are not affected by the OWC tilt. 88

4.13 Oil saturation distribution at the end of the secondary production stages (50 years). 89

4.14 Reservoir performance under primary production and secondary waterflood. 89

4.15 Cumulative CO_2 injection for the six scenarios. 91

4.16 Reservoir performance in terms of oil production for the proposed cases (a) oil production rate (top), and (b) cumulative oil production (bottom). 92

4.17 Reservoir performance in terms of CO_2 storage for the proposed cases (a) cumulative CO_2 stored (top), and (b) net CO_2 utilization (bottom). 93

4.18 Summary of MPZ-ROZ development cases. The expansion development strategy should be proportional to CO_2 investment strategy. Moderate/moderate or

aggressive/aggressive investment scenarios are recommended. 96

4.19 CO_2 storage performance plots demonstrating (a) the effect of recoverable oil volume on the performance of all cases and (b) the effects of biodegradation and diagenesis on the performance of Case 6. The diagonal lines represent constant net CO_2 utilizations. The performance of Case 2, i.e. MPZ *only* development with a total CO_2 injection volume of 140 Bscf, is presented for comparison. 98

4.20 Comparison of the water production of the MPZ-only and MPZ-ROZ development scenarios. The difference between the total produced and injected water should be considered for disposal. 101

5.1 Summary of the methodologies investigated in this dissertation. 103

A.1 The concept of lateral pressure gradient or potentiometric surface. Regional flow of water through sand from higher to lower outcrop results in continuous drop in potential. This figure is adopted from Hubbert (1954). 124

A.2 Force intensity vector and the physical interpretation of Darcy's law. Adopted from Hubbert (1954). 125

A.3 (a) Impelling forces on water, oil and gas in hydrodynamic environment (left) and (b) vector analysis (right). Adopted from Hubbert (1954). 127

A.4 Divergent migration of oil and gas in hydrodynamic environment. Adopted from Hubbert (1954). 128

A.5 Theoretical vs simulated OWC tilts for the case studies presented in Table A.1. 130

CHAPTER I

INTRODUCTION

The standard lifecycle of an oil field includes primary, secondary, and tertiary recovery stages. In the primary recovery phase, the reservoir's natural energy source is the main driver of hydrocarbon production. In the secondary recovery phase, pressure management methods such as water or gas injection and artificial lift are used to maintain a favorable production. The tertiary recovery phase involves the injection of fluids that do not typically exist in the reservoir. For instance, Enhanced Oil Recovery (EOR) methods such as CO_2-EOR are typically implemented in this phase. If the production through the primary and secondary phases has declined significantly, the oil field is considered mature (Figure 1.1).

1.1. Motivation Behind this Study

With most of the world's potential oil reserves having already been explored and major new onshore discoveries becoming increasingly rare, mature fields will play an ever more prominent role in energy supply. Nearly 70% of the worldwide oil production comes from mature oil fields (*Mature Fields Solution*, 2014). Oil companies' capacity

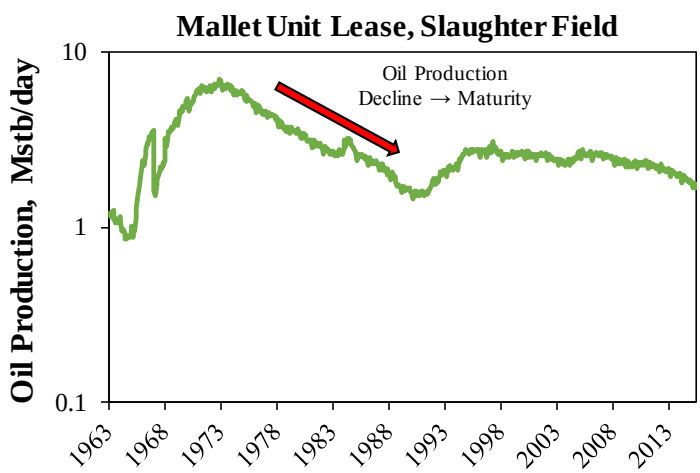

Figure 1.1 The onset of maturity in a mature field (Mallet Unit lease in the Slaughter field).

to meet rising world demand will therefore depend on their ability to get the most out of existing resources. In addition, a recent oil bust has resulted in the termination of drilling activities across the US. Consequently, the oil field operators are currently eager to increase their investment in mature oil fields to squeeze every last drop of oil out of the existing resources.

The West Texas Permian Basin reaches from south of Lubbock to south of Midland and extends westward into the southeastern part of New Mexico. Producing approximately 1.3 million barrels of oil per day, the Permian Basin is the largest oil play in North America. This basin is unique in its diversity. Comprised of a collection of regional conventional and unconventional plays, the Permian Basin covers a wide area and more than a dozen productive formations. One of the most prolific reservoirs within the Permian Basin is the San Andres formation. The majority of the oil fields producing from this formation are approaching maturity, encouraging the oil filed operators to come up with new and innovative methods for revitalizing those fields.

According to the industry standards, a wide variety of well development and reservoir development strategies are widely applicable to mature oil fields (Babadagli, 2007). In this study, three methods are investigated for improving recovery from mature oil fields: (1) Application of Capacitance Resistance Models, (2) Maximized Workover Benefits through Stimulation of Better Producers, (3) CO_2 Enhanced Oil Recovery in the Residual Oil Zone. The contribution of this work to the literature is shown in Figure 1.2.

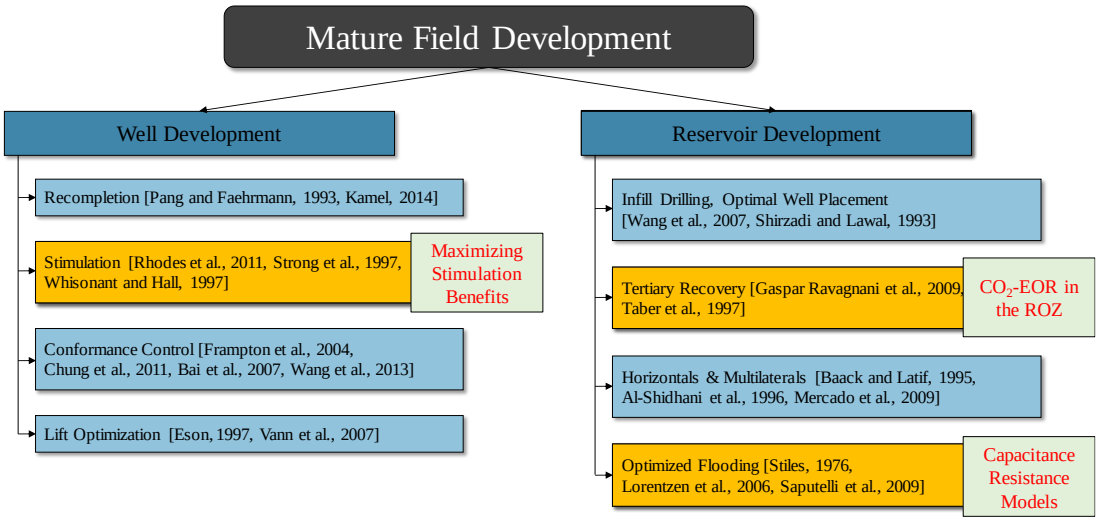

Figure 1.2 General mature field solution and the three methods investigated in this study.

1.2. Application of Capacitance Resistance Models

Capacitance Resistance Models (CRM) are data driven methods for characterizing a reservoir and optimizing oil production without taking up complex and time-consuming geological modeling and reservoir simulation practices. These models leverage injection and production data for history-matching and optimizing the performance of field-scale waterflood and CO_2-flood operations (Yousef et al., 2006Al-Yousef, 2006). As a part of a collaborative project with Apache Corporation, we investigated the application of CRM to large-scale fields with an emphasis on overcoming the practical challenges frequently encountered in large-scale mature oil fields. Application of CRM to large-scale mature oil fields has its own limitations: the optimization problem that needs to be solved grows exponentially with the increasing number of injectors and producers in the field.

We investigate several strategies to optimize the solution method of large-scale CRM problems. These include the implementation of a global optimization algorithm, parameter scaling, analytical development of gradient vector and Hessian matrix of the CRM objective function, and restriction of optimization variables according to their

physical meaning. Using these strategies, the solution time is improved at least by a factor of ten. Using this fast solver, it is confirmed that the CRM objective function has only one local minimum within its feasible region. These improvements enable the application of CRM to large-scale problems with more than 500 wells. A new procedure and analysis technique is presented that greatly improves the significance of CRM's output. With this information in hand operators can redirect the CO_2 resources to where they are needed the most. Furthermore, in one example the CRM connectivities are confirmed by comparing CO_2 injection signal and its response in the corresponding producers. This observation is of particular importance because it brings credibility to CRM (Jamali and Ettehadtavakkol, 2017a).

1.3. Maximized Workover Benefits through Stimulation of Better Producers

The majority of stimulation treatments are performed on wells that do not match their expected productivity indices or produce oil below a certain economic limit. While this may appear as an intuitively sound strategy, the potential oil production from stimulation of more productive wells should not be underestimated. Data analysis of the past workovers can be used to improve the decision-making process, leading to a better ranking of the candidate wells for stimulation. We have analyzed oil production data from four mature leases, producing from San Andres carbonate reservoir in the West Texas Permian Basin, for identifying potential correlation between the historical oil production and the oil production improvement resulted from well stimulation.

The results indicate a strong positive correlation between the historical oil production and the well response after the stimulation process. This has important implications in identifying wells with greater potential for oil production improvement from well stimulation. While the success of the treatment strongly depends on the selection, design, and implementation of the appropriate stimulation method, priority should be given to the wells that exhibit high historical oil production, or the wells that are located in highly productive zones. This practice will increase the statistical likelihood of max-

imized workover benefits. Based on the results and observations, a data-driven workflow is proposed for the preliminary screening of workover candidates which helps maximize the stimulation benefits. This workflow is applied to maximizing the workover benefits of a large-scale reservoir simulation model and the results are compared to conventional workover candidate selection workflows (Jamali et al., 2017a, Jamali et al., 2018).

1.4. CO_2 Enhanced Oil Recovery in the Residual Oil Zone

Residual Oil Zones (ROZs) are formed as the result of secondary tectonic activities which trigger extensive oil remobilization after the primary petroleum migration. The ROZs are attractive targets for CO_2 Enhanced Oil Recovery (CO_2-EOR) and storage: first, because in many cases, the thickness of the ROZ ensures an overall recoverable volume of oil comparable to that of the Main Pay Zone (MPZ) and second, because the ROZ has favorable containment and capacity for large-scale and long-term EOR-storage projects. We investigate one of the underlying theories of the ROZ formation, called the Altered Hydrodynamic Flow Fields (AHFF). The impact of the AHFF process on the formation of ROZs is specifically investigated using a field-scale simulation model for a Permian Basin San Andres reservoir. The simulation model is tuned and verified by validating the ROZ's characteristics, such as the thickness of the ROZ, the shape of the saturation profile, and the tilt of the Oil Water Contact.

Depending on the CO_2 availability and ROZ development strategy, six different development scenarios are specified. The corresponding simulations are performed to find the optimum EOR-storage strategies for the MPZ-ROZ through the extensive comparison of key performance parameters, including the cumulative oil recovery and CO_2 storage. Our results have confirmed the technical viability of CO_2-EOR and storage in the ROZ. The most favorable expansion strategy in terms of oil production and CO_2 storage is the simultaneous development of the MPZ and the ROZ from the beginning of the EOR-storage process. Most importantly, the study demonstrates that the volume of the utilized CO_2 has a substantial effect on the success of the EOR-storage. While other expansion strategies such as sequential development also provide reasonable oil

production response and CO_2 storage potential, early project expansion into the ROZ without sufficient investment in CO_2 resources is shown to be detrimental to the economics of the project. Finally, several important technical considerations for CO_2 storage are qualitatively discussed, including assessment of the ROZ storage capacity, saltwater disposal requirements, and reduced risk of CO_2 leakage in the ROZ (Jamali and Ettehadtavakkol, 2017b).

1.5. Scope and Organization of this Dissertation

The analysis requires medium- to large-scale data compilation as well as development of three field-scale reservoir simulation models and other internal software. These are explained separately for each method in their corresponding chapter. Chapter II discusses numerical improvements made to Capacitance Resistance Models and show their application to eliminating out of zone CO_2 injectors and/or identifying the water injectors that are suitable for CO_2 injection. Chapter III investigates a correlation between historical oil production and well stimulation response and presents its applicability as a well stimulation candidate screening criterion. Finally, Chapter IV explains

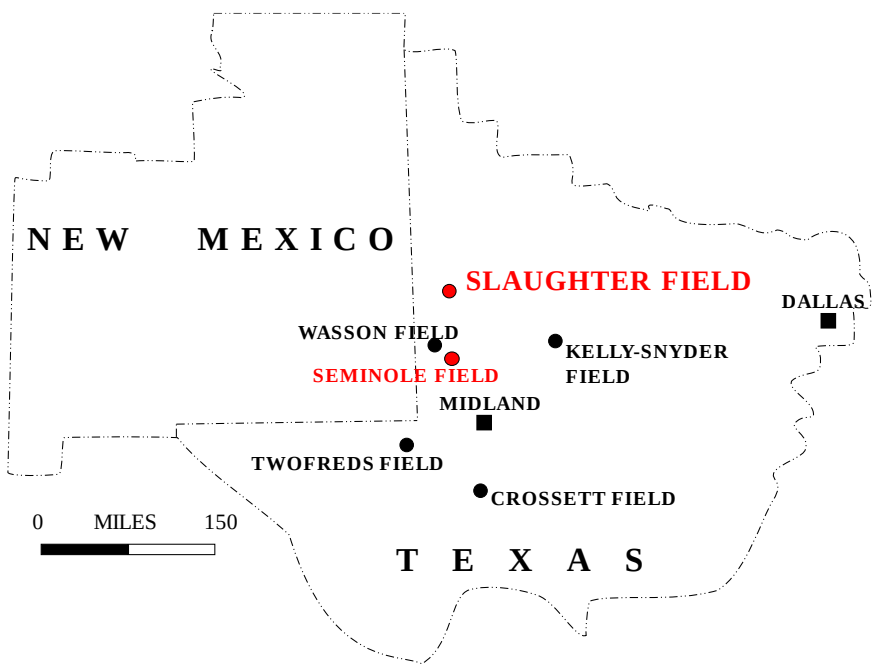

Figure 1.3 Fields analyzed in this study. Data from the Slaughter field is analyzed in Chapter II and Chapter III and data from the Seminole field is analyzed in Chapter IV.

and evaluates the prominent theory on the origin of Residual Oil Zones and investigates the effect of various design variables and expansion strategies on the performance of CO_2-EOR in the Residual Oil Zone (Figure 1.3).

CHAPTER II

APPLICATION OF CAPACITANCE RESISTANCE MODELS[1]

This chapter presents the application of Capacitance Resistance Models (CRMs) to large-scale fields with an emphasis on overcoming the practical challenges frequently encountered in mature oil fields. This analysis is especially valuable for mature oil fields located in West Texas because of the particular characteristics they possess. These fields are rapidly approaching a marginal incremental recovery; however, their performance can be enhanced with proper management of injection fluids and injection rates. The interpretation of the CRM solution is an important step that leads to practical recommendations for the improvement of the waterflood or CO_2-flood performance for individual producers and injectors.

Capacitance Resistance Model for Producers (CRMP) is selected for this analysis because of its adequacy. Mature fields are specified as large-scale systems with specific characteristics that make them suitable for the application of CRMP. Several strategies are presented to optimize the solution method of large-scale CRMP problems. These include the implementation of a global optimization algorithm, parameter scaling, analytical development of gradient vector and Hessian matrix of the CRMP objective function, and restriction of optimization variables according to their physical meaning. Using these strategies, the solution time is improved at least by a factor of ten. Using this fast solver, it is confirmed that the CRMP objective function has only one local minimum within its feasible region. These improvements enable the application of CRMP to large-scale problems with more than 500 wells.

The CRMP delivers a fieldwide connectivity map that signifies what portion of each injector's fluid is received at each producer. A new procedure and analysis technique is presented that greatly improves the significance of CRMP's output. With this

[1] Parts of this chapter are published in:
Jamali, A., Ettehadtavakkol, A., 2017b. Application of capacitance resistance models to determining interwell connectivity of large-scale mature oil fields. Petroleum Exploration and Development 44, 132–138. doi:10.1016/S1876-3804(17)30017-4

information in hand operators can redirect the CO_2 resources to where they are needed the most. Furthermore, in one example the CRMP connectivities are confirmed by comparing CO_2 injection signal and its response in the corresponding producers. This observation is of importance because it brings credibility to CRMs. The limitations and merits of CRMP are discussed at the end of this chapter.

2.1. Problem Definition

The standard lifecycle of an oil field includes primary, secondary, and tertiary recovery stages. In the primary recovery phase, the reservoir natural energy source is the main driver of hydrocarbon production. In the second recovery phase pressure management methods, such as water or gas injection and artificial lift, are used to maintain a favorable production. Secondary recovery activities are an industry standard through which most information about the reservoir geology and fluid properties are collected. The tertiary recovery phase involves the injection of fluids that do not typically exist in the reservoir. For instance, enhanced oil recovery (EOR) methods such as CO_2-EOR are typically implemented in this phase. If the production through the primary and secondary phases has declined significantly, the oil field is considered mature. In this chapter the application of Capacitance Resistance Models (CRMs) to large-scale mature oil fields is discussed.

Analyzing injector-producer pairs to determine reservoir characteristics have a long-lasting history and involves several methods, including tracer testing and/or monitoring producers' response to an injection signal. Recently, several researchers have used statistical approaches to leverage injection and production data in order to determine interwell communications. Heffer et al. (1997) calculated the Spearman rank correlation coefficient between injector-producer pairs to find the interaction between them as a potential measure of flow directionalities. Their analysis indicated that the injection signal received by producers have some components coupled to geomechanics. Panda and Chopra (1998) used artificial neural networks to predict oil production rate and to estimate the interaction between well-pairs. They applied this method to small simulation case studies and concluded that the application of artificial neural networks to such

complex systems has some limitations. In addition, it is well known that the physical interpretation of such models is a challenge. Albertoni and Lake (2003) used the multivariate linear regression analysis to quantify the interwell communications.

Yousef et al. (2006) developed a mathematical model to calculate producers' total fluid production responses to injection signals and to bottomhole pressure variations. This was essentially the solution to the mass balance differential equation for a closed control volume containing a set of injectors and producers. The model contained unknown coefficients that relate the production response to the producers' effective drainage volume, fluid compressibility, productivity index, and the connectivity coefficient between the injector-producer pairs. These parameters could effectively describe the *capacity* of the system to produce fluids. In addition, there is a unique similarity between this equation and the one used to describe the flow of electrical currents in a system of capacitors and resistors; therefore, this model and its variants are known as Capacitance Resistance Models (CRMs).

Several researchers contributed to the development of CRMs, following their introduction by Yousef. Sayarpour et al. (2009) expanded the solution of the mass balance differential equation to three different control volumes, namely the entire field (CRMT), a single producer (CRMP), and an injector-producer pair's shared volume (CRMIP). They coupled CRM with fractional flow models to predict the oil production rate along with the total fluid production rate of each producer.

The implementation of CRMs to large-scale problems encounters several challenges on the accuracy and reliability of the results. The early studies limited the problem size to a subset of less than 60 wells to keep the optimization problem size manageable. Weber et al. (2009) classified several heuristic procedures for problem size reduction, including the removal of inactive wells and restraining the connectivities by setting a connectivity radial cutoff. In light of a reduced problem size, they suggested that the result of nonlinear regression is more likely to be statistically significant. Nguyen et al. (2011) introduced the Integrated Capacitance Resistance Model (ICR) with a linearized

objective function. They concluded that the ICR will converge to a *unique* solution regardless of the number of fitting parameters because it uses linear regression.

This chapter focuses on overcoming some of the current limitations of this technique and on delivering a simplified procedure for applying CRMs to mature oil fields. First, we explain the characteristics of mature oil fields and the challenges they bring. Then, we review the Capacitance Resistance Model for Producers (CRMP), its components, and the recommended optimization routine that makes CRMP easily applicable to large-scale problems. This is followed by a step by step procedure on how to apply this technique and interpret the results. The methodology is applied to several leases located in Slaughter field, West Texas, and the results are presented.

The problem investigated in this chapter is commonly encountered in mature oil fields of West Texas. However, this does not impose any restrictions on applying this methodology to other fields with similar characteristics. Consider a mature oil field that has undergone waterflood or CO_2-EOR for a sufficiently long period of time and possesses the following characteristics:

- The current drilling activity is very low, but the injector/producer interruptions are frequent due to high workover and maintenance activities. This is further illustrated in Figure 2.1 for four leases located in Slaughter field, West Texas.
- A variety of artificial lift techniques can be used; however, the majority of producers are equipped with sucker rod pumps. The presence of such pumps guarantees that the fluid level and consequently the flowing bottomhole pressure varies within a relatively small range.
- The field has a fairly compact well spacing of 10-30 acres and there are no further plans for drilling new wells.

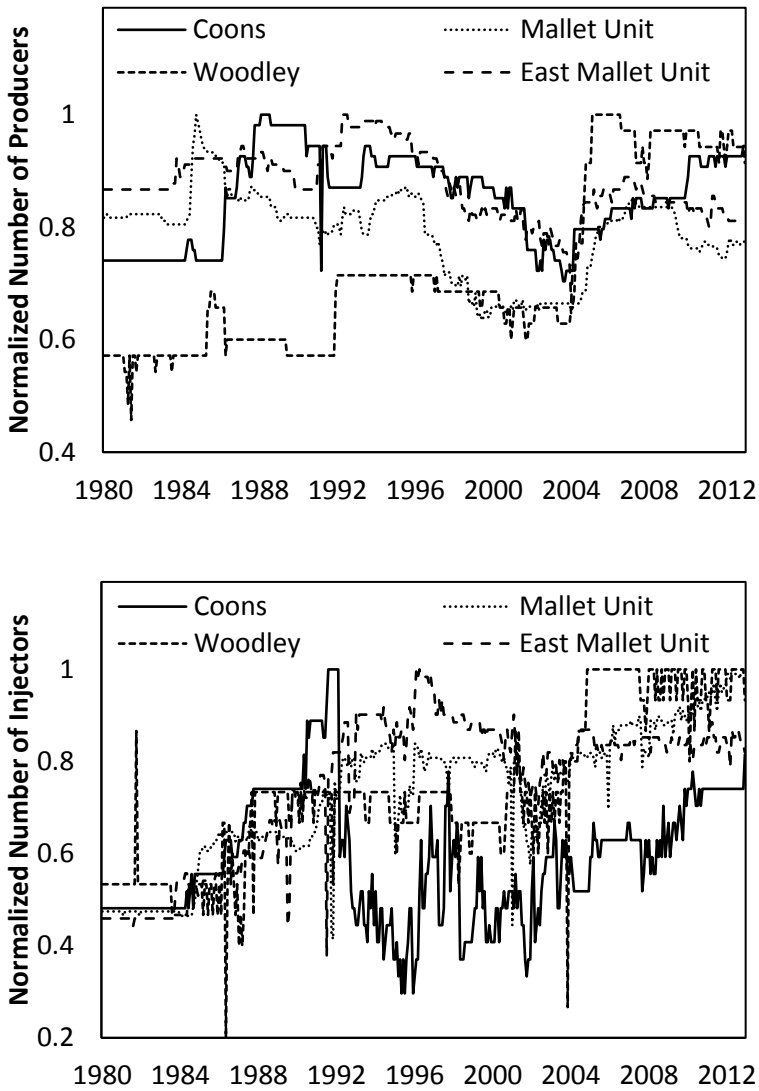

Figure 2.1 (a) Variations in number of active producers in four leases located in Slaughter field, West Texas (top) and (b) Variations in number of active injectors. Normalized number of producers is the ratio of active lease producers to the largest number of active lease producers (bottom).

While approaching a marginal oil recovery, such fields usually suffer from declined oil production, excessive water/CO_2 production, and many other unwanted problems. These issues encourage the operators to seek options that can help revitalizing the field. These fields have already undergone extensive evaluations throughout their lifespan. This is particularly important because CRMs can be used as fast and inexpen-

sive tools to minimize the investment risks for the operators at such late stages of reservoir development. In this chapter CRMs are effectively used to provide recommendations that can remediate these problems, especially for large-scale fields.

2.2. Procedure

The procedure of CRM derivation is widely discussed in the literature (Morteza Sayarpour et al., 2009; Yousef et al., 2006). We adopt their method and present a simplified derivation based on the assumption of single-phase slightly-compressible fluid. The isothermal compressibility of a fluid is defined as the relative volume change of that fluid as a response to a pressure change while temperature remains constant,

$$c = -\frac{1}{v}\frac{dv}{dp}\,, \tag{2.1}$$

where c is the isothermal compressibility of the fluid, v is the fluid volume, and p is the fluid pressure. Consider an arbitrary hydrocarbon reservoir control volume under injection and production (Figure 2.2a). We assume that the system is dominantly occupied by a single fluid and describe it by a unique compressibility, c_t. The total compressibility for this system after applying the chain rule is,

$$c_t = -\frac{1}{v_p}\frac{dv_p}{d\bar{p}} = -\frac{1}{v_p}\frac{dv_p}{dt}\frac{dt}{d\bar{p}}\,, \tag{2.2}$$

where $\bar{p}$ and v_p are the average fluid pressure and the pore volume of this arbitrary control volume, respectively. For a closed system containing one producer and one injector, the accumulation of the fluid in the system with respect to time is equal to the algebraic sum of fluid inflow and outflow,

$$-\frac{dv_p}{dt} = I - Q = c_t v_p \frac{d\bar{p}}{dt}\,, \tag{2.3}$$

where Q and I are production and injection rates of the system, respectively. The measurement of average pressure usually requires well test analysis and therefore cannot be continuously provided. Although steady-state behavior is a common assumption for a reservoir that is being waterflooded, the operational interruptions, such as frequent in-

jector/producer shut-ins, render this assumption inaccurate. Therefore, a linear productivity model is used instead to eliminate the average pressure term and reduce the complexity,

$$\bar{p} = \frac{Q}{J} + p_{wf} \ , \tag{2.4}$$

where J and p_{wf} are the productivity index and the flowing bottomhole pressure of the producer, respectively. Substituting Equation 2.4 in Equation 2.3,

$$\frac{c_t v_p}{J}\frac{dQ}{dt} + c_t v_p \frac{dp_{wf}}{dt} = I - Q. \tag{2.5}$$

We define the time constant, τ, as the product of the total compressibility, pore volume, and the inverse of the productivity index as follows,

$$\tau = \frac{c v_p}{J} \ , \tag{2.6}$$

and by using $e^{t/\tau} = e^{\int (1/\tau \, dt)}$ as the integrating factor, the solution to Equation 2.5 is obtained as,

$$Q(t) = Q(t_1)e^{\left(-\frac{t-t_1}{\tau}\right)} + \frac{e^{-\frac{t}{\tau}}}{\tau}\int_{t_1}^{t} e^{\frac{\xi}{\tau}} I(\xi)d\xi + J\begin{bmatrix} p_{wf(t_1)}e^{\left(-\frac{t-t_1}{\tau}\right)} - p_{wf}(t) \\ + \frac{e^{-\frac{t}{\tau}}}{\tau}\int_{t_1}^{t} e^{\frac{\xi}{\tau}} p_{wf}(\xi)d\xi \end{bmatrix}. \tag{2.7}$$

2.2.1. Discrete Producer Model

To determine injector-producer interactions, the model is extended for individual producers. It is assumed that a certain fraction of the injected fluid in injector i flows towards producer j (Figure 2.2b). This fraction, f_{ij}, is referred to as the connectivity of injector i and producer j. We assume that the variations of the flowing bottomhole pressure are negligible. The viability of this assumption is explained in the next section. The discrete form of Equation 2.7 for producer j during the kth month of its production is,

$$Q_j(t_k) = Q_j(t_{k-1})e^{\left(-\frac{t_k - t_{k-1}}{\tau_j}\right)} + \sum_{i=1}^{N_{inj}}\left[\frac{e^{-\frac{t_k}{\tau_j}}}{\tau_j}\int_{t_{k-1}}^{t_k} e^{\frac{\xi}{\tau_j}} f_{ij} I_i(\xi)d\xi\right], \tag{2.8}$$

where f_{ij} is the connectivity between injector i and producer j, and I_i is the injection rate of injector i. Assuming a fixed monthly injection rate of I_{ik} is established during the kth month, Equation 2.8 is reduced to,

$$Q_j(t_k) = Q_j(t_{k-1})e^{\left(-\frac{t_k - t_{k-1}}{\tau_j}\right)} + \sum_{i=1}^{N_{inj}} \left[f_{ij} I_{ik} \left(1 - e^{\left(-\frac{t_k - t_{k-1}}{\tau_j}\right)} \right) \right]. \tag{2.9}$$

After applying successive substitution of the flow rate terms, the downhole fluid production rate of producer j at the end of the nth month of production is,

$$Q_j(t_n) = Q(t_1)e^{\left(-\frac{t_n - t_1}{\tau_j}\right)} + \sum_{k=2}^{N_t} \left\{ e^{-\left(\frac{t_n - t_k}{\tau_j}\right)} \left(1 - e^{\left(-\frac{t_k - t_{k-1}}{\tau_j}\right)} \right) \left[\sum_{i=1}^{N_{inj}} f_{ij} I_{ik} \right] \right\}. \tag{2.10}$$

Equation 2.10 is the Capacitance Resistance Model for Producers (CRMP) under stepwise change of injection rates and constant flowing bottomhole pressure. For simplicity, we represent the time variable as a subscript,

$$Q_{jn} = Q_{j1} e^{\left(-\frac{n-1}{\tau_j}\right)} + \sum_{k=1}^{N_t} \left\{ e^{-\left(\frac{n-k}{\tau_j}\right)} \left(1 - e^{\left(-\frac{1}{\tau_j}\right)} \right) \left[\sum_{i=1}^{N_{inj}} f_{ij} I_{ik} \right] \right\}. \tag{2.11}$$

Equation 2.11 indicates that the response of producer j to a series of injection signals I_{ik} is a function of the initial production rate Q_{j1}, the producer's time constant τ_j, and the connectivity factor between that producer and individual injectors, f_{ij}. These parameters are not directly known; however, one can estimate them through the analysis of the production and injection history.

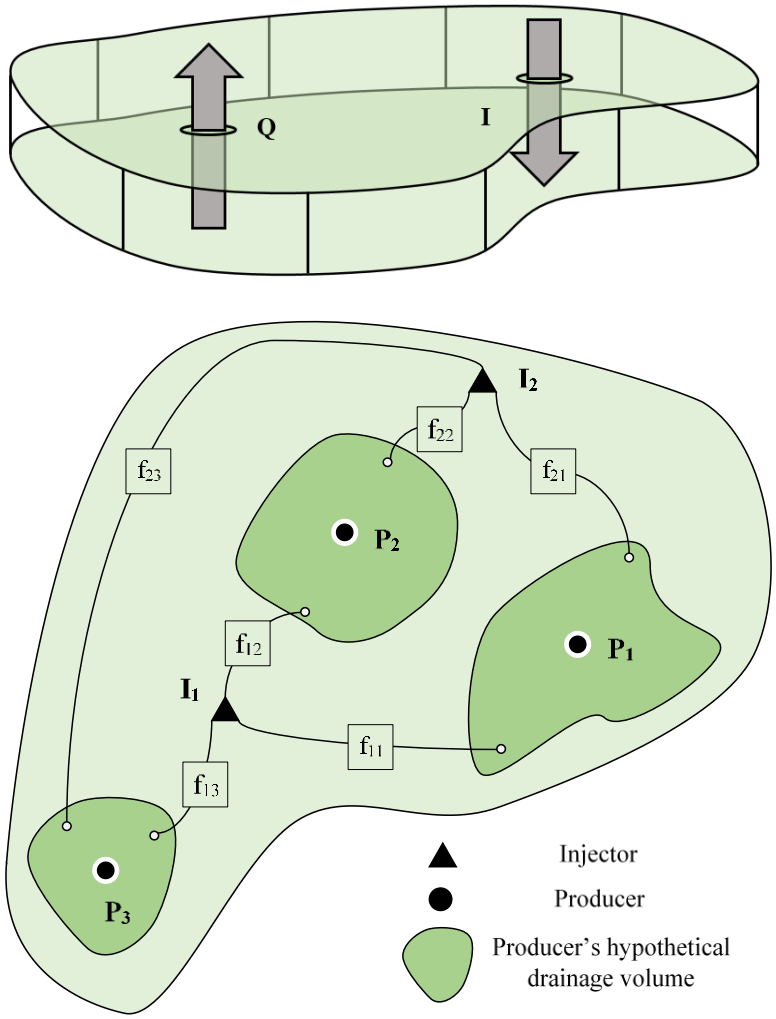

Figure 2.2 (a) Schematic of the base CRM (top). The total production response, *Q*, is a function of the total injection signal, *I*, control volume properties and the operating conditions (b) Schematic of CRMP. Each producer is assumed to be receiving a certain fraction of each injector's fluid (bottom).

2.2.2. Flowing Bottomhole Pressure

For the particular problem defined earlier, a discussion on the flowing bottomhole pressure in Equation 2.7 is of importance. The flowing bottomhole pressure data from permanent downhole gauges is ideally preferred for the CRMP implementation; however, such data are not normally available for mature fields. The installation of the permanent downhole pressure gauges and periodic recording is an expensive practice for mature fields, and therefore, the majority of the mature fields are unlikely to have

such long-term pressure data. In addition, at least 90% of mature wells in the Onshore US are equipped with sucker rod pumps, and in the presence of such pumps, the calculation of the downhole pressure requires extensive additional information and analysis which are not normally available (Athichanagorn et al., 1999; Cutler and Mansure, 1999).

We investigated the impact of the absence of flowing bottomhole pressure data on the quality of the CRMP connectivity maps using a tuned reservoir simulation model (Ettehadtavakkol et al., 2014a) for the Sacroc oil field, Permian Basin. In the absence of flowing bottomhole pressure data, the resulting connectivity values varied within a ±20% of their actual values obtained in the presence of flowing bottomhole pressure data. Although the absence of flowing bottomhole pressure data reduces the quality of the CRMP history matches, the connectivity maps remain favorably intact for the analysis. Also, the larger connectivities that contain the most important information have the smallest relative errors. We conclude that any analysis that is based on these large connectivities remains fairly unbiased in the absence of flowing bottomhole pressure data. The reader may refer to the next subsection for a detailed discussion of this subject.

2.2.3. Effect of Flowing Bottomhole Pressure Variations

In order to ensure that CRMP can be safely applied to fields that lack flowing bottomhole pressure data, a tuned reservoir simulation model for the Sacroc field, Permian Basin with eight producers and six injectors is used. Figure 2.3 shows the permeability map and the locations of individual wells. The permeability distribution introduces sufficient heterogeneity into the reservoir to create a diverse connectivity map. CRMP is sensitive to changes in the injection signal and uses such variations to determine connectivities; therefore, shut-in frequencies for the injectors are extracted from real field data to make the problem more realistic.

All producers are active under a minimum flowing bottomhole pressure constraint and reach a constant bottomhole pressure shortly after any changes are applied to this constraint. A flowing bottomhole pressure constraint signal with normal distribution having a standard deviation of 100 psi is then introduced for each producer (Figure 2.4). The results are analyzed using CRMP. The flowing bottomhole pressure variations are taken into account in Case I and are ignored in Case II. The results are compared in Table 2.1 for half of the injectors. It is evident from these results that the average relative error introduced when ignoring the flowing bottomhole pressure variations is less than 20%. Furthermore, no false large connectivities are reported. These large

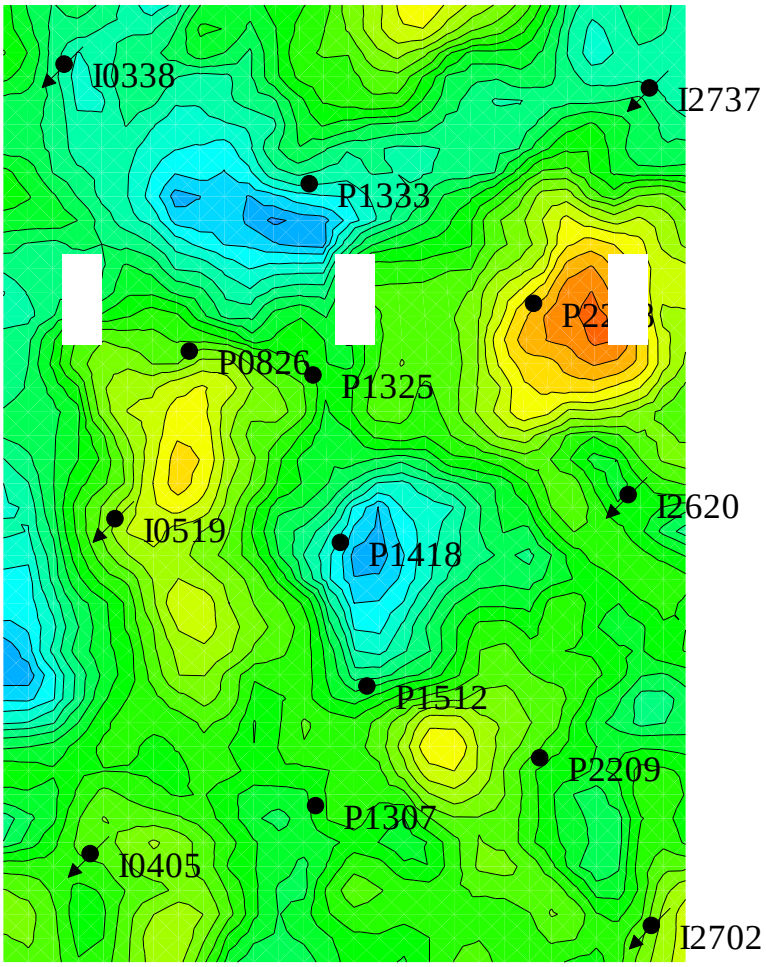

Figure 2.3 The permeability map of the 8P-6I model. This model is used to investigate the effect of bottomhole pressure variations on CRMP connectivity maps.

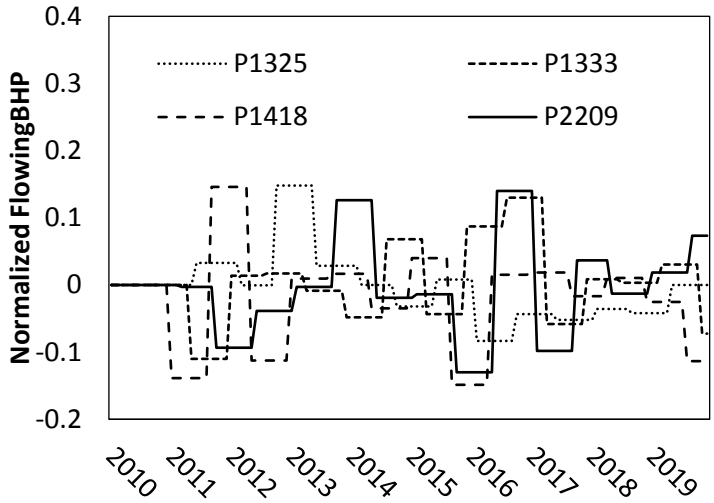

Figure 2.4 Flowing bottomhole pressure variations for some of the producers, normalized to the initial flowing bottomhole pressure.

connectivities are particularly important because they determine the future well management strategies presented in this chapter. Note that although the connectivity map is relatively intact, the quality of history match is decreased in the absence of flowing bottomhole pressure data (also see Appendix E of Sayarpour (2008) for field examples). However, our analysis focuses on the connectivity maps and not the quality of CRMP history match.

This observation can be further explained by a cursory analysis of Equation 2.5. Consider a well that on average produces 5000 bbl/month of fluids with a total fluid compressibility of 0.00001 1/psi from a 20 acres drainage area. If this volume was to be solely produced through pressure drop, an approximate value of 500 psi/month would be required. This is clearly not the case because otherwise the flowing bottomhole pressure would drop to zero in a short amount of time. It is therefore concluded that since more than 95% of the production signal is supplied through the injection signals, the connectivity maps generated from CRMP are not significantly influenced if the bottomhole pressure is assumed to be constant. This is especially correct for larger connectivities.

Table 2.1 Effect of bottomhole pressure variations on the value of connectivities inferred from CRMP.

	Results for I2620							
	P0826	**P1307**	**P1325**	**P1333**	**P1418**	**P1512**	**P2209**	**P2228**
Case I	0.036	0.08	0.074	0.031	0.016	0.07	0.124	0.568
Case II	0	0.081	0.05	0.05	0.014	0.07	0.184	0.547
Rel. Err.		0.013	0.324	0.613	0.125	0.000	0.484	0.037

	Results for I0405							
	P0826	**P1307**	**P1325**	**P1333**	**P1418**	**P1512**	**P2209**	**P2228**
Case I	0.106	0.25	0.096	0.024	0.055	0.115	0.096	0.258
Case II	0.051	0.274	0.079	0.031	0.064	0.084	0	0.279
Rel. Err.	0.519	0.096	0.177	0.292	0.164	0.270		0.081

	Results for I0519							
	P0826	**P1307**	**P1325**	**P1333**	**P1418**	**P1512**	**P2209**	**P2228**
Case I	0.1679	0.191	0.1348	0.0311	0.0512	0.115	0.061	0.2189
Case II	0.163	0.185	0.163	0.019	0.047	0.136	0.076	0.211
Rel. Err.	0.029	0.031	0.209	0.389	0.082	0.183	0.246	0.036

2.2.4. Estimation of the CRMP Parameters

Consider a mature oil field with N_p producers and N_{inj} injectors for which the well locations and the allocated monthly injection/production rates are available. The objective is to find the CRMP parameters, including the average response time, τ_j, of the producers, the initial production rates, Q_{j1}, and the individual injector-producer well-pairs connectivities, f_{ij}. The connectivity distance between the injector-producer pairs has an upper bound, r_i, above which the injector-producer pairs may not effectively communicate. This is referred to as the *radius of influence* of that injector and is mainly set by the field-expert geologists and reservoir engineers with experience on the field operation.

We use an optimization method to estimate the unknown parameters of the CRMP. We use Equation 2.11 to build the objective function and use physical signifi-

cance of the unknowns to define the feasible region. This equation models the bottom-hole production rate of each producer, generally as a function of the known injection rates and the unknown fitting parameters, namely Q_{j1}, τ_j, and f_{ij}.

The optimization model will minimize the difference between the computed rates, Q_{jn}, and the observed rates, Q_{jn}^{obs} within the physical range of the fitting parameters, Q_{j1}, τ_j, and f_{ij}.

$$minimize\ f_{CRMP} = \sum_{j=1}^{N_p}\sum_{n=1}^{N_t}\left(Q_{jn} - Q_{jn}^{obs}\right)^2 , \tag{2.12}$$

$$subject\ to\ \tau_j > 0, Q_{j1} > 0, f_{ij} \geq 0, and\ \sum_{j=1}^{N_p} f_{ij} \leq 1\ (for\ i = 1, \dots, N_i) , \tag{2.13}$$

$$and\ subject\ to\ f_{ij} < f_0\ if\ r_{ij} > r_i , \tag{2.14}$$

This optimization problem is classified as large-scale, constrained, and nonlinear. We use the interior-point algorithm through a commercial nonlinear programming solver.

The large-scale and nonlinear natures of this problem lead to challenges in the solution convergence and time that are not addressed in the other studies. This study is the first to systematically classify these challenges and presents a strategy to resolve them, as we will explain in the following.

2.2.5. Global and Local Minima

The optimization problem in Equation 2.12 has one set of fitting parameters over the feasible region for which f_{CRMP} is minimized. This set is called the global minimum. A local minimum, on the other hand, occurs in a specific neighborhood of the function. Nonlinear optimization problems such as CRMP can have more than one local minimum. Therefore, depending on the initial point, the solver may converge to a local minimum instead of the global minimum. Our objective is to ensure that the CRMP problem will converge to the global minimum by using a global optimization method. In global

optimization, the true global solution of the optimization problem is found, and the compromise is efficiency. Even small problems with a few tens of variables, can take a very long time (e.g., hours or days) to solve.

The key to resolving this problem is to be *sufficiently* confident that CRMP objective function is convex within its feasible region. The CRMP feasible region is convex. Therefore, the objective function is convex if the corresponding Hessian matrix is positive definite (Lasdon and Waren, 1983). If the objective function and feasible region are both convex, then any local minima is a global minimum. The mathematical proof of the convexity of the CRMP objective function is beyond the scope of this work. Instead, we investigate the convexity of this function numerically.

A small-scale CRMP problem including 10 years of data for six injectors and eight producers is set up. This problem has 64 variables and 70 constraints. The local optimization solver takes about one minute to converge to the solution. The global optimization solver uses the local optimization solver with 1,000 set of initial points and compares the results for the global minimum. The distributions of the start points are shown in Figure 2.5. The global optimization solver completed the runs from all start points while all local solver runs converged to the *same solution* within an acceptable tolerance of 10^{-6} for all fitting parameters.

The above example, and many other field-scale problems practiced by the author, do not serve as a proof of the convexity of the optimization problem. However, we investigated many small- to large-scale CRMP problems. In all cases the global optimizer consistently converged to a *unique* solution.

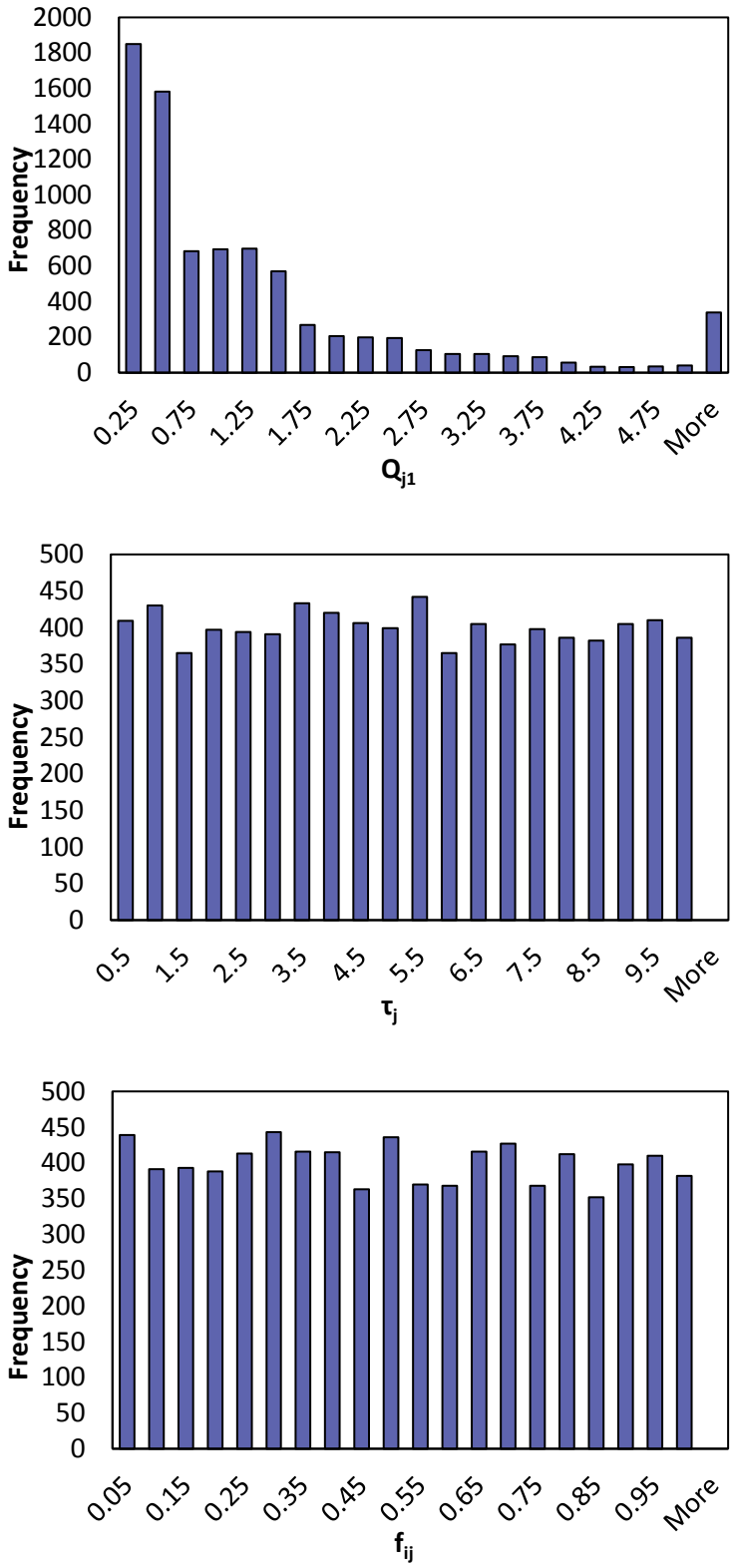

Figure 2.5 Distribution of start points used for the global optimization solver.

2.2.6. Solution Time and Convergence Rate

Previous studies documented large solution time and convergence failure as common challenges encountered in handling large-scale fields (Weber et al., 2009). We present two strategies for the first time to significantly improve the solution time and convergence rate:

1. Calculate the analytical gradient vector, and
2. Calculate the analytical Hessian matrix.

The solver usually estimates the gradient vector and Hessian matrix of the objective function using finite differences. Computing these numerical approximations is extremely inefficient in terms of the solution time. The alternative for the solver is to use the user-supplied analytic gradient vector and Hessian matrix of the objective function.

2.2.7. The Gradient of the CRMP Objective Function

The gradient of a scalar function is defined as,

$$\nabla f = grad\ f = (\partial f/\partial x_1\,, \partial f/\partial x_2\,, \dots, \partial f/\partial x_n)\ . \tag{2.15}$$

Therefore, the gradient vector of CRMP objective function is,

$$\nabla f_{CRMP} = ([\partial f_{CRMP}/\partial Q_{l1}], [\partial f_{CRMP}/\partial \tau_l], [\partial f_{CRMP}/\partial f_{ml}])\ (for\ l = 1 \dots N_p\ and\ m = 1 \dots N_{inj})\ . \tag{2.16}$$

The gradient vector of the CRMP objective function is in the form of recursive sequence. The derivation and the final form of this vector is presented in the following section.

2.2.8. Analytical Derivation of the Gradient Vector of the CRMP Objective Function

The CRMP objective function is defined as follows,

$$F = \sum_{j=1}^{N_p} \sum_{n=1}^{N_t} \left(Q_{jn} - Q_{jn}^{obs}\right)^2\ , \tag{2.17}$$

where

$$Q_{jn} = Q_{j1} e^{\left(-\frac{n-1}{\tau_j}\right)} + \sum_{k=1}^{n} \left\{ e^{-\left(\frac{n-k}{\tau_j}\right)} \left(1 - e^{\left(-\frac{1}{\tau_j}\right)}\right) \left[\sum_{i=1}^{N_i} f_{ij} I_{ik}\right] \right\}. \tag{2.18}$$

The derivative of this function with respect to an arbitrary parameter, *x*, is,

$$\frac{dF}{dx} = 2 \sum_{j=1}^{N_p} \sum_{n=1}^{N_t} \left[\left(Q_{jn} - Q_{jn}^{obs}\right) \frac{dQ_{jn}}{dx} \right]. \tag{2.19}$$

If x is only associated with producer *l*,

$$\frac{dQ_{jn}}{dx_l} = 0 \ (for\ j \neq l)\ . \tag{2.20}$$

Therefore,

$$\frac{dF}{dx_l} = 2 \sum_{n=1}^{N_t} \left[\left(Q_{ln} - Q_{ln}^{obs}\right) \frac{dQ_{ln}}{dx_l} \right]. \tag{2.21}$$

Derivation of $\frac{\mathbf{dF}}{\mathbf{dQ_{l1}}}$

$$\frac{dF}{dQ_{l1}} = 2 \sum_{n=1}^{N_t} \left[\left(Q_{ln} - Q_{ln}^{obs}\right) \frac{dQ_{ln}}{dQ_{l1}} \right], \tag{2.22}$$

$$\frac{dQ_{lk}}{dQ_{l1}} = \frac{dQ_{l,k-1}}{dQ_{l1}} e^{-\frac{1}{\tau_l}} \ (for\ k = 1 \ldots n) \rightarrow \frac{dQ_{ln}}{dQ_{l1}} = \frac{dQ_{l1}}{dQ_{l1}} \times e^{-\frac{1}{\tau_l}} \times \ldots \times e^{-\frac{1}{\tau_l}} = e^{-\frac{n-1}{\tau_l}}, \tag{2.23}$$

$$\frac{dF}{dQ_{l1}} = 2 \sum_{n=1}^{N_t} \left[\left(Q_{ln} - Q_{ln}^{obs}\right) e^{-\frac{n-1}{\tau_l}} \right]. \tag{2.24}$$

Derivation of $\frac{\boldsymbol{dF}}{\boldsymbol{d\tau_l}}$

$$\frac{dF}{d\tau_l} = 2 \sum_{n=1}^{N_t} \left[\left(Q_{ln} - Q_{ln}^{obs}\right) \frac{dQ_{ln}}{d\tau_l} \right], \tag{2.25}$$

$$\frac{dQ_{lk}}{d\tau_l} = Q_{l,k-1} \frac{1}{\tau_l^2} e^{-\frac{1}{\tau_l}} + e^{-\frac{1}{\tau_l}} \frac{dQ_{l,k-1}}{d\tau_l} - \frac{1}{\tau_l^2} e^{-\frac{1}{\tau_l}} \left\{ \sum_{i=1}^{N_{inj}} [f_{il} I_{ik}] \right\} \ (for\ k = 1 \ldots n), \tag{2.26}$$

where,

$$\frac{dQ_{l1}}{d\tau_l} = 0\ .$$

This recursive sequence must be computed numerically.

Derivation of $\frac{dF}{df_{ml}}$

$$\frac{dF}{df_{ml}} = 2\sum_{n=1}^{N_t}\left[\left(Q_{ln} - Q_{ln}^{obs}\right)\frac{dQ_{ln}}{df_{ml}}\right], \tag{2.27}$$

$$\frac{dQ_{lk}}{df_{ml}} = \frac{dQ_{l,k-1}}{df_{ml}}e^{-\frac{1}{\tau_l}} + \left(1 - e^{\left(-\frac{1}{\tau_l}\right)}\right)I_{mk}\ (for\ k = 1 \dots n)\ , \tag{2.28}$$

where,

$\frac{dQ_{l1}}{df_{ml}} = 0$. This recursive sequence must be computed numerically.

2.2.9. The Hessian of the CRMP Objective Function

The Hessian of a scalar function is a square matrix defined as,

$$H = \nabla^2 f = Hessian\ f\ ,\ H_{i,j} = \frac{\partial^2 f}{\partial x_i \partial x_j}\ . \tag{2.29}$$

The Hessian for a constrained problem is the Hessian of the Lagrangian. Considering an objective function, *f*, nonlinear inequality constraints vector, $\bar{c}_{eq}$, and nonlinear equality constraint vector, c_{eq}, the Lagrangian is,

$$L = f + \sum_i \lambda_i \bar{c}_{eq,i} + \sum_j \lambda_j c_{eq,j}\ , \tag{2.30}$$

where λ_j's are Lagrange multipliers. Therefore, the Hessian of the Lagrangian is,

$$H = \nabla^2 f + \sum_i \lambda_i \nabla^2 \bar{c}_{eq,i} + \sum_j \lambda_j \nabla^2 c_{eq,j}\ . \tag{2.31}$$

All linear constraints have Hessian of zero. Therefore, if no nonlinear constraints exists, as is the case here, only the objective function contributes non-trivially to the Hessian of the Lagrangian,

$$H_{CRMP} = \nabla^2 f_{CRMP}\ , \tag{2.32}$$

$$H_{CRMP} = \begin{pmatrix} \left[\frac{\partial^2 f_{CRMP}}{\partial Q_{l1}\partial Q_{r1}}\right] & \left[\frac{\partial^2 f_{CRMP}}{\partial \tau_l \partial Q_{l1}}\right] & \left[\frac{\partial^2 f_{CRMP}}{\partial f_{ml}\partial Q_{l1}}\right] \\ \left[\frac{\partial^2 f_{CRMP}}{\partial \tau_l \partial Q_{l1}}\right] & \left[\frac{\partial^2 f_{CRMP}}{\partial \tau_l \partial \tau_r}\right] & \left[\frac{\partial^2 f_{CRMP}}{\partial \tau_l \partial f_{ml}}\right] \\ \left[\frac{\partial^2 f_{CRMP}}{\partial f_{ml}\partial Q_{l1}}\right] & \left[\frac{\partial^2 f_{CRMP}}{\partial \tau_l \partial f_{ml}}\right] & \left[\frac{\partial^2 f_{CRMP}}{\partial f_{ml}\partial f_{sl}}\right] \end{pmatrix} \qquad (for\ l, r = 1 \dots N_p\ and\ m, s = 1 \dots N_i). \tag{2.33}$$

The Hessian matrix of CRMP objective function is in the form of recursive sequence. The derivation and the final form of this matrix is presented in the following section

2.2.10. Analytical Derivation of the Hessian Matrix of CRMP Objective Function

CRMP objective function is defined as follows,

$$F = \sum_{j=1}^{N_p} \sum_{n=1}^{N_t} \left(Q_{jn} - Q_{jn}^{obs}\right)^2 , \tag{2.34}$$

where,

$$Q_{jn} = Q_{j1} e^{\left(-\frac{n-1}{\tau_j}\right)} + \sum_{k=1}^{n} \left\{ e^{-\left(\frac{n-k}{\tau_j}\right)} \left(1 - e^{\left(-\frac{1}{\tau_j}\right)}\right) \left[\sum_{i=1}^{N_i} f_{ij} I_{ik}\right] \right\} . \tag{2.35}$$

The Hessian of this function with respect to an arbitrary parameter, *x*, is,

$$\frac{d^2F}{dx^2} = \frac{d}{dx}\left(\frac{dF}{dx}\right) = \frac{d}{dx}\left(2 \sum_{j=1}^{N_p} \sum_{n=1}^{N_t} \left(Q_{jn} - Q_{jn}^{obs}\right) \frac{dQ_{jn}}{dx}\right) = 2 \sum_{j=1}^{N_p} \sum_{n=1}^{N_t} \left[\left(Q_{jn} - Q_{jn}^{obs}\right) \frac{d^2 Q_{jn}}{dx^2} + \left(\frac{dQ_{jn}}{dx}\right)^2\right] . \tag{2.36}$$

Derivation of $\frac{d^2F}{dQ_{l1}{}^2}$

$$\frac{d^2F}{dQ_{l1}{}^2} = 2 \sum_{n=1}^{N_t} \left[\left(Q_{ln} - Q_{ln}^{obs}\right) \frac{d^2 Q_{ln}}{dQ_{l1}{}^2} + \left(\frac{dQ_{ln}}{dQ_{l1}}\right)^2\right] , \tag{2.37}$$

$$\frac{dQ_{ln}}{dQ_{l1}} = e^{-\frac{n-1}{\tau_l}} . \tag{2.38}$$

Therefore,

$$\frac{d^2 Q_{ln}}{dQ_{l1}^2} = 0 , \tag{2.39}$$

and,

$$\frac{d^2F}{dQ_{l1}{}^2} = 2 \sum_{n=1}^{N_t} \left[\left(Q_{ln} - Q_{ln}^{obs}\right) e^{-2\frac{n-1}{\tau_l}}\right] . \tag{2.40}$$

Derivation of $\frac{d^2F}{d\tau_l{}^2}$

$$\frac{d^2F}{d\tau_l{}^2} = 2 \sum_{n=1}^{N_t} \left[\left(Q_{ln} - Q_{ln}^{obs}\right) \frac{d^2 Q_{ln}}{d\tau_l{}^2} + \left(\frac{dQ_{ln}}{d\tau_l}\right)^2\right] , \tag{2.41}$$

where,

$$\frac{d^2Q_{lk}}{d\tau_l{}^2} = \frac{d^2Q_{l,k-1}}{d\tau_l{}^2}e^{-\frac{1}{\tau_l}} + \frac{1}{\tau_l^2}e^{-\frac{1}{\tau_l}}\frac{dQ_{l,k-1}}{d\tau_l} - \frac{2}{\tau_l^3}e^{-\frac{1}{\tau_l}}Q_{l,k-1} + \frac{1}{\tau_l^4}e^{-\frac{1}{\tau_l}}Q_{l,k-1} + \left[\frac{2}{\tau^3}e^{-\frac{1}{\tau_l}} - \frac{1}{\tau_l^4}e^{-\frac{1}{\tau_l}}\right]\left[\sum_{i=1}^{N_i} f_{il}I_{ik}\right](for\ k = 1 \dots n)\ , \tag{2.42}$$

where $\frac{dQ_{lk}}{d\tau_l}$ can be calculated from Equation 2.26. This recursive sequence must be computed numerically.

Derivation of $\frac{d^2F}{df_{ml}{}^2}$

$$\frac{d^2F}{df_{ml}{}^2} = 2\sum_{n=1}^{N_t}\left[\left(Q_{ln} - Q_{ln}^{obs}\right)\frac{d^2Q_{ln}}{df_{ml}{}^2} + \left(\frac{dQ_{ln}}{df_{ml}}\right)^2\right]. \tag{2.43}$$

By using Equation 2.28,

$$\frac{d^2F}{df_{ml}{}^2} = \frac{d}{df_{ml}}\left(\frac{dQ_{lk}}{df_{ml}}\right) = \frac{d}{df_{ml}}\left(\frac{dQ_{l,k-1}}{df_{ml}}e^{-\frac{1}{\tau_l}} + \left(1 - e^{\left(-\frac{1}{\tau_l}\right)}\right)I_{mk}\right) = \frac{d^2Q_{l,k-1}}{df_{ml}{}^2}e^{-\frac{1}{\tau_l}}, \tag{2.44}$$

where,

$$\frac{d^2Q_{l,1}}{df_{ml}{}^2} = 0.$$

Therefore,

$$\frac{d^2F}{df_{ml}{}^2} = 0\ , \tag{2.45}$$

and,

$$\frac{d^2F}{df_{ml}{}^2} = 2\sum_{n=1}^{N_t}\left(\frac{dQ_{ln}}{df_{ml}}\right)^2\ . \tag{2.46}$$

This recursive sequence can must be computed numerically using Equation 2.28.

Derivation of $\frac{d^2F}{df_{ml}dQ_{l1}}$

$$\frac{d^2F}{df_{ml}dQ_{l1}} = \frac{d}{df_{ml}}\left(\frac{dF}{dQ_{l1}}\right). \tag{2.47}$$

Using Equation 2.24,

$$\frac{d}{df_{ml}}\left(\frac{dF}{dQ_{l1}}\right) = \frac{d}{df_{ml}}\left(2\sum_{n=1}^{N_t}\left[\left(Q_{ln} - Q_{ln}^{obs}\right)e^{-\frac{n-1}{\tau_l}}\right]\right) = 2\sum_{n=1}^{N_t}\left[\frac{dQ_{ln}}{df_{ml}}e^{-\frac{n-1}{\tau_l}}\right], \tag{2.48}$$

where $\frac{dQ_{lk}}{df_{ml}}$ can be calculated from Equation 2.28. This recursive sequence must be computed numerically.

Derivation of $\frac{d^2F}{d\tau_l dQ_{l1}}$

$$\frac{d^2F}{d\tau_l dQ_{l1}} = \frac{d}{d\tau_l}\left(\frac{dF}{dQ_{l1}}\right). \tag{2.49}$$

Using Equation 2.24,

$$\frac{d}{d\tau_l}\left(\frac{dF}{dQ_{l1}}\right) = \frac{d}{d\tau_l}\left(2\sum_{n=1}^{N_t}\left[\left(Q_{ln} - Q_{ln}^{obs}\right)e^{-\frac{n-1}{\tau_l}}\right]\right) = 2\sum_{n=1}^{N_t}\left[\frac{dQ_{ln}}{d\tau_l}e^{-\frac{n-1}{\tau_l}} + \frac{n-1}{\tau_l^2}e^{-\frac{n-1}{\tau_l}}\left(Q_{ln} - Q_{ln}^{obs}\right)\right], \tag{2.50}$$

where $\frac{dQ_{lk}}{d\tau_l}$ can be calculated from Equation 2.26. This recursive sequence must be computed numerically.

Derivation of $\frac{d^2F}{d\tau_l df_{ml}}$

$$\frac{d^2F}{d\tau_l df_{ml}} = \frac{d}{d\tau_l}\left(\frac{dF}{df_{ml}}\right). \tag{2.51}$$

Using Equation 2.27,

$$\frac{d}{d\tau_l}\left(\frac{dF}{df_{ml}}\right) = \frac{d}{d\tau_l}\left(2\sum_{n=1}^{N_t}\left[\left(Q_{ln} - Q_{ln}^{obs}\right)\frac{dQ_{ln}}{df_{ml}}\right]\right) = 2\sum_{n=1}^{N_t}\left[\frac{dQ_{ln}}{d\tau_l}\frac{dQ_{ln}}{df_{ml}} + \frac{d}{d\tau_l}\left(\frac{dQ_{ln}}{df_{ml}}\right)\left(Q_{ln} - Q_{ln}^{obs}\right)\right]. \tag{2.52}$$

Using Equation 2.28,

$$\frac{dQ_{lk}}{d\tau_l}\frac{dQ_{lk}}{df_{ml}} = \frac{d}{d\tau_l}\left(\frac{dQ_{l,k-1}}{df_{ml}}e^{-\frac{1}{\tau_l}} + \left(1 - e^{\left(-\frac{1}{\tau_l}\right)}\right)I_{mk}\right) = \frac{d^2Q_{l,k-1}}{{df_{ml}}^2}e^{-\frac{1}{\tau_l}} + \frac{1}{\tau^2}e^{-\frac{1}{\tau_l}}\frac{dQ_{l,k-1}}{df_{ml}} - \left(\frac{1}{\tau_l^2}e^{-\frac{1}{\tau_l}}\right)I_{mk}\ (for\ k = 1 \dots n)\ , \tag{2.53}$$

where,

$$\frac{d^2Q_{l1}}{{df_{ml}}^2} = 0\ ,$$

and,

$$\frac{dQ_{l1}}{df_{ml}} = 0\ .$$

This recursive sequence must be computed numerically.

Derivation of $\frac{d^2F}{d\tau_l d\tau_r}$

$$\frac{d^2F}{d\tau_l d\tau_r} = 0 \ . \tag{2.54}$$

Derivation of $\frac{d^2F}{dQ_{l1} dQ_{r1}}$

$$\frac{d^2F}{dQ_{l1} dQ_{r1}} = 0 \ . \tag{2.55}$$

Derivation of $\frac{d^2F}{df_{ml} df_{sl}}$

$$\frac{d^2F}{df_{sl} df_{ml}} = \frac{d}{df_{sl}}\left(\frac{dF}{df_{ml}}\right) . \tag{2.56}$$

Using Equation 2.27,

$$\frac{d}{df_{sl}}\left(\frac{dF}{df_{ml}}\right) = \frac{d}{df_{sl}}\left(2\sum_{n=1}^{N_t}\left[\left(Q_{ln} - Q_{ln}^{obs}\right)\frac{dQ_{ln}}{df_{ml}}\right]\right) = 2\sum_{n=1}^{N_t}\left[\frac{dQ_{ln}}{df_{sl}}\frac{dQ_{ln}}{df_{ml}} + \frac{d}{df_{sl}}\left(\frac{dQ_{ln}}{df_{ml}}\right)\left(Q_{ln} - Q_{ln}^{obs}\right)\right] = 2\sum_{n=1}^{N_t}\left[\frac{dQ_{ln}}{df_{sl}}\frac{dQ_{ln}}{df_{ml}}\right] , \tag{2.57}$$

where $\frac{dQ_{lk}}{df_{ml}}$ and $\frac{dQ_{ln}}{df_{sl}}$ can be calculated from Equation 2.28. This recursive sequence must be computed numerically.

2.2.11. Improvements from the use of Analytical Gradient and Hessian

By supplying the analytical gradient vector and Hessian matrix to the solver, the solution time and the convergence rate are improved. For a large-scale problem with more than 500 wells, this strategy will reduce the solution time from several days to several hours, depending on the choice of r_i. The results of implementing the Hessian matrix and the gradient vector are shown in Figure 2.6 for four leases located in the West Texas Permian Basin. As the number of wells increases, the number of fitting parameters and consequently the CRMP solution time increase exponentially. By using the Hessian matrix and the gradient vector and depending on the problem size, a 90-99% decrease in convergence time is observed. For very large problems such as Mallet Unit, the number of fitting parameters is so large (17,000) that practically the problem cannot be solved with a powerful computer (Intel Xeon E5 with 32 Gigabytes memory). The projection of the CRMP runtime without Hessian matrix and gradient vector for the

Mallet Unit problem shows that the solution time is approximately in the order of thousands of hours. While such high runtimes render the CRMP completely impractical. The use of the Hessian Matrix and the gradient vector reduced the convergence time from order of several thousand hours down to approximately 3 hours.

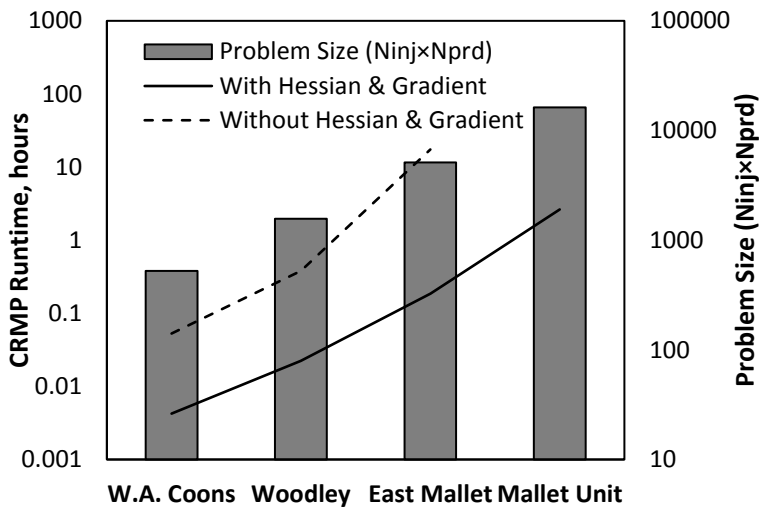

Figure 2.6 CRMP runtime for small- to large-scale problems.

2.2.12. Scaling the Fitting Parameters

Scaling is the process of gauging all variables so that their magnitudes are approximately within the same range, e.g. [0, 10]. This can help solve convergence problems, improve numerical stability, and in many cases improve the quality of the solution. If a problem contains variables with different scales, the solver will allocate more time on smaller variables because the objective function is more sensitive to a change in a small variable compared to a large variable. In CRMP, both the time constants and the connectivities are approximately centered around 1. Initial flow rates, on the other hand, can have a magnitude of 10^3 RB/m. The solution is simple: multiply all injection/production rates by an appropriate scaling factor, e.g. 10^{-3}, so that the values are centered around 1. For most practical purposes, changing the units of the rates from RB/m to MRB/m will suffice.

2.3. Analysis of Mature Oil Fields

The assumptions for CRMs are the following: linear well productivity, slightly compressible fluids, no producer extended shut-in, no new production wells, and no new completions. CRMs assume that the interwell connectivities and producers' time constants are constant over the evaluated time period. In reality, various large- and small-scale events occur, and the above-mentioned assumptions are often violated. These include conversion to injections, well abandonment, changes in maintenance plans, workovers, and limited infill drilling. These changes bring a dynamic nature to the problem, especially over longer time periods. Therefore, assigning a single connectivity map to the field or characterizing a producer's control volume with a single time constant is not correct.

We apply the stepwise model fitting method to break down the lease production history into smaller periods. This method accounts for changes due to the major lease events and to compare the solutions. If two independent analyses generate similar connectivity patterns, the conclusions will be more reliable. Therefore, for each injector three to four connectivity maps are extracted, each covering eight to 12 years of production history. If a producer-injector well-pair shows strong connectivity in at least two of these connectivity maps, their connectivity is reliable. This methodology cannot completely eliminate the errors generated due to deviation from ideal assumptions, but it will greatly reduce the introduction of false large connectivities.

2.3.1. Radius of Influence of the Injectors (ri)

This term is defined for each injector, as the threshold radius beyond which a flow communication between the injector-producer pairs is improbable and is shown by r_i (see Equation 2.14). Producers located farther than r_i are assumed to be in indirect communication with the injector. The value of r_i is a strong function of the reservoir geology and heterogeneity.

We present a method to estimate r_i based on the CRMP as follows. The radius of influence condition is honored by setting an upper bound constraint, f_0, for the well connectivities in Equation 2.14. The values of r_i and f_0 are determined by performing a

set of CRMP runs for different values of these parameters and monitoring the history match quality. The field expert input is required to determine the range of r_i. Figure 2.7 presents the fieldwide history match error as a function of r_i. The error is significantly high for r_i values smaller than 1500 feet. However, the error reaches a plateau between 1500 feet and 2500 feet for all leases. For each lease, the corresponding value of r_i after which a minimal error reduction is expected is extracted from this plot and used for the rest of the analysis.

Using greater values of r_i will result in an only slightly better history match; the downside, however, is the introduction of extremely distant connectivities (over 0.5 miles) which contradict the conventional judgement of the field operators. We believe that such distant connectivities are simply the artifact of simplified models and of the errors involved with allocated flow rates, as well as the absences of flowing bottomhole pressure; therefore, they do not carry any physical meaning.

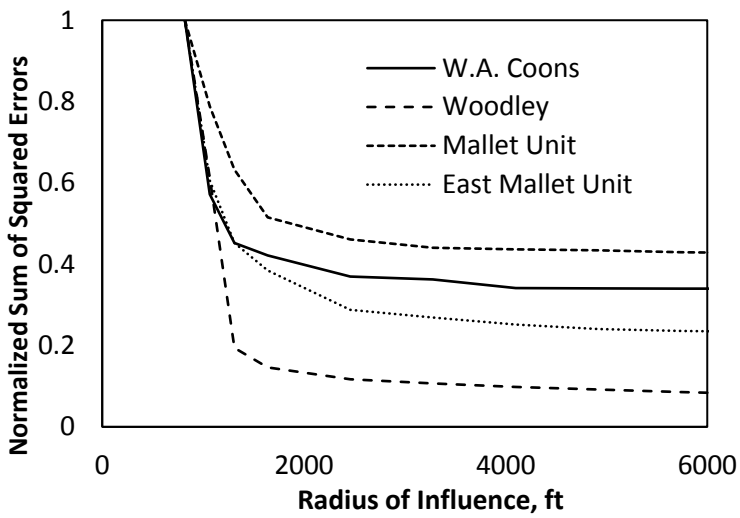

Figure 2.7 Normalized history match error as a function of radius of influence for four leases located in Slaughter field, West Texas.

2.4. Results: Application to Large-Scale Mature Oil Fields

The methodology is applied to several leases located in Slaughter field, West Texas (Figure 2.8). This field produces oil from the lower Permian San Andres Dolomite at an average depth of approximately 5000 ft. This includes three porous zones

each approximately 40 feet thick separated by anhydritic dolomite or anhydrite. Primary and secondary productions in this field were initiated in 1930s and 1960s, respectively. CO_2 injection was initiated between 1985 and 1995 for different leases located in this field.

The largest lease examined in this study has up to 400 wells. Such a large problem can now be easily solved by applying the solution time and convergence rate management strategies discussed earlier. With the information obtained from the connectivity maps, the operator can develop more successful well management strategies to improve the waterflood and CO_2-EOR performance. Overall, the performance of about 300 injectors and 500 producers are analyzed. We present three examples with important features and implications.

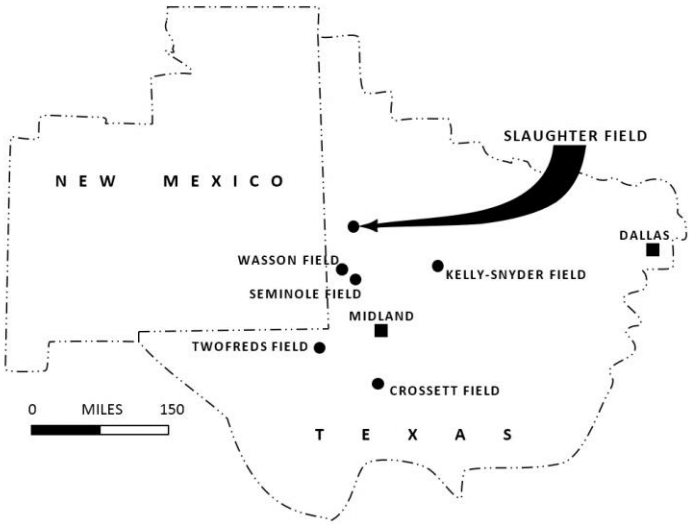

Figure 2.8 The study area: the Slaughter field in West Texas.

2.4.1. Example 1: Validation of CRMP Results

CRMP results and their interpretation for several injectors in the East Mallet Unit lease are presented in this example. Figure 2.9 shows the well identity map of the East Mallet Unit lease in the Slaughter field. The injector CTI01 and its nearby producers are identified. The results of CRMP runs for CTI01 for three different time periods of 1985-1991, 1992-2004, and 2005-2013 are summarized in Table 2.2a. These time

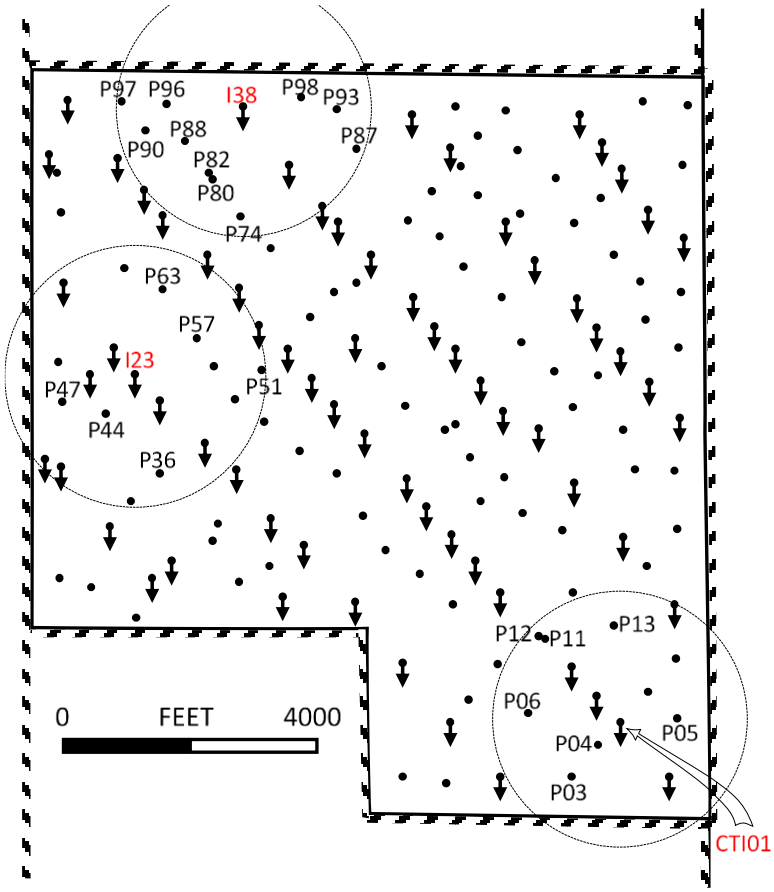

Figure 2.9 East Mallet Unit. The circles show the radius of influence (approximately 2000 feet for this lease).

intervals were selected based on major lease-wide operations, in particular the beginning of CO_2 flood in 1992 and the beginning of a series of workover operations in 2005. For any other lease, the analyst is recommended to select appropriate intervals after studying the fields' history.

The results indicate that this injector has considerable connectivities to P03, P04, P05, and P11/P12 and shows trivial total connectivities to the producers beyond its radius of influence. The producer P12 was replaced by P11 in 2004 due to completion deficiencies; therefore, the results for these two producers are combined and reported as one producer (P11/P12). Figure 2.10a illustrates the CO_2 injection rate of CTI01 and CO_2 production rates of P04 and P05. Since the beginning of CO_2 injection in 1990, the injection rate has peaked several times. All these peaks correspond to peaks in CO_2 production responses of P04 and P05 with an approximate six to 12 months delay of

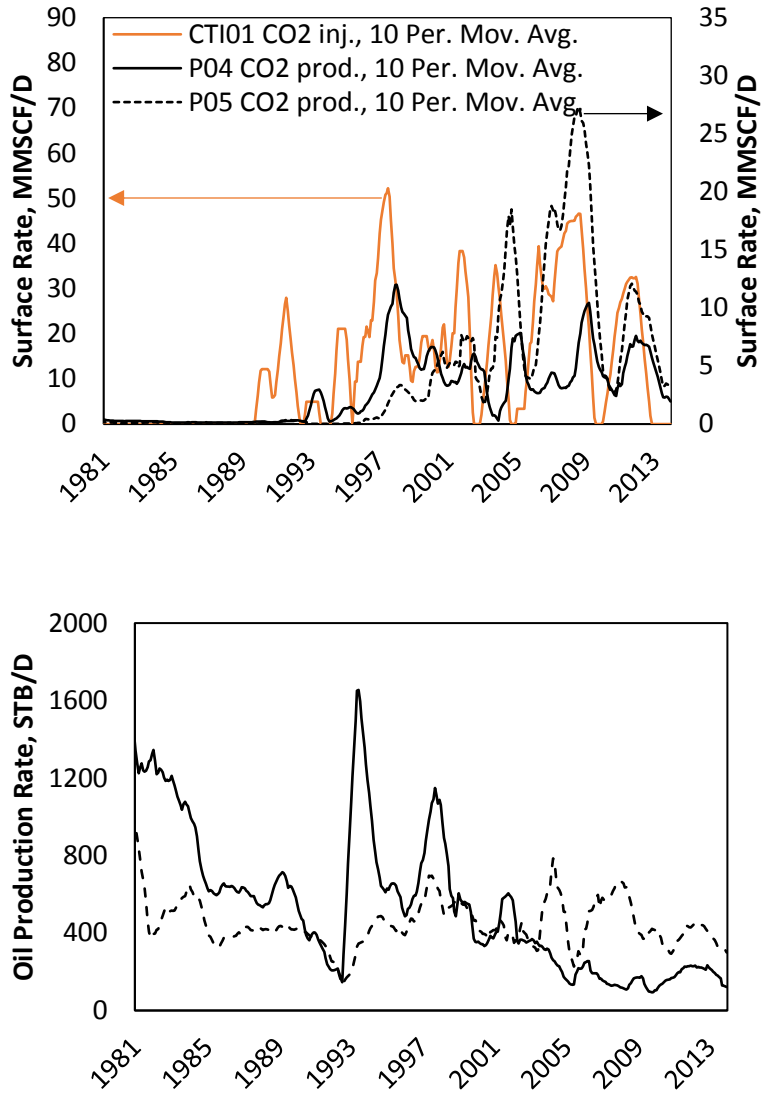

Figure 2.10 (a) CTI01 CO_2 injection signal and P04 and P05 CO_2 production response (top), and (b) P04 and P05 oil production response (bottom).

response. Furthermore, oil production rates of these producers indicate that each peak in CO_2 production corresponds to a peak in oil production demonstrating the successful application of CO_2-EOR in this injector (Figure 2.10b).

The author found numerous other examples to verify the CRMP results based on this method which are not presented here. The analyst may use other sources of information, such as radioactive tracer testing and determine the connectivity with greater confidence. The economic justification of such tests for the mature fields, however, is a challenge.

2.4.2. Example 2: Determining Current Water Injectors Suited for CO_2 Injection

Figure 6b also identifies the injector I38 and its nearby producers in the East Mallet Unit lease. Table 2.2b summarizes the CRMP connectivity results for this injector for the same time periods as mentioned in Example 1. Producer P82 was replaced by P80 in 2000 due to completion deficiencies; therefore, the results for these two producers are combined and reported as one producer (P80/P82). Injector I38 has significant connectivity to the nearby producers and moderate connectivities to the region beyond its radius of influence. I38 has been an active water injector throughout the life of this lease but has not been used for CO_2 injection. Given the strong connectivities between this injector and its nearby producers, this injector is recommended for CO_2 injection because the injection fluid is confined to the system. Such injectors are recommended for a one-year trial period of CO_2 injection while monitoring the production response of the producers with confirmed connectivities. Upon confirmation, this injector is recommended for further CO_2 injection.

2.4.3. Example 3: Determining Current CO_2 Injectors Not Suited for CO_2 Injection

Figure 6b also identifies I23 and its nearby producers in the East Mallet Unit lease. Table 2.2c summarizes the CRMP connectivity results for this injector for the same time periods as mentioned in Examples 1 and 2. The results indicate that unlike the injectors in Examples 1 and 2, injector I23 is only weakly connected to the nearby producers. This is a potential indicator of out of zone injection. For more than 20 years since the beginning of its activity in 1991, I23 has injected nearly 4 BSCF of CO_2. Given the weak connectivities to the nearby producers, an injection log should be performed to determine the conformance issues.

Table 2.2 CRMP connectivity results (f_{ij}) for CTI01, I38 and I23; BRI: Beyond the Radius of Influence, C: Connected, NC: Not Connected. Refer to Figure 6b for the well locations.

(a) Results for CTI01

	Period1	**Period2**	**Period3**	**Status**
P03	0.16	0.11	≈0	C
P04	≈0	0.26	0.05	C
P05	0.30	0.27	0.48	C
P06	≈0	≈0	≈0	NC
P09	≈0	0.02	≈0	NC
P10	0.24	≈0	≈0	NC
P11/P12	≈0	0.04	0.32	C
P13	≈0	≈0	0.07	NC
BRI	0.15	0.20	0.10	—

(b) Results for I38

	Period1	**Period2**	**Period3**	**Status**
P69	0.07	≈0	≈0	NC
P74	0.04	≈0	≈0	NC
P80/P82	0.10	≈0	0.10	C
P88	≈0	0.07	0.05	C
P90	0.14	0.42	0.06	C
P93	≈0	0.13	0.07	C
P96	≈0	0.11	0.26	C
P98	0.16	0.17	0.19	C
BRI	0.34	0.1	0.25	—

(c) Results for I23

	Period1	**Period2**	**Period3**	**Status**
P36	≈0	0.54	≈0	NC
P44	≈0	0.05	0.24	C
P47	≈0	≈0	0.13	NC
P51	≈0	≈0	0.22	NC
P57	0.07	≈0	0.09	C
P63	≈0	0.14	0.07	C
BRI	0.15	0.25	0.3	—

2.5. Discussion

Figure 2.11 shows the overall CRMP match for the Mallet Unit lease, another lease located in the Slaughter field. The overall match is satisfactory, but major workover events have significant effect on the results. In this example, a five-year period of data is used for the history matching and data tuning. Then the model is set to predict the production rates over the next three years. While CRMP successfully matches the observed rates during the first year subsequent to history matching, it underestimates the production rate for the next two years. This period corresponds to major lease-wide workover operations. In such cases the reliability of the resultant connectivity maps is rather compromised. In future studies, CRMP may be adjusted so that the producer workovers are accounted in the CRMP formulation.

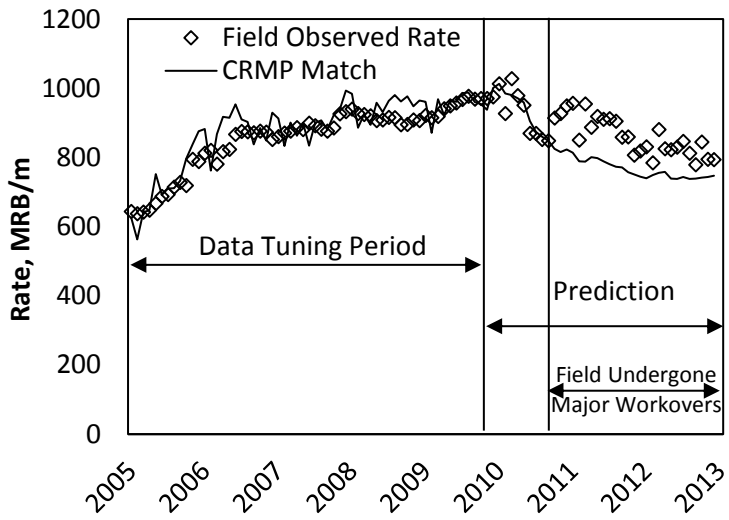

Figure 2.11 Application of CRMP to predicting future performance of Mallet Unit lease. The model underestimates the fluid production rates in the presence of major workover operations starting in 2011.

In addition, many studies concentrated on improving the quality of various CRMs' history match by introducing more complex models, such as CRMIP and CRM-Block, taking producer-producer interaction into account, and including multiphase equations in the model's formulations (M. Sayarpour et al., 2009). While these approaches are acceptable, the adequacy of CRMP in its presented form must not be underestimated. CRMP may not yield a *visually* acceptable match for all wells, however,

such cases do not necessarily affect reliability of the CRMP matches. The author observed many unforeseen events in the analysis that may not be easily modeled for a field with 500 wells, such as lease acquisition, extensive workovers, and out of zone influx and outflux. Adding more fitting parameters does not necessarily result in better models. This raises the concept of a *useful* model from a statistical viewpoint.

The CRM's degree of freedom determines the flexibility to match a given set of data. Degree of freedom is defined as the number of observations minus the number of relationships between dependent and independent variables. Small degrees of freedom will result in "perfect fitting" and "overfitting." Overfitting must be avoided because a less fitted model resulting from more degrees of freedom carries more merits (Hawkins, 2004). A model that includes too many variables without sufficient observations to support the model will overfit the observed data. In such cases, although a satisfactory match is easily obtainable, the model will lack the power to capture actual features of the system and cannot be used for predicting its future performance. We recommend CRMP over more complex models with a greater number of fitting parameters, especially considering the data shortage often encountered in such problems.

CHAPTER III

MAXIMIZED WORKOVER BENEFITS: STIMULATION OF BETTER PRODUCERS[2]

Effective candidate selection is an important consideration in planning successful stimulation campaigns. Identifying "high potential" wells—those that would provide the largest incremental production—has been the subject of several studies, some of which have suggested that stimulation of better producers is a good practice to maximize stimulation benefits. An evidence-based investigation of this idea is lacking and is the subject of this study.

This chapter hypothesizes that a positive correlation exists between a well's oil production performance and its stimulation incremental oil production. We test this hypothesis by investigating three independent methods: (1) analysis of aggregate results of case studies in the literature; (2) analysis of production data from four mature Permian Basin San Andres leases; and (3) analysis of the simulation results from a tuned reservoir model.

The results confirm the existence and statistical significance of a positive correlation between pre-stimulation oil rate and stimulation incremental oil production. This observation is used to rank stimulation candidates based on their potential for incremental oil recovery. The performance of this ranking method is shown to be nearly equal to candidate selection with perfect information in which the true ranking is known.

While the success of the treatment depends on the design and implementation of the appropriate stimulation method, priority should be given to the wells that exhibit high oil production. This practice will statistically increase the likelihood of maximized workover benefits, while imposing only a slight increase on analysis cost and time.

[2] Parts of this chapter are published in:
Jamali, A., Ettehadtavakkol, A., 2018. Good wells make better stimulation candidates: An evidence-based analysis. Journal of Petroleum Science and Engineering.

3.1. Problem Definition

Well stimulation refers to any treatment performed to restore or improve the productivity of an oil/gas well. The purpose of well stimulation is to enhance oil/gas field economics through faster and higher hydrocarbon delivery without significant investment (Economides and Nolte, 2000; Schechter, 1992). Depending on the nature of production impairment, reservoir characteristics, and operators' preference and past experience, a number of stimulation techniques have been practiced, including matrix acidizing, acid fracturing, hydraulic fracturing, recompletion, and fracpack (Bartko et al., 1992; Hainey and Troncoso, 1992; Hopkinson et al., 1982; Kalfayan, 2008; Meese et al., 1994; Pang and Faehrmann, 1993; Strong et al., 1997; Whisonant and Hall, 1997; Zillur et al., 2002). A generic stimulation workflow can be defined which comprises five stages, namely: candidate selection, treatment selection, treatment design, execution, and evaluation. While each stage should be carefully addressed, successful candidate selection (i.e. identifying wells that would provide largest incremental production) is particularly important and can significantly boost the economic benefits. On the other hand, if a wrong well is selected, even good treatment design and operation does not guarantee success in terms of economic return (Kartoatmodjo et al., 2007; Moore and Ramakrishnan, 2006; Nitters et al., 2000; Nnanna et al., 2009; Sinson et al., 1988; Zoveidavianpoor et al., 2012b).

Well stimulation optimization and effective candidate selection strategies have been the subject of many studies. Table 3.1 summarizes selected studies on candidate selection, the proposed candidate selection technique, and a summary of the results and conclusions. More than ten candidate selection strategies have been practiced and documented using actual field data, analytical models, and reservoir simulation models. These techniques include well-test-driven techniques (e.g. well performance analysis, identification of formation damage source and severity), production data analysis techniques (e.g. production comparison with nearby wells), and computerized optimization techniques (e.g. Artificial Neural Networks and Genetic Algorithms). Despite the considerable effort devoted to this problem, there is no general agreement on the optimal

candidate selection strategy. Moore and Ramakrishnan (2006) concluded that no selection criteria can be universally applied to every situation, and a reservoir specific selection criteria should be formulated based on the existing experience for that particular field. Zoveidavianpoor et al. (2012a) reviewed conventional candidate selection techniques for hydraulic fracturing and reported that candidate selection is not a straightforward procedure, lacking an agreed-upon approach to universally identify stimulation candidates across different geological settings. Reeves et al. (1999a) applied three different candidate selection techniques and showed that each technique provides a completely different list of candidate wells, indicating the uncertainty involved with each technique. The complex nature of this problem and the lack of agreement among various candidate selection techniques can be associated with (1) the considerable amount of data required to accurately determine the sources of well impairment and to identify the optimal remedial action; (2) the variations in the performance of each reservoir stimulation technique; and (3) the uncertainty of operational parameters during well stimulation.

Several researchers have intimated that stimulation of "good producers", may provide better results when compared to the more complex analytical models. Reeves et al. (2000) applied various candidate selection techniques to a field-scale reservoir simulation model. They concluded that while some of those techniques can identify a majority of top stimulation candidates, their performance is inferior to selecting better producers as better stimulation candidates. Shelley (1999) concluded that wells with higher production rates are generally the best candidates for recompletion. Jennings (1991) concluded that high deliverability wells benefit from fast payout time and effective well cleanup, making them attractive candidates for stimulation. The list of studies that have supported the stimulation of good producers is presented in Table 3.2. These studies are mainly based on analytical or simulation models and present only a very limited number of case studies; therefore, they lack sufficient field data to establish a compelling case.

Table 3.1 Selected publications on well stimulation optimization with focus on candidate selection.

Reference	Location/Field	Technique	Summary and Findings
Xiong and Holditch, 1995	theoretical	fuzzy logic	Eight fuzzy evaluators are developed to improve decision making of candidate selection, treatment type selection, and fluid & additive selection.
Shelley, 1999; Shelley et al., 1998	Red-Oak field, OK; Red Deer Creek field, TX	Artificial Neural Networks (ANNs)	The commonly available well and reservoir characteristics and production response to past stimulations are used to evaluate the recompletion re-stimulation potential in the remaining wells.
Zarei et al., 2014	simulation, anonymous field	Genetic Algorithms (GA)	Long-term effect of workovers is emphasized. GA and engineer-guided GA are used to allocate limited stimulation resources and to determine optimal workover timing.
Reeves et al., 2000, 1999a, 1999b	Green River, Piceance, East TX, and TX Gulf Coast Basins	production data comparison; ANNs & GA; type curve matching	Top candidates ranked by each analytical method are unique to that method, indicating the uncertainty of each method. Stimulation of underperforming wells (production data comparison) is less effective than ANNs or GAs.
Nitters et al., 2000	theoretical	structured candidate selection	Candidate wells are selected by comparing actual performance and theoretical potential. The sources of poor performance are identified to help with treatment selection and design.
Kartoatmodjo et al., 2007	simulation, Bokor filed, East Malaysia	risk-based candidate selection	Risk likelihood and severity are evaluated to reflect potential monetary and time loss.

			Risk analysis is performed using Monte-Carlo simulation to select optimal candidates.
Krasey, 1988	Pembina field, Alberta, Canada	high-grading candidate selection	Pressure transient analysis is used to measure the skin factor. Stimulation candidates are ranked by comparing stabilized production rate before and after skin removal.
Jennings, 1991	P/6 gas field, The Netherlands	high-productivity wells	High-productivity wells possess most critical characteristics related to stimulation success, e.g. fast payout. The notion that little benefit comes from stimulating good wells is wrong.
Nnanna et al., 2005, 2009	Niger Delta, Nigeria	formation damage identification	Identification of damage radius and its components can help in choosing right candidates for acid stimulation.
Sinson et al., 1988	theoretical	constrained non-linear optimization	For stimulation economics optimization, an objective function is formulated to reflect the relationship between reservoir and well characteristics, treatment type and design.

Other Relevant Works

Hashemi et al., 2012; Zoveidavianpoor et al., 2012b; Zoveidavianpoor and Gharibi, 2016 (fuzzy logic); Ugbenyen et al., 2011 (constrained non-linear optimization); Mohaghegh et al., 2001; Popa et al., 2005 (Artificial Neural Networks, ANNs); Afolabi et al., 2008; Sencenbaugh et al., 2001; Strong et al., 1997 (identifying sub-performing wells and analyzing sources of impairment); Moore and Ramakrishnan, 2006 (detailed analysis of well and reservoir characteristics and operator's field experience)

In this chapter, we apply correlation analysis to several stimulation datasets to verify a correlation between pre-stimulation oil rate and the stimulation incremental oil production, and to measure the strength of such correlation. We then use a field-scale reservoir simulation model to test the applicability and performance of this screening criterion.

Table 3.2 Selected publications supporting stimulation of good producers.

Reference	Observation/Conclusion
Ely et al., 2000	Best producers are often best candidates for stimulation; however, stimulation of such wells is performed reluctantly because of the risk of losing production from an excellent well.
Sencenbaugh et al., 2001	After re-stimulation of 110 wells, the need for re-stimulation of better producers was recognized and those producers were added to the list of potential candidates.
Moore and Ramakrishnan, 2006	In the past, candidate selection has focused on underperforming wells. This approach has yielded disappointing results. Eliminating the under-performing well is recommended as a candidate screening criterion.
Ugbenyen et al., 2011	Analytical models are applied to determine an optimal candidate selection strategy. Results show that the stimulation benefits are higher when pre-stimulation productions are higher.

3.2. Solution Method

A good producer is defined as a well that, when compared to other producers, has relatively higher oil/gas production rates. A good stimulation candidate is a well that, when compared to other producers, would deliver larger incremental oil/gas production if stimulated. These definitions are selected because of their simplicity and ease of use; they can be readily applied to various production datasets to identify good producers and good stimulation candidates without the need for in-depth well and reservoir characterization. While they do not consider the operational aspects of the stimulation jobs or the differences among various stimulation techniques, these definitions will deliver meaningful results, as discussed in the next section.

We quantify a good producer using average oil production rate in years prior to well stimulation. We further define two-year stimulation incremental oil production rate, Δq_{2y}, as,

$$\Delta q_{2y} = \frac{\Delta Q_{2y}}{\Delta \mathrm{t}} = \frac{Q_{+2y} - Q_{-2y}}{\Delta \mathrm{t}} \tag{3.1}$$

where Q_{-2y} and Q_{+2y} are the cumulative oil production in the two years preceding, and succeeding well stimulation. This is schematically shown in Figure 3.1. The value of the two-year incremental oil production quantifies the difference between stimulated and unstimulated well performance in terms of incremental oil production, and is used as a measure of stimulation potential or benefits; a good stimulation candidate is one with larger two-year incremental oil production. This definition provides a first-order estimation of the stimulation incremental oil production.

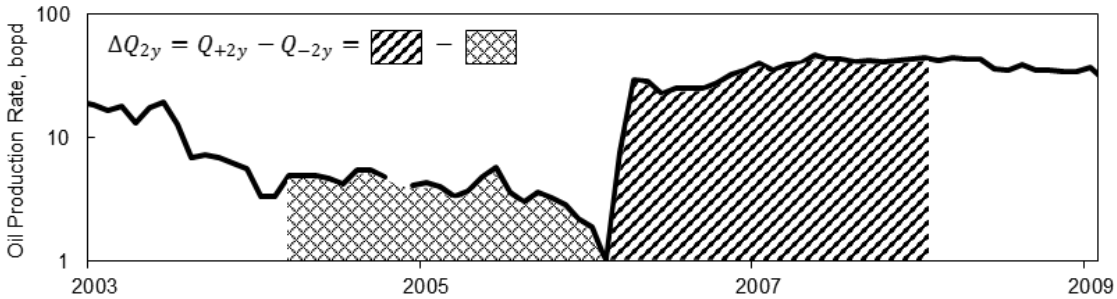

Figure 3.1 Two-year stimulation incremental oil production.

3.3. Results

3.3.1. Literature Data

The literature was surveyed for stimulation case studies to build a dataset for analysis. Eleven studies were found that reported before and after stimulation oil production rates. The works presented in these studies comprises a variety of stimulation methods (e.g. hydraulic fracturing, water-frac, acidizing, fracture acidizing, and microbial stimulation) and were performed in a variety of geological settings (e.g. Austin Chalk, unconsolidated sands in Venezuela, complex carbonate reservoirs). Figure 3.2 and Figure 3.3 show the incremental oil production rates as a function of pre-stimulation average oil rates for each of these studies and for the combined dataset. We use simple linear regression for our analysis which implies that the incremental oil rate depends only on the pre-stimulation oil rate. Furthermore, the strength of association between the two correlated parameters is measured using correlation coefficient, *r*, and the statistical significance of the observations is measured using *p*-value. The *p*-value indicates

the probability of obtaining by chance results equal or more extreme than what is observed if *no correlation* existed. The results show a positive correlation between the two parameters, both for the individual studies and for the combined dataset. For the combined dataset, r and *p*-value are calculated to be *0.8* and 10^{-20}, respectively. The somewhat high value of the correlation coefficient indicates that while pre-stimulation oil rate is a strong predictor for the response variable (incremental oil production), other parameters should be incorporated into the model to increase its accuracy and its predictive power. The extremely low value of the *p*-value indicates that the model is statistically significant. Therefore, pre-stimulation rate is in fact one of the predictors of the stimulation incremental oil production.

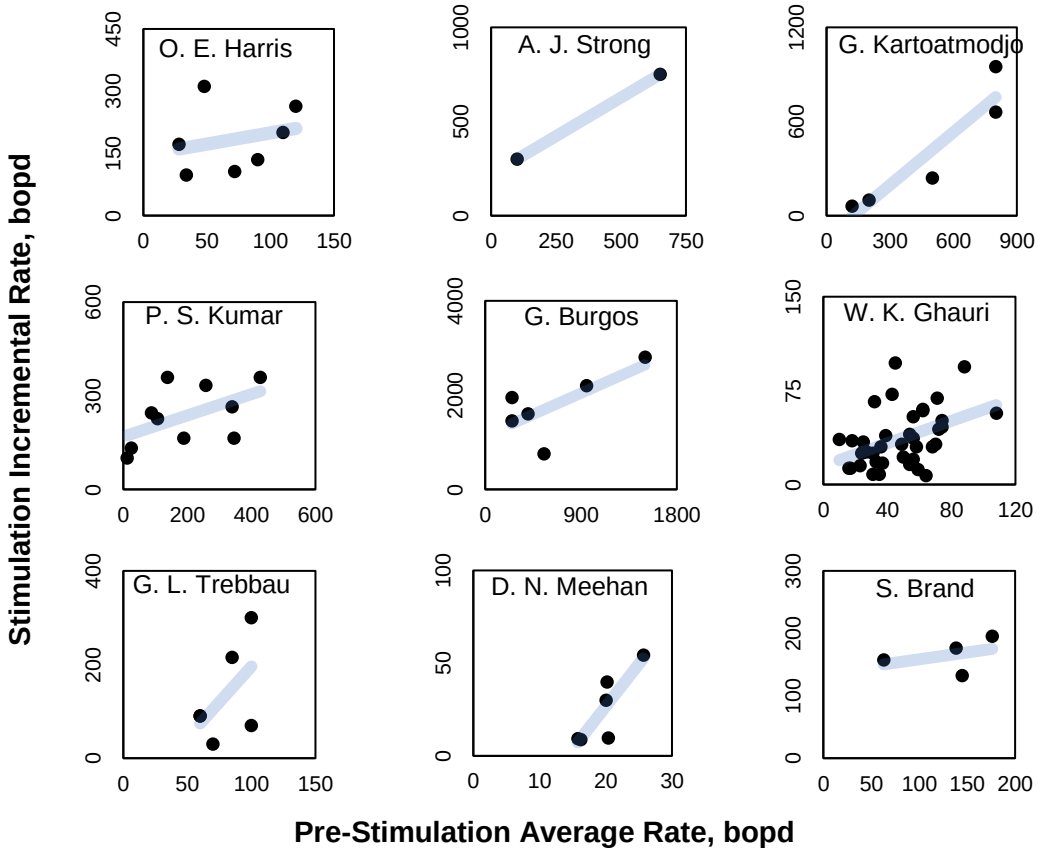

Figure 3.2 Incremental recovery from well stimulation reported by numerous studies (Afolabi et al., 2008; Brand, 2010; Burgos et al., 2005; Ghauri, 1960; Harris et al., 1966; Kartoatmodjo et al., 2007; Kumar et al., 2005; Meehan, 1995; Sencenbaugh et al., 2001; Strong et al., 1997; Trebbau et al., 1999).

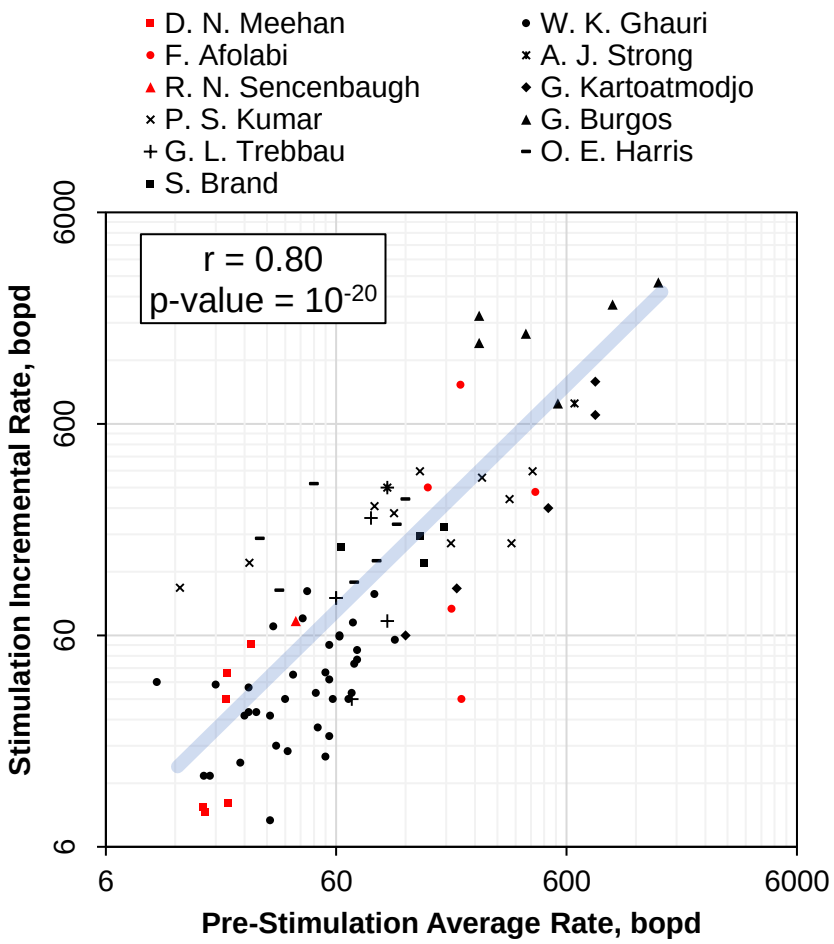

Figure 3.3 Combined plot of incremental recovery from well stimulation reported by numerous studies (Afolabi et al., 2008; Brand, 2010; Burgos et al., 2005; Ghauri, 1960; Harris et al., 1966; Kartoatmodjo et al., 2007; Kumar et al., 2005; Meehan, 1995; Sencenbaugh et al., 2001; Strong et al., 1997; Trebbau et al., 1999).

3.3.2. Analysis of Field Data

Located in the Northern Shelf of the Midland Basin, Slaughter field is 100,000-acre oil and gas producing area, producing primarily from structural and stratigraphic traps in the lower San Andres Dolomite at approximately 5,000 ft (Figure 3.4a). We analyze oil production and well stimulation data from four leases in this field, namely: East Mallet Unit, F. L. Woodley, Mallet Unit, and W. A. Coons (Figure 3.4b).

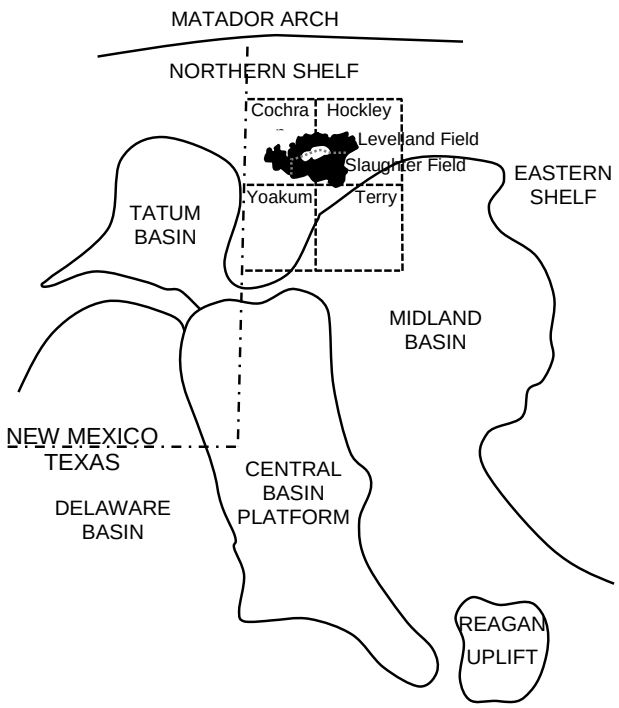

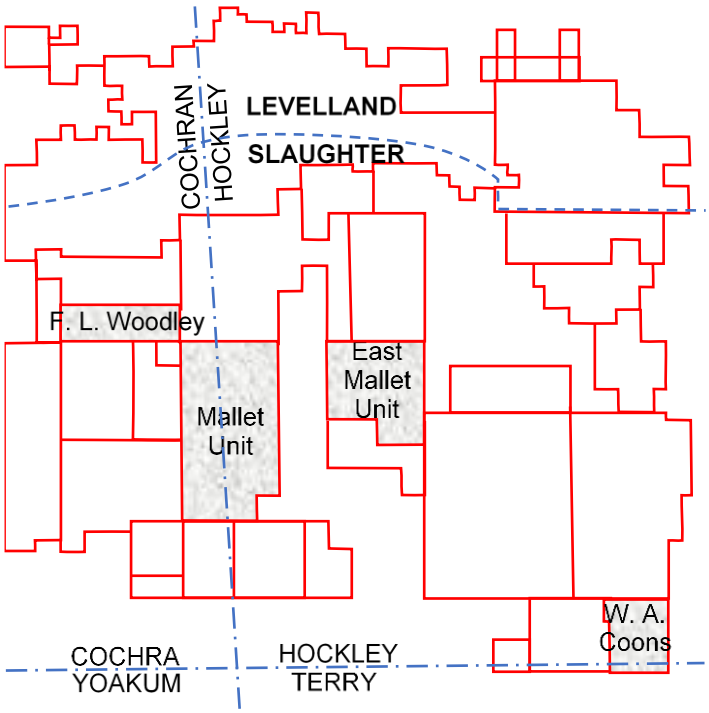

Figure 3.4 Locations of (a) Slaughter field (modified after Behm and Ebanks Jr., 1984, 1984) (top) and (b) the four leases investigated in this study (modified after Watson, 2005) (bottom).

All four leases share similar development history. Initial development started in late 1930s and early 1940s while waterflood and CO_2 flood were initiated in early 1960s and early 1990s, respectively. By 2004, all four leases had undergone extensive flooding and experienced declining oil production. Apache Corporation acquired these four leases and several other leases in this area in 2004. The declining oil production encouraged the operator to initiate multiple stimulation and infill drilling campaigns to rejuvenate oil production and improve field economics (Jamali and Ettehadtavakkol, 2017a). Matrix acidizing, acid frac, and reperforation are the major workover operations performed during these stimulation campaigns. Figure 3.5 is the rate-cum decline curve for Mallet Unit, indicating the positive effect of stimulation campaign in accelerating production and improving the estimated ultimate recovery.

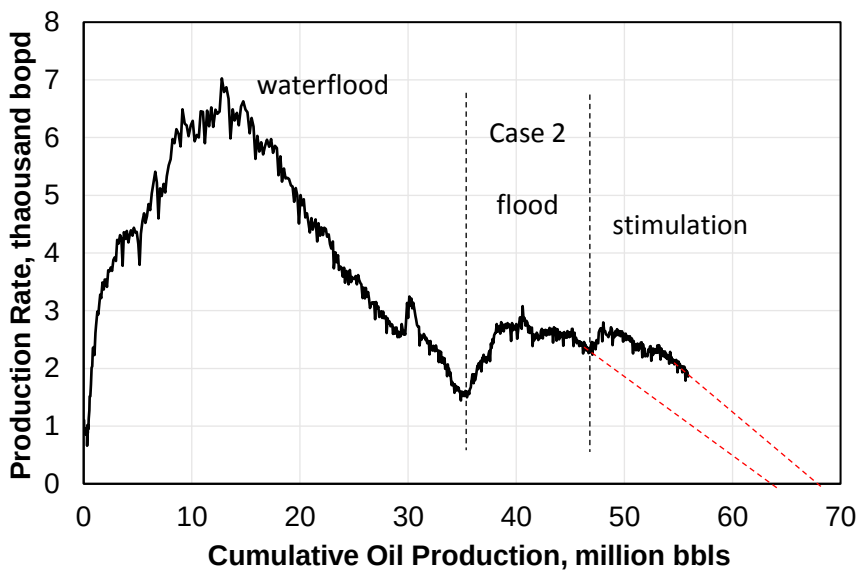

Figure 3.5 Stimulation campaign started in 2004 and slowed down production decline in Mallet Unit.

We use parameters defined earlier to analyze the well-by-well stimulation results. Figure 3.6 and Figure 3.7 show the two-year incremental oil production rates as a function of pre-stimulation average oil rates for each of the four leases and for the combined dataset. The results of regression analysis are summarized in Table 3.3. Correlation coefficients between 0.4 to 0.6 indicate that the predictor, i.e. pre-stimulation rate,

is not the only factor determining the response variable. In other words, for more accurate prediction of the response variables, other parameters such as reservoir characteristics and development history, stimulation design and implementation, etc. should be accounted for. Furthermore, *p*-values may be used to determine the statistical significance of the results. Most of the calculated *p*-values fall below a 0.05 threshold, indicating that the changes in the predictor are well-associated with changes in the response variable.

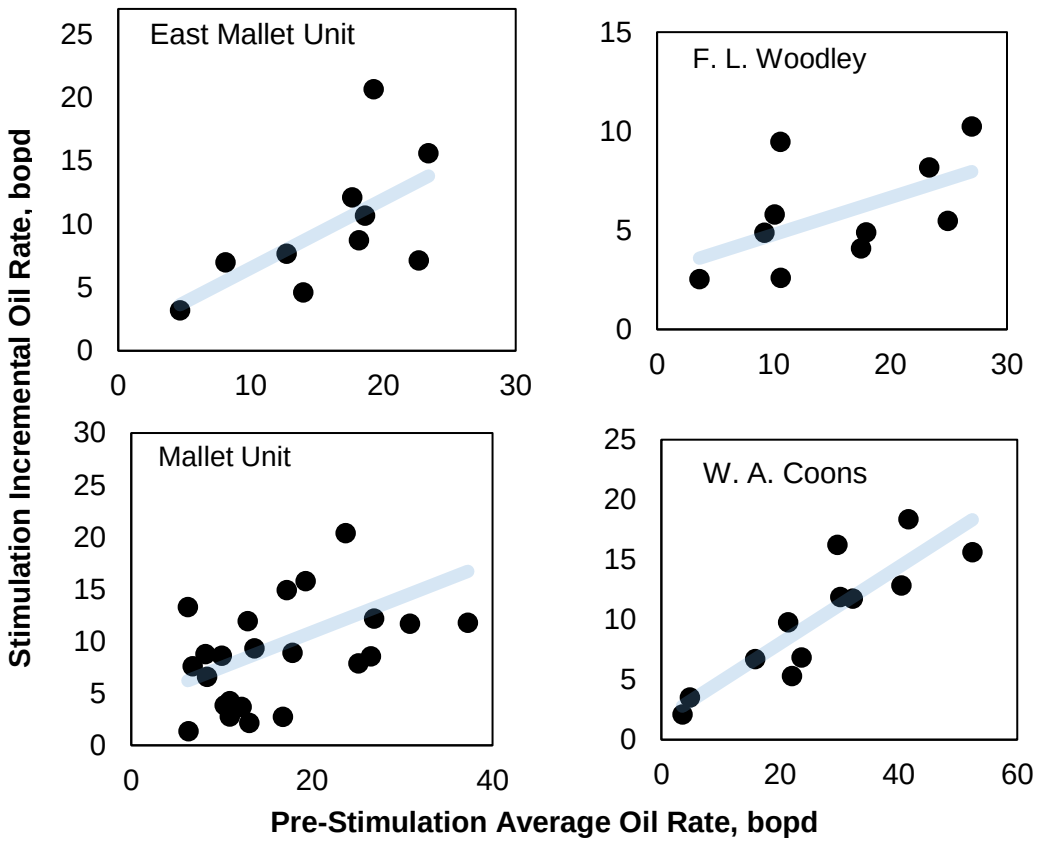

Figure 3.6 Stimulation incremental oil recovery for the four leases of the Slaughter field.

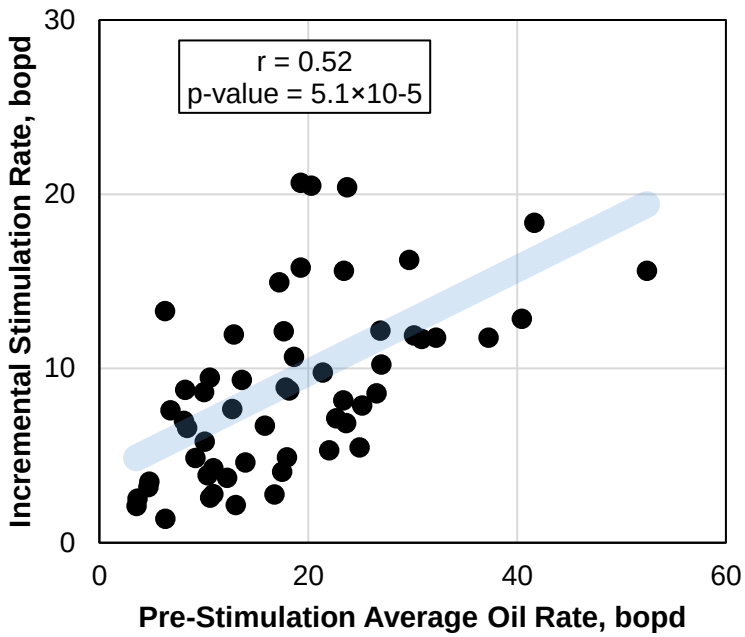

Figure 3.7 Combined plot of stimulation incremental oil recovery for the four leases of the Slaughter field.

Table 3.3 Results of regression analysis for Mallet Unite, East Mallet Unit, W. A. Coons, and F. L. Woodley leases in the Slaughter field.

Lease	Number of observations	Correlation coefficient, r	p-value
East Mallet Unit	10	0.6247	0.0485
F. L. Woodley	10	0.5474	0.1015
Mallet Unit	23	0.4215	0.0402
W. A. Coons	12	0.8805	0.0002
Combined	55	0.5181	0.000051

Note that the Slaughter field is a mature oil field with high in-fill drilling, workover, and EOR activities. Therefore, both correlated parameters are continuously affected by workover failure, errors in production data, ongoing water and CO_2 floods, and other factors. One way to minimize such bias in analysis is to use spatial grouping of producers. In this technique, producers are divided into several groups based on their spatial

proximity and the average values of the two parameters are calculated for each region. Figure 3.8 shows the results of spatial grouping for Mallet Unit. The lease is arbitrarily divided into 8 groups, each with 2 to 4 producers (Figure 3.8a). The average values of pre-stimulation oil and two-year incremental oil rate for each group are plotted in (Figure 3.8b). As a result of applying the spatial grouping method, the correlation parameter increased to 0.85 and the *p*-value reduced 0.0081.

3.4. Application to Stimulation Well Screening

Reservoir Simulation Study. A field-scale 3D reservoir simulation model is developed to test the applicability of our hypothesis and to evaluate its effectiveness as a stimulation well screening criterion. The reservoir simulation model represents a layered carbonate reservoir comprising two adjacent anticlines with an approximate thickness of 150 ft. All the major reservoir properties, such as the permeability and porosity distribution, relative permeability and capillary pressure curves, and fluid properties, are adopted from the published data as a proxy for Permian Basin carbonate reservoirs and incorporated in the model using the proper procedures (Ettehadtavakkol et al., 2014a). Major reservoir properties are summarized in Table 3.4. The next section presents a complete description of the geological model, rock, and fluid properties.

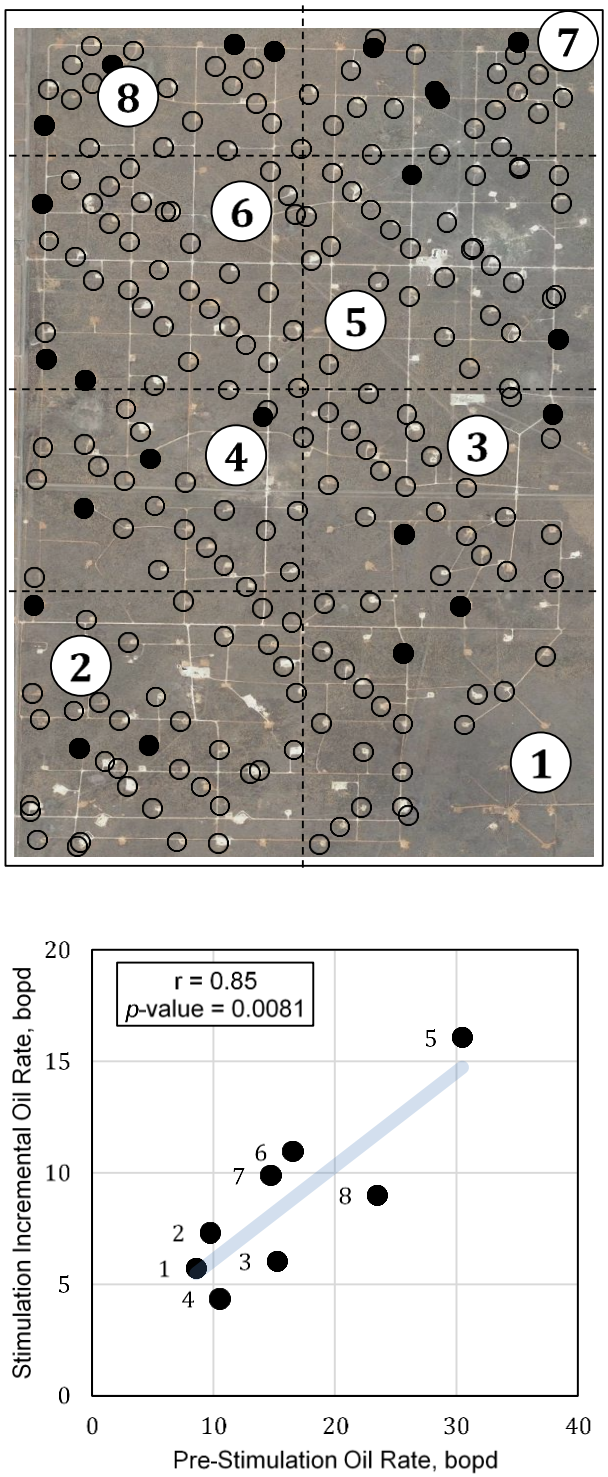

Figure 3.8 Results of spatial grouping for Mallet Unit, (a) grouping map (○: unstimulated, ●: stimulated), (top) and (b) stimulation response for each region (bottom) (pre-stimulation and incremental oil rates are average values for each region.)

Table 3.4 Reservoir model description for the anticlinal model used to evaluate the proposed candidate selection scheme

Dimension	8500×11500×150 ft
Average porosity	0.12
Average horizontal permeability	17 md
Vertical permeability	$0.1 \times k_h$
Temperature	120 °F
Depth	6000 ft
Initial reservoir pressure	3000 psi
Grid Type	Corner point
Number of gridblocks	84×120×15
Dimension of gridblocks	100×95×10 ft
Initial oil in saturation	80%
Total number of wells	130

3.5. Reservoir Simulation Model

The reservoir simulation model represents a layered carbonate reservoir and is built based on appropriate data compilations as follows:

1. The reservoir geological structure comprises two adjacent anticlinal domes with an average thickness of 150 ft (Figure 3.9).

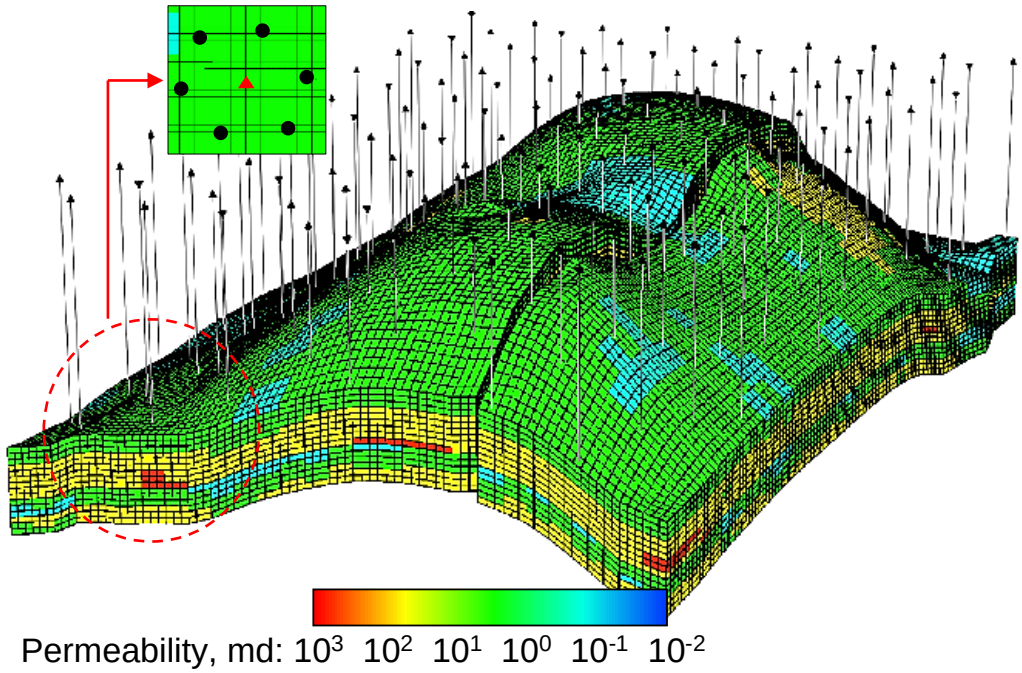

Figure 3.9 Well locations and permeability map of the reservoir simulation model.

2. The reservoir comprises 75% intermediate-wet and 25% water-wet rocks. It is characterized by low-to-moderate permeability, high permeability contrast between the layers, and high degree of heterogeneity within each layer. The heterogeneity is accounted for using a high value for the Dykstra-Parsons coefficient of 0.9. The average horizontal permeability for each layer is presented in Figure 3.10. A vertical to horizontal permeability ratio of 0.1 is used to calculate vertical permeability.

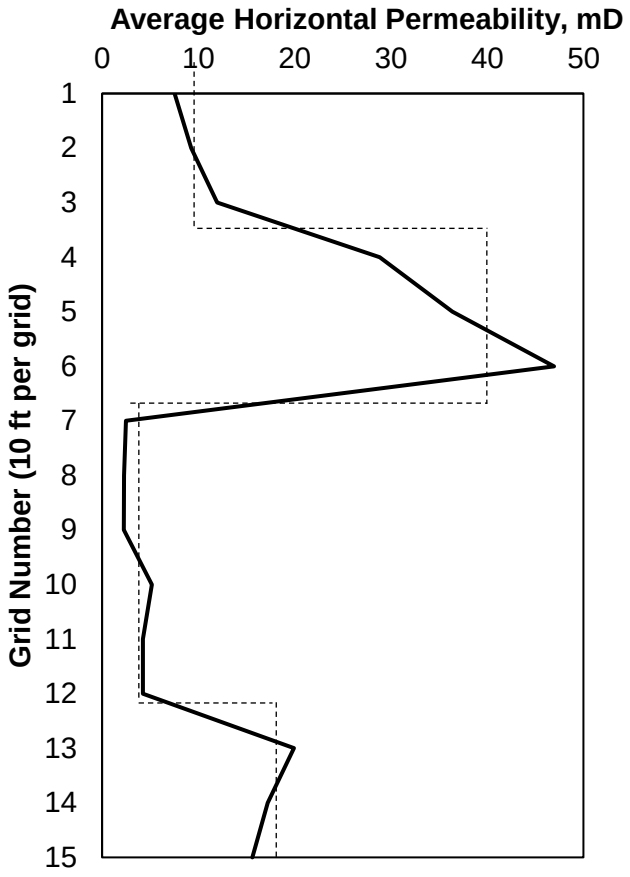

Figure 3.10 Average horizontal permeability of each layer. The low, medium, and high sequence of permeabilities represent different depositional regimes throughout geologic time.

3. The relative permeabilities for the intermediate-wet and the water-wet rock are presented in Figure 3.11.

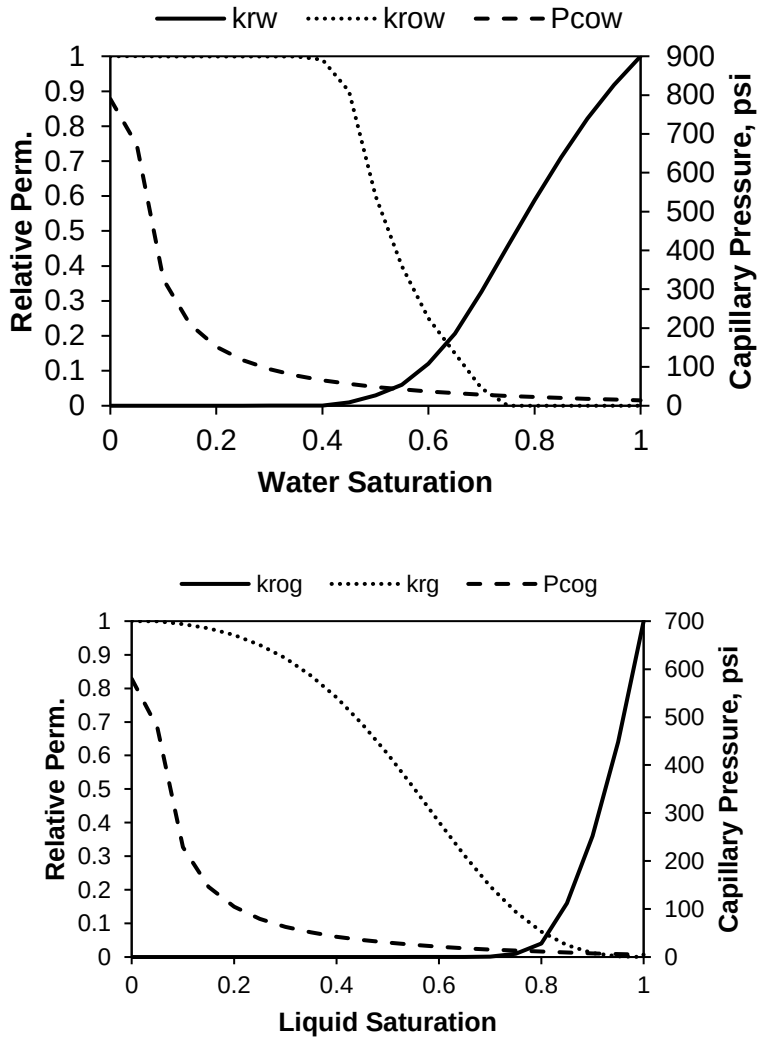

Figure 3.11 Relative permeability curves for (a) water-wet oil-water system (top), (b) water-wet gas-liquid system (second from top), (c) intermediate-wet oil-water system (second from bottom), and (d) intermediate-wet gas-liquid system (bottom).

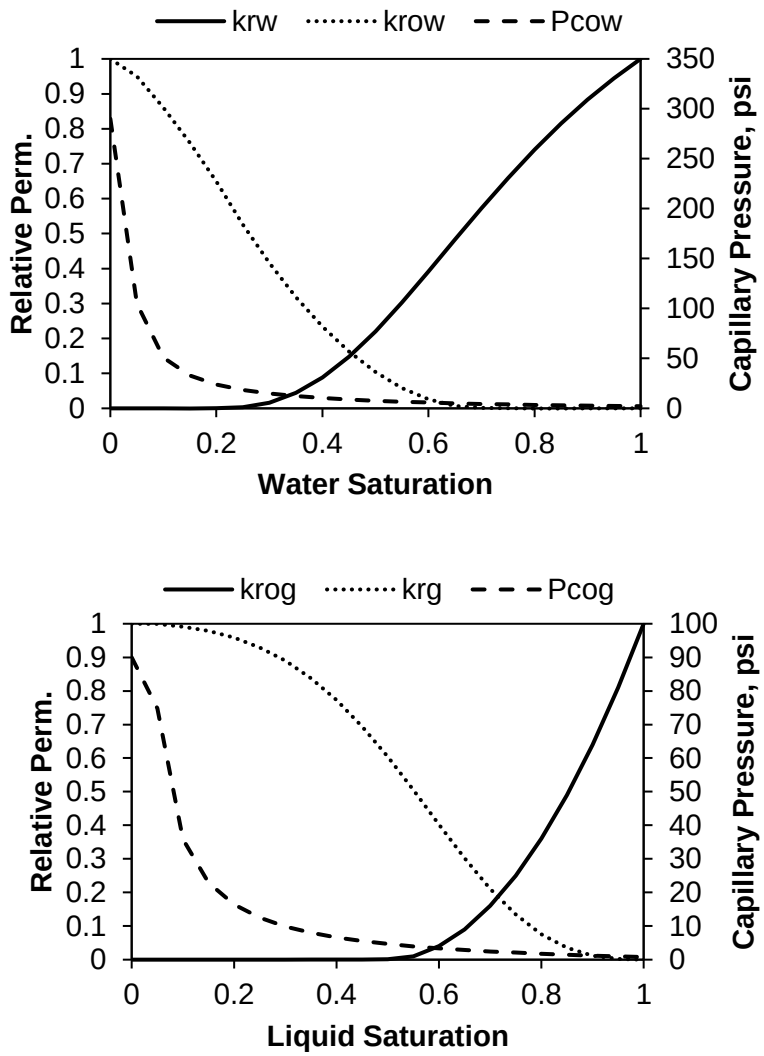

Figure 3.11 Relative permeability curves for (a) water-wet oil-water system (top), (b) water-wet gas-liquid system (second from top), (c) intermediate-wet oil-water system (second from bottom), and (d) intermediate-wet gas-liquid system (bottom).

4. The following porosity-permeability correlations are assigned to the two dominant rock types with porosity in fraction and permeability in millidarcy:

$$k = 2 \times 10^6 \Phi^{4.8} \tag{3.2}$$

$$k = 5 \times 10^6 \Phi^{7.1} \tag{3.3}$$

5. The fluid compositions correspond to Sacroc Unit in Kelly-Snyder field as summarized in Table 3.5. These compositions are used to generate black oil PVT tables using Computer Modeling Group's phase behavior and fluid property program (CMG WinProp).

Component	Reservoir, %	Injected Gas, %
CO_2	0.32	100
N_2	0.83	0
CH_4	28.65	0
C_2H_6	11.29	0
C_3H_8	12.39	0
IC_4	1.36	0
NC_4	6.46	0
IC_5	1.98	0
NC_5	2.51	0
FC_6	4.06	0
C_{7+}	30.15	0

Table 3.5 Reservoir and injected gas fluid composition (Ettehadtavakkol, 2013).

3.6. Results

An important consideration in this analysis is incorporating a representative field development history that captures the complexities encountered in development of an actual oil field. The field development history comprises the following six stages:

1. Primary development under solution gas drive for 25 years with two drilling campaigns at t = 0 and t = 10 years.
2. Peripheral water injection introduced at t = 25 years.
3. Line drive waterflood introduced at t = 30 years converted later to inverted five-spot.
4. Infill drilling campaign initiated at t = 40 years to update the injection pattern to inverted seven-spot.
5. Solvent injection started at t = 50 years and lasted for 10 years.

6. Stimulation campaign initiated at t = 60 years.

During the drilling campaigns, approximately one well is drilled each month and completed through all layers. The total number of active injectors and producers prior to initiation of the stimulation campaign are 44 and 86, respectively, resulting in a field-wide 25-acre well spacing. Producers with a water cut greater than 99% are abandoned. Geological structure, layering, and distribution of horizontal permeability is shown in Figure 3.9 along with well locations at t = 60 years.

Near wellbore damage is accounted for using an effective radial skin factor which is eliminated or reduced after stimulation. The field's stimulated and unstimulated oil production performances are shown in Figure 3.12. It is desirable to determine producers with the highest stimulation potential solely from oil production data. Three scenarios are considered: (1) "High Pre-Stim" in which better producers are considered better stimulation candidates, (2) "Random" in which wells are ranked randomly, and (3) "Low Pre-Stim" in which worse producers are considered better stimulation candidates. For comparison, two additional scenarios are defined in which *perfect information* is available: (1) "Best Candidates" and (2) "Worst Candidates". Perfect information refers to the cases where the true ranking of stimulation candidates is known from comparing the stimulated and unstimulated performances.

Figure 3.13a shows the normalized sum of incremental rates as a function of the fraction of wells stimulated. This is calculated by first ranking the wells for each method and then adding up their stimulation incremental oil rates. The sum is normalized with respect to the total incremental oil rate from stimulation of all wells. A concave down plot indicates an improved candidate selection method over the Random selection scenario while a concave up plot represents the opposite. The High Pre-Stim scenario has a great advantage over Random scenario. Most importantly, selecting wells based on the worst pre-stimulation rates, i.e. Low Pre-Stim scenario, which is a common industry practice, provides the worst performance. For the top half of the stimulation candidates, a bar plot of normalized sum of stimulation rates are presented in Figure 3.13b. While Best Candidates ranking scheme can detect wells with 65% of the total incremental oil

potential from the stimulation of all wells, the High Pre-Stim scheme detects wells which with 62% of the total incremental oil production.

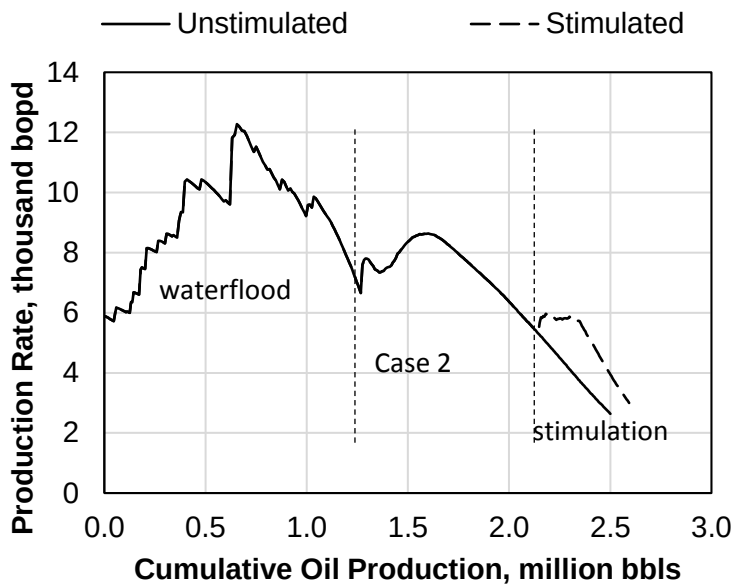

Figure 3.12 Post waterflood stimulated and unstimulated oil production performance for the reservoir model.

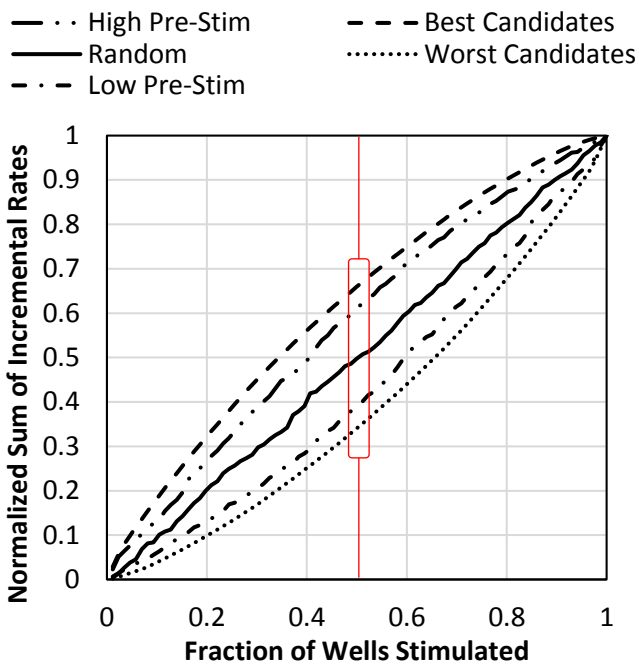

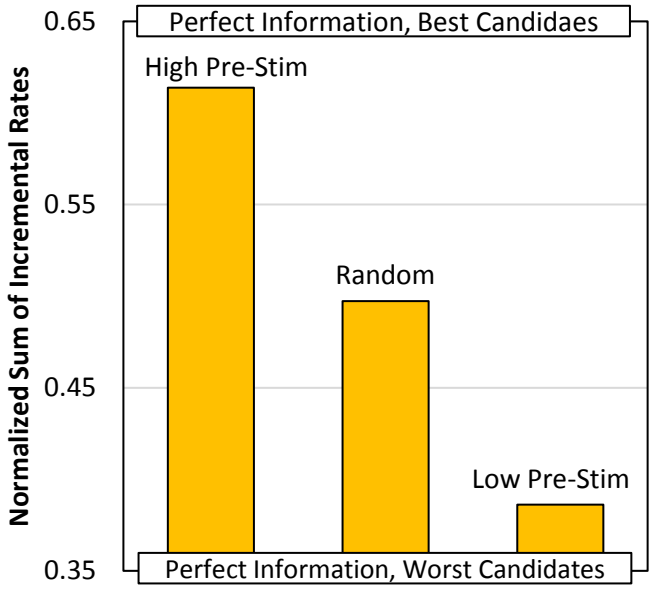

Figure 3.13 Performance of various candidate selection schemes (a) as a function of the fraction of wells stimulated (top), and (b) when half of producers are stimulated (bottom).

3.7. Discussion

The method presented in this work has several important advantages: (1) it uses oil production rates which are frequently recorded and readily available; (2) the analysis requires minimal computational resources; and (3) the method can be used before or after applying other candidate selection methods to further narrow down the list of candidates. It is important to note that stimulation of good producers has an inherent risk of losing a good well due to a failed stimulation job (e.g. fracing below the oil-water contact). This may dissuade operators from stimulating highly productive wells. The presented comparisons show that a risk-averse approach towards candidate selection will significantly reduce workover benefits. Therefore, in the practical applications, it is recommended that both the operator concern and the potential benefit of selecting the best wells are considered. Especially when considering large stimulation campaigns, the conclusions of this study may be used to ensure that resources are properly allocated among competing candidate wells.

CHAPTER IV

CO_2 ENHANCED OIL RECOVERY IN THE RESIDUAL OIL ZONE[3]

Residual Oil Zones (ROZs) are formed as the result of secondary tectonic activities which trigger extensive oil remobilization after the primary petroleum migration. The ROZs are attractive targets for CO_2 Enhanced Oil Recovery (CO_2-EOR) and storage: first, because in many cases, the thickness of the ROZ ensures an overall recoverable volume of oil comparable to that of the Main Pay Zone (MPZ) and second, because the ROZ has favorable containment and capacity for large-scale and long-term EOR-storage projects.

This study investigates one of the underlying theories of the ROZ formation, called the Altered Hydrodynamic Flow Fields (AHFF). The impact of the AHFF process on the formation of ROZs is specifically investigated using a field-scale simulation model for a Permian Basin San Andres reservoir. The simulation model is tuned and verified by validating the ROZ's characteristics, such as the thickness of the ROZ, the shape of the saturation profile, and the tilt of the OWC. The tuned Permian Basin San Andres reservoir model is used to simulate the primary recovery and the secondary waterflooding phases in the MPZ. Depending on the CO_2 availability and ROZ development strategy, six different development scenarios are specified beyond the waterflooding phase. The corresponding simulations are performed to find the optimum EOR-storage strategies for the MPZ-ROZ through the extensive comparison of key performance parameters, including the cumulative oil recovery, CO_2 storage and net CO_2 utilization.

The results confirm the technical viability of CO_2-EOR and storage in the ROZ. The most favorable expansion strategy in terms of oil production and CO_2 storage is the simultaneous development of the MPZ and the ROZ from the beginning of the EOR-

[3] Parts of this chapter are published in:
Jamali, A., Ettehadtavakkol, A., 2017b. CO_2 storage in Residual Oil Zones: Field-scale modeling and assessment. International Journal of Greenhouse Gas Control 56, 102–115. doi:10.1016/j.ijggc.2016.10.005

storage process. Most importantly, the study demonstrates that the volume of the utilized CO_2 has a substantial effect on the success of the EOR-storage. While other expansion strategies such as sequential development also provide reasonable oil production response and CO_2 storage potential, early project expansion into the ROZ without sufficient investment in CO_2 resources is shown to be detrimental to the economics of the project. Finally, several important technical considerations for CO_2 storage are qualitatively discussed, including assessment of the ROZ storage capacity, saltwater disposal requirements, and reduced risk of CO_2 leakage in the ROZ.

4.1. Problem Definition

CO_2 Enhanced Oil Recovery (CO_2-EOR) is a widely accepted EOR method that has been practiced for more than 50 years (Chapel et al., 1999; Gozalpour et al., 2005; Ren et al., 2015). This technique serves a twofold purpose. On one hand, large amounts of residual oil that are left behind during the conventional recovery processes can be targeted by CO_2-EOR (Lake, 2010; Thomas, 2008). On the other hand, strong correlation have been shown to exist between climate change and the increased concentration of the greenhouse gasses, especially CO_2 (Crowley, 2000; Mitchell et al., 1995; Petit et al., 1999). CO_2-EOR is one of the geologic options for CO_2 sequestration as an attempt to mitigate the problem of climate change in the medium- and long-term (Bachu, 2003; Herzog et al., 1997; Lackner, 2003).

As a widely accepted option, CO_2 sequestration through CO_2-EOR can help minimize storage costs by using the substantial existing infrastructure in the oil and gas industry, and benefiting from the incremental oil production revenue which offsets the CO_2 capture costs (Ettehadtavakkol et al., 2014b; Hill et al., 2013; Metz et al., 2005). While developing storage options for CO_2 sequestration remains a challenge, a new option for CO_2-EOR and storage, best known as Residual Oil Zone (ROZ), has recently drawn much attention (Hill et al., 2013; Melzer, 2006). This option is mainly investigated in the Texas Permian Basin because of the region's ever-increasing number of enhanced oil recovery projects, particularly for mature oil fields. Revitalizing the performance of mature fields requires novel and economically-viable methods, as well as

proper reservoir management strategies (Babadagli, 2007; Manrique et al., 2013). While such strategies are widely sought after, considerable volumes of oil in the ROZ are left unrecovered or even unnoticed and should be considered as the target of alternative development options (Melzer, 2006).

A Residual Oil Zone (ROZ) is defined as a considerably thick column of oil at residual or near-residual oil saturation to water, technically recoverable only through the application of unconventional methods. The documented examples of ROZs are typically observed below the producing Oil Water Contact (OWC) of the Main Pay Zone (MPZ) (Melzer, 2006). The reported MPZ-ROZ reservoirs are accompanied by a tilted OWC which is the primary indirect indication of the presence of ROZs (West, 2014). This type of ROZ is widely known as a Brownfield ROZ and is mainly recoverable through solvent injection methods. Existence of ROZs with effectively no MPZ is also plausible and has been documented (Gratton and LeMay, 1969). This type of ROZ is referred to as a Greenfield ROZ and is currently under investigation and development using methods such as Depressuring the Upper ROZ (DUROZ) (Melzer, 2016).

The theory of oil migration under hydrostatic capillary-gravity equilibrium can explain neither the presence nor the characteristics of tilted OWCs. The theory of oil entrapment under hydrodynamic conditions provides a better explanation for tilted OWCs. This theory was first introduced by Hubbert (1954) and later discussed by other researchers (Brown, 2001; Dahlberg, 1995; Dennis et al., 2000; Hiss, 1980; Lindsay, 1998), and states that lateral pressure variations may exist during the migration of hydrocarbons. This pressure variation is introduced by elevated outcrops as an indirect result of tectonic activities such as regional tilting of a basin. Under such hydrodynamic forces, regional groundwater movement occurs from a charge point in a higher outcrop to a discharge point in a lower outcrop (higher to lower potential) (Figure 4.1). Examples of hydrodynamic effects are becoming collectively abundant in many international oil and gas fields, some of which are listed in Table 4.1. Related studies on these fields indicate that the hydrodynamic effects may properly justify the existence of such zones in regions like the Permian and Bighorn basins (Melzer, 2006; Peigui Yin et al., 2012).

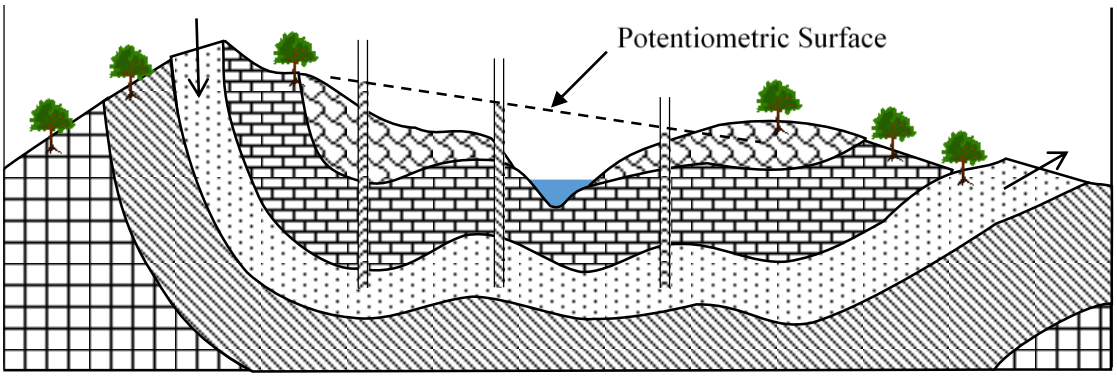

Figure 4.1 The concept of lateral pressure gradient or potentiometric surface. Regional flow of water through sand from higher to lower outcrop results in continuous drop in potential. This figure is adopted from Hubbert (1954).

In addition to hydrodynamics, other hypotheses on the origin of ROZs in the Permian Basin are discussed by Melzer (2006) and West (2014). These hypotheses mainly include breached and reformed seals and regional or local basin tilt both accompanied by buoyant displacement of oil by the underlying formation water; however, in light of several direct and indirect evidences in favor of the hydrodynamic effects and the failure of these two hypotheses in explaining the tilted OWCs, they concluded that hydrodynamics is the primary mechanism in the Permian Basin.

This chapter addresses the following aspects of the ROZ development for CO_2 storage: (1) the formation and characteristics of the ROZ as a result of hydrodynamic effects, (2) the potential of the ROZ for CO_2-EOR and storage, and (3) important considerations for CO_2 storage in the ROZ. We develop a reservoir simulation model that is tuned to represent Permian Basin San Andres reservoirs. Using this tuned model, we investigate six ROZ-MPZ development scenarios. In determining the foremost development strategy, a significant emphasis is given to both oil production performance and CO_2 storage capacity.

Table 4.1 Several basins with documented effect of hydrodynamics on oil and gas entrapment.

Location	Reference
San Juan Basin, New Mexico	McNeal, 1961
Permian Basin, Texas	McNeal, 1965
Indian Basin gas field, New Mexico	Hubbert, 1967
Maracaibo Basin, Venezuela	Hubbert, 1967
Panhandle oil field, Texas Panhandle	Hubbert, 1967
Hugoton-Amarillo gas field, West OK & KS	Hubbert, 1967
North Sakhalin Basin, Russia	Ostistyy et al., 1967
Illizi Basin, Algeria	Chiarelli, 1978
Gulf Basin, Qatar	Wells, 1988
Big Horn Basin, Wyoming	Towler et al., 1992
Danish Central Graben, North Sea	Thomasen and Jacobsen, 1994
Williston Basin, North Dakota	Berg et al., 1994
Papuan Basin, Papua New Guinea	Eisenberg et al., 1994
Putumayo Basin, Colombia	Estrada and Mantilla, 2000
The North Sea	Dennis et al., 2000
Lublin Basin, Poland	Zawisza, 2006
Kutei Basin, Indonesia	Jauhari, 2012

4.2. Permian Basin San Andres Reservoir Model

Several ROZ instances have been observed in the Permian Basin. It is hypothesized that Late Tertiary tectonics triggered massive recharge of meteoric water into the subsurface of the Permian Basin (Lindsay, 1998). For the San Andres formation, this hypothesis is supported by direct and indirect evidence, including the presence of a lateral pressure gradient—also known as potentiometric gradient— tilted OWC, imbibition oil saturation profile, and several signs of interaction between oil and meteoric water (e.g. low salinity formation water, secondary dolomitization, biodegradation, evidence of anaerobic reducing bacteria, etc.) (West, 2014). Most importantly, the slope of OWC tilts corresponds to the field observations and to Hubbert's theoretical tilt formula

(Brown, 2001; Gratton and LeMay, 1969; Hubbert, 1954). Based on the available geologic and hydrologic information, documented OWC tilts, log-based data, and identification of ROZs in nearby fields, Koperna et al. (2013) predicted the presence of ROZs in more than 50 fields across the Permian Basin. Figure 4.2 summarizes those fields with potential, proved, or commercially developed ROZs in the Permian Basin. Several CO_2-EOR projects have been extended from the MPZ to the ROZ and are currently co-developing both zones.

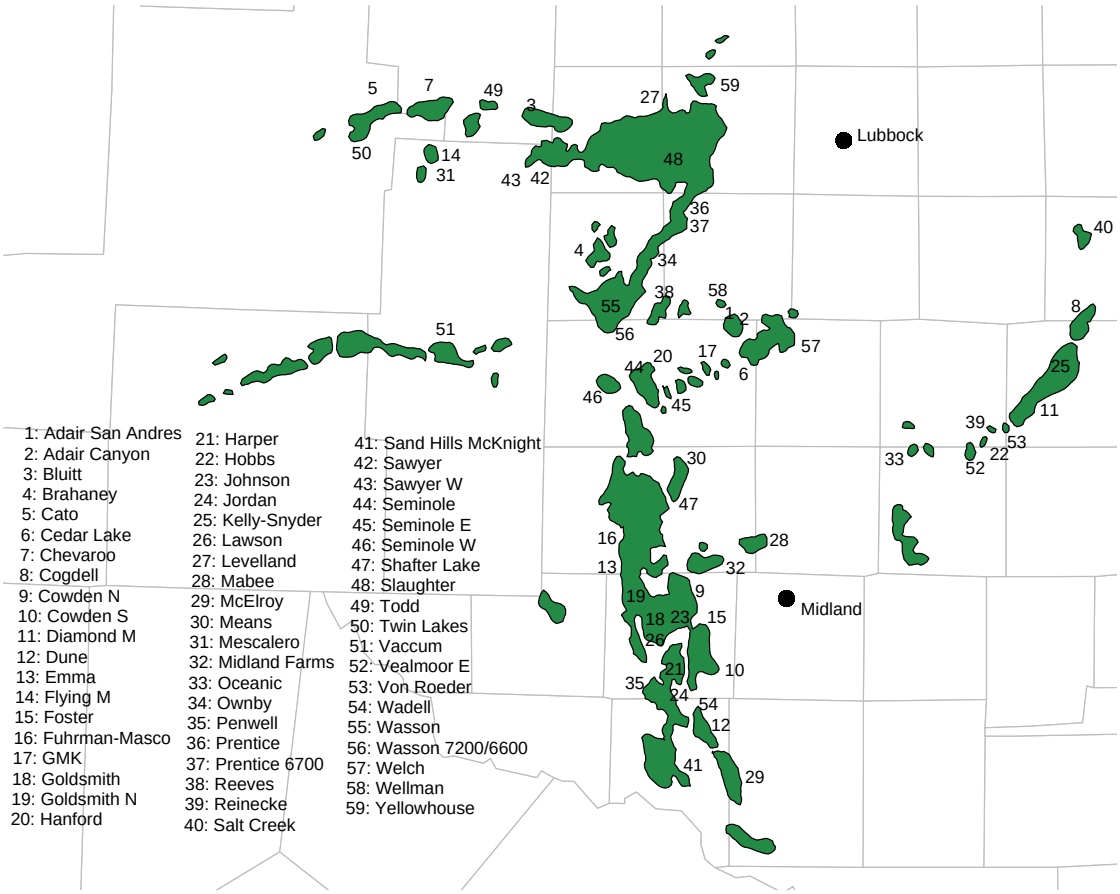

Figure 4.2 Location of San Andres, Grayburg, and Canyon & Cisco oil fields with proved (Cowden S, Goldsmith, Hanford, Kelly-Snyder, Means, Salt Creek, Seminole, Vacuum, Wasson) and/or predicted (others) ROZs. Data compiled from Koperna et al. (2013) and West (2014). Other map details are constructed based the maps presented in Ward et al. (1986).

The hydrodynamic effect is referred to as Altered Hydrodynamic Flow Fields (AHFF). The underground flow of water is triggered by the AHFF and can potentially

result in extensive remobilization of the existing oil over extremely long periods of time. This is an irreversible process (similar to waterflood) that leaves behind large volumes of oil in the swept zone at saturations near the residual oil saturation to water. The well-known hydrostatic capillary-gravity equilibrium is not applicable under these conditions. Instead, a new equilibrium takes place that is characterized by an elevated free water level, tilted OWC, and a potentially elongated transition zone with near residual oil saturation to water (Honarpour et al., 2010; Melzer, 2006). We refer to the new equilibrium conditions as the capillary-gravity-hydrodynamic equilibrium. An idealized diagram of oil distribution in a reservoir with ROZ is shown in Figure 4.3. The reservoir height is divided into three zones: MPZ, CTZ (Capillary Transition Zone), and ROZ. The MPZ is the uppermost interval confined between the top of the reservoir and the OWC. This zone has near zero water mobility and therefore, during the primary recovery will predominantly produce oil. The CTZ is the zone below the OWC in which water saturation increases from irreducible water saturation to unity. In the presence of the AHFF, a new CTZ is formed as a result of capillary imbibition where oil saturation gradually decreases from the MPZ oil saturation at the top to near-residual oil saturation at the bottom. The ROZ is a thick volume of reservoir rock containing near-residual saturation below the CTZ (Arps, 1964; Brown, 2001; Melzer, 2006; West, 2014). A tuned reservoir model should properly predict the oil saturation profile under the AHFF equilibrium conditions.

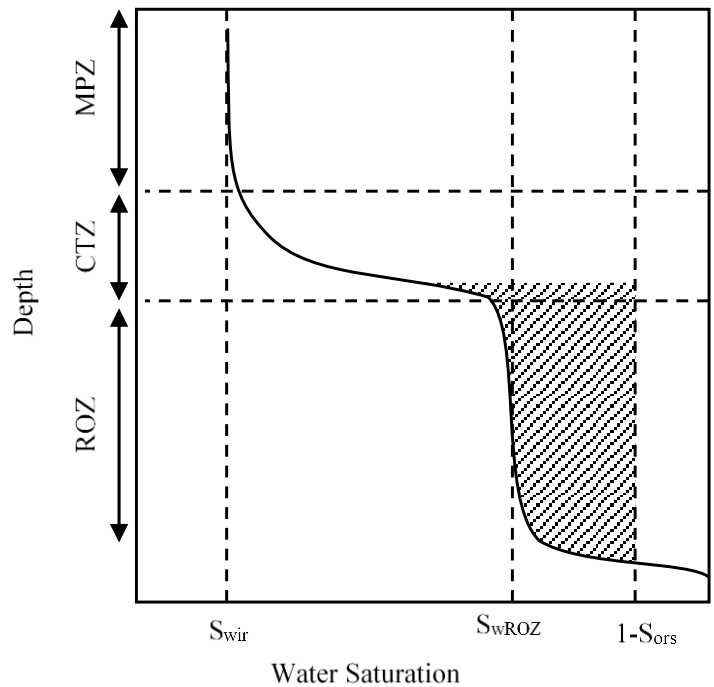

Figure 4.3 Idealized oil saturation profile under the capillary, gravitational and hydro-dynamic equilibrium. The average oil saturation in the ROZ is slightly greater than the residual oil saturation to waterflood. Recoverable ROZ trapped oil is shaded.

A reservoir simulation model is developed and tuned to verify the MPZ-ROZ development in the Permian Basin using the following steps:

1. The oil initially maintains a vertical capillary-gravity equilibrium with the underlying water and a small gas cap. The primary drive mechanism for the majority of the San Andres reservoirs is solution gas drive (*Selected oil & gas fields in West Texas*, 1982). A number of fields with confirmed ROZs under development, such as Wasson and Seminole, possess gas caps (Hsu et al., 1997; Wang et al., 1998).

2. The AHFF is introduced using an injector-producer well pair. These wells are far away from the boundaries of the area of study, which ensures that the local boundary effects will not influence the pressure and saturation distributions. The aquifer flow remains active for a long period of time. The in-

jector and the producer are active under constant and equal injection/production rate constraints. This constraint is set to a value that satisfies the required lateral pressure gradient.

3. The resulting saturation and pressure distribution of the AHFF model is supplied as the initial condition for quantifying the EOR-storage potential of the MPZ-ROZ reservoirs.

The reservoir model is developed using a black oil simulator. The reservoir dimensions are 10000 ft × 1000 ft × 600 ft. The reservoir grid is a 100 × 1 × 60 corner point grid system, with approximate grid dimensions of 100 ft × 1000 ft × 10 ft. The primary objective of this simulation is to tune the model and match the observed characteristics of ROZs in the Permian Basin. This requires a high vertical resolution and long simulation time to properly capture and match the vertical oil saturation distribution, the slope of the OWC, and the relative heights of the MPZ, CTZ, and ROZ. A 2D grid system is selected to achieve the desired vertical resolution and to enable the long simulation of the AHFF process (of the order of one hundred thousand years). A pseudo-miscible flood model is used after extensive tuning of the black oil model against the lab experimental data and compositional PVT models. Comparison of miscible flood simulators has shown excellent agreement between compositional and pseudo-miscible models when the reservoir pressure is maintained above the minimum miscibility pressure (Killough and Kossack, 1987; Todd and Longstaff, 1972).

All the major reservoir properties, such as the permeability and porosity distribution, relative permeability and capillary pressure curves, and fluid properties, are adopted from the published data for the San Andres formation and incorporated to the model using the proper procedures (Amaefule et al., 2013; Brown, 2001; Honarpour et al., 2010; Killough, 1976; Lucia, 2000; Pedersen et al., 2014; Treiber and Owens, 1972; Wang et al., 1998). The majority of the reservoir model data are from Seminole San Andres Unit (SSAU) because of the extensive availability of SSAU reservoir data in the literature; however, the model may be used as a proxy for all Permian Basin San Andres reservoirs. The geological structure, layering, and horizontal permeability distribution

are shown in Figure 4.4. A complete description of the model and its components is presented in the next section.

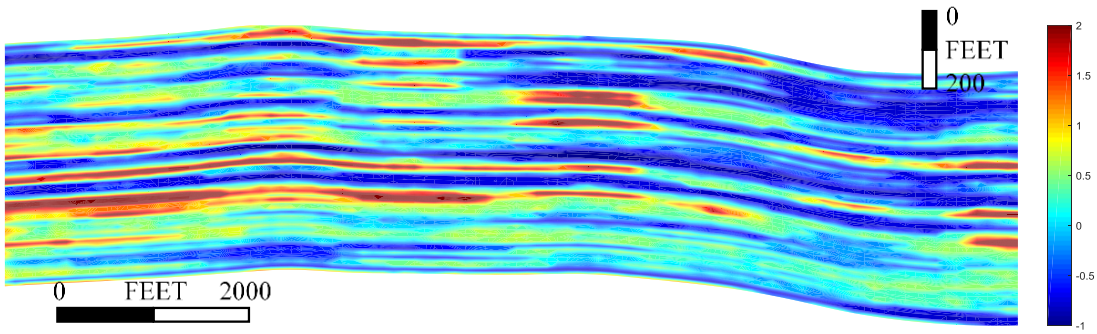

Figure 4.4 Logarithm of horizontal permeability with an average of 15 md. Model dimensions are 10000 ft × 600 ft. Data adapted from Wang et al. (1998).

4.3. Reservoir Model Description

The MPZ-ROZ model is developed based on an extensive data compilation for the San Andres formation, especially the Seminole Unit (SSAU). The Seminole Unit is specifically studied because the ROZ is commercially developed. The MPZ-ROZ model assumes that the MPZ is a vertical continuation of the ROZ. The data used for this model are compiled from the following sources:

1. The geological structure, layering, and horizontal permeability distribution are adopted from Wang et al. (1998) and shown in Figure 4.4.
2. The vertical permeability is generated based on the joint probability distribution of the horizontal-vertical permeability (Honarpour et al., 2010) and using the sample generation method for 2D discrete distributions (Ursell, 2012). This distribution is shown in Figure 4.5a.
3. The experimental permeability-porosity measurements of whole cores for SSAU (Honarpour et al., 2010) are analyzed with the hydraulic unit identification method (Amaefule et al., 2013). Three rock types were identified. Each rock type has a unique permeability-porosity joint distribution. These distributions are used to generate the reservoir porosity distribution as shown in Figure 4.5b.

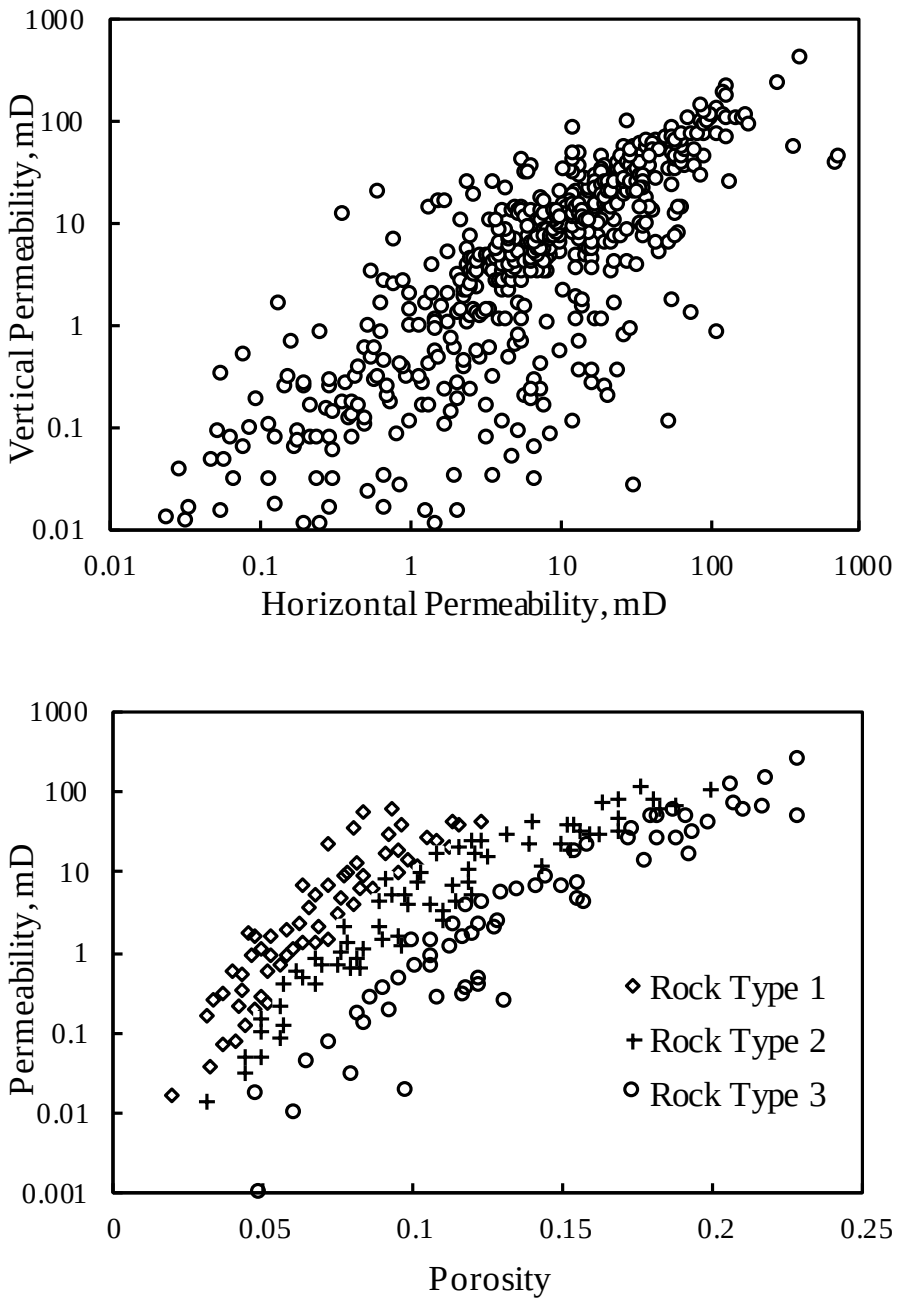

Figure 4.5 Major rock and rock-fluid properties of the MPZ-ROZ simulation model (a) Experimental data for vertical to horizontal permeability correlation (Honarpour et al., 2010) used to generate the joint probability distribution of vertical-horizontal permeability (top), and (b) Experimental permeability-porosity correlation (Honarpour et al., 2010) used to generate the joint distribution of permeability-porosity (bottom).

4. The relative permeability data are shown in Figure 4.6. The experimental core flood data (Honarpour et al., 2010) are fitted using the Corey-type relative permeability model (Corey, 1954):

$$k_{row}(S_w) = (1 - S_{wD})^{n_o} \tag{4.1}$$

$$k_{rw}(S_w) = k_{rw}^0 S_{wD}^{n_w} \tag{4.2}$$

$$S_{wD} = \frac{S_w - S_{wi}}{1 - S_{wi} - S_{orw}} \tag{4.3}$$

The corresponding fitting parameters are: $n_o = 3.2$, $n_w = 2.3$, $S_{wi} = 0.13$, $S_{orw} = 0.25$, $k^0_{rw} = 1$. There are two major processes modeled in this study: (1) the slow AHFF process in which capillary forces are dominant, and (2) the waterflood and miscible flood processes in which viscous forces are dominated. These two cases correspond to the two ends of the capillary number scale. Nguyen et al., (2006) showed that for high contact angles (which is the case for the intermediate wettability reservoir presented here), the relative permeability curves for a wide range of capillary numbers are fairly similar. Therefore, it is sufficient to use one set of relative permeability curves for modeling both processes.

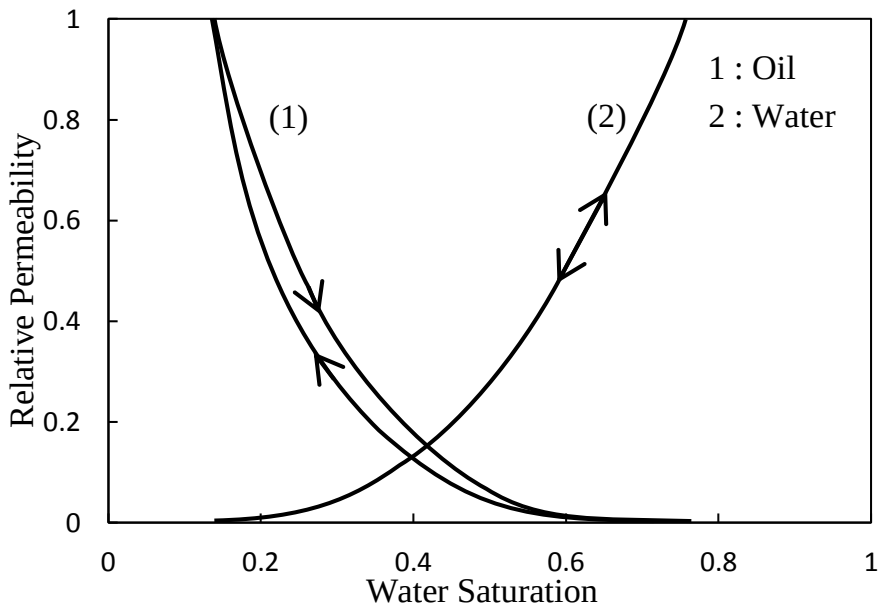

Figure 4.6 Major rock and rock-fluid properties of the MPZ-ROZ simulation model: Water-oil imbibition relative permeability curves (Honarpour et al., 2010)

5. Drainage capillary pressure curves are widely measured and accessible for San Andres formation; however, the imbibition curves are not frequently reported (Lucia, 2000). Honarpour et al. (2010) reported intermediate to oil-wet wettability for the ROZ region of the SAAU which may apply to other Permian Basin reservoirs in the absence of wettability data (Treiber and Owens, 1972). Capillary pressure curves are adapted from Killough (1976), and rescaled to match reported capillary pressure at initial water saturation for Permian Basin San Andres formation. Brown, 2001 reported capillary pressures in the order of tens of psi at initial water saturation for Willard Unit, Wasson Field in the Permian Basin. These data are used as a proxy for the Permian Basin San Andres formation. The capillary height curves are presented in Figure 4.7. Also, we use the capillary hysteresis model (Killough, 1976) to account for the saturation path dependence of the relative permeabilities during the alternate drainage and imbibition cycles.

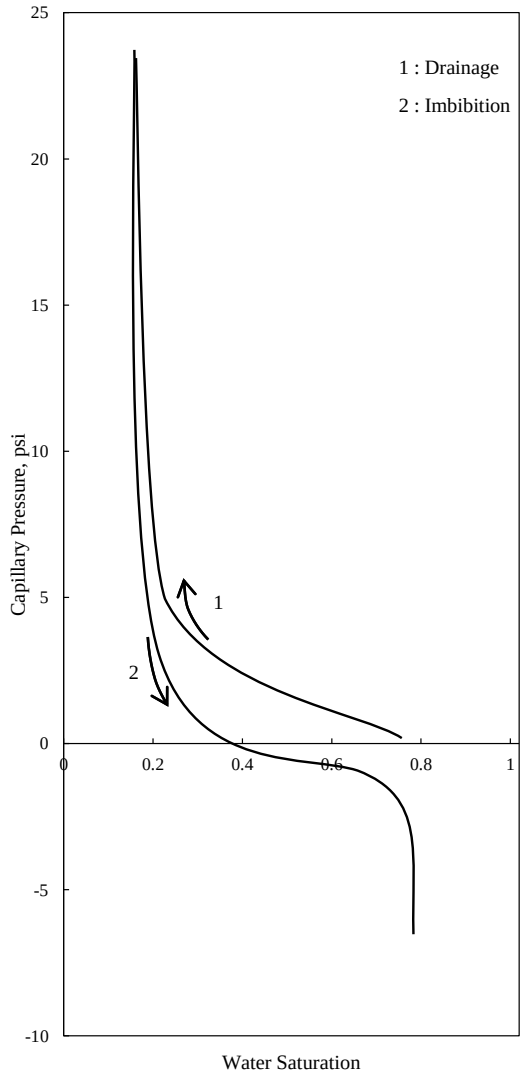

Figure 4.7 Major rock and rock-fluid properties of the MPZ-ROZ simulation model: Drainage and imbibition capillary pressure curves (Brown, 2001; Killough, 1976). Related concepts adopted from Abdallah et al. (2007)

6. The oil composition and properties are presented in Table 4.2. Regression method (Pedersen et al., 2014) is used to tune the corresponding PVT model with the reported experimental data (Honarpour et al., 2010). The mixing parameter, $\omega_{o,}CO_2$, is an indicator of the degree of CO_2-oil miscibility and depends on the pressure, temperature and oil composition. This predictions of the tuned PVT model are verified against the experimental slim tube tests (Honarpour et al., 2010) and computational multi contact miscibility test

(Pedersen et al., 2014). The minimum miscibility pressure (MMP) is approximately 1350 psi. Table 4.3 summarizes the PVT data of the MPZ-ROZ simulation model.

Table 4.2 MPZ and ROZ fluid composition (Honarpour et al., 2010). Oil biodegradation can affect reservoir oil attributes in several ways, including raising the oil viscosity and reducing the oil API gravity both resulting from significant com-position difference between MPZ and ROZ oil.

Component	**Mole fraction, original oil**	**Mole fraction, degraded oil**
N_2	0.51	0.02
CO_2	2.47	0.02
H_2S	1.96	0
C1	24.65	20.12
C2	9.1	9.04
C3	7.57	6.86
iC4-nC4	5.44	3.84
iC5-nC5	3.79	2.33
C6	3.54	2.82
C7+	40.97	54.95
MWC7+	224	252

Table 4.3 PVT data of the MPZ-ROZ simulation model based on the oil composition in Table 4.2. The bubble point pressure and minimum miscibility pressure are 1400 psi and 1350 psi respectively. These results consistently match the experimental data (Honarpour et al., 2010).

P	**R_s**	**B_o**	**B_g**	**B_o**	**μ_o**	**μ_g**	**μCO_2**	**ω_o,CO_2**
psi	scf/STB	RB/STB	RB/SCF	RB/STB	cP	cP	cP	
14.7	0.0	1.01	0.1907	0.193	2.33	0.009	0.016	0
200	139.3	1.09	0.0133	0.013	1.36	0.012	0.017	0
400	213.6	1.13	0.0064	0.006	1.16	0.012	0.017	0
600	276.0	1.16	0.0042	0.004	1.02	0.013	0.018	0
800	335.0	1.19	0.0030	0.002	0.92	0.013	0.019	0
1000	392.6	1.22	0.0024	0.002	0.83	0.014	0.021	0
1200	449.8	1.24	0.0019	0.001	0.76	0.014	0.031	0.3
1300	478.3	1.25	0.0018	0.001	0.73	0.015	0.051	0.5
1400	501.0	1.26	0.0017	0.001	0.71	0.015	0.058	1.0

7. Other major reservoir properties are summarized in Table 4.4.

Table 4.4 Major reservoir properties of the MPZ-ROZ simulation model (Honarpour et al., 2010)

Parameter	Units	Value
Average Porosity	—	0.13
Average Horizontal Permeability	mD	15
OWC Depth*	ft	5400
GOC Depth*	ft	4975
Oil Density, ST Conditions	lb_m/ft^3	49.9
Gas Density, ST Conditions	lb_m/ft^3	0.08
Reservoir Pressure, 5000 ft	psi	2000
Reservoir Temperature	°F	105
Residual Oil Saturation to Water	—	0.25
Residual Oil Saturation to CO_2	—	0.12

*prior to initiation of the hydrodynamics

4.4. Results and Discussion

The objectives of this section are (1) to simulate the formation of ROZ in a Permian Basin San Andres MPZ-ROZ reservoir and under AHFF, and (2) to determine the CO_2 storage capacity of the MPZ-ROZ reservoir under various development strategies.

4.4.1. ROZ History Matching and Model Verification

The AHFF is modeled as an injector-producer well pair operating under equal rate constraints. The average slope of the potentiometric surface for Seminole San Andres Unit (SSAU) is 7.5 feet per mile (McNeal, 1965) which corresponds to a lateral pressure gradient of 3.3 psi per mile. The rate constraints are changed until the required lateral pressure gradient is obtained. The resulting lateral pressure variations are shown in Figure 4.8. The injector flow rate corresponds to an underground flow velocity of 0.5 feet per year. The simulation is completed at 10^5 years when the average MPZ and ROZ gross thicknesses correspond to the field observations.

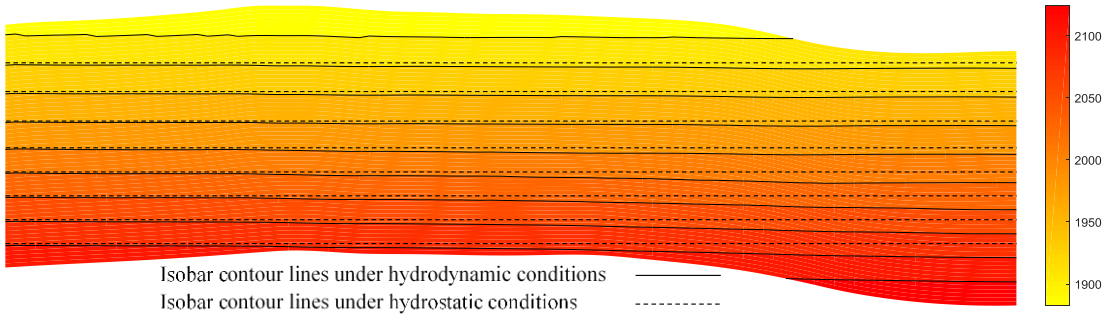

Figure 4.8 Effect of AHFF on lateral pressure variation. A potentiometric surface slope of 7.5 feet per mile corresponding to a lateral pressure gradient of 3.3 psi per mile is introduced to the system. The solid lines are the isobar contour lines under hydrodynamic conditions. The dashed lines are the isobar contour lines under hydrostatic condition and are shown only for comparison.

Figure 4.9 presents the fieldwide oil saturation distribution at 0.03×10^5, 0.50×10^5, and 1.00×10^5 years. The important observations follow:

1. The fieldwide OWC tilt remains fairly constant at the value of 30 feet per mile after 3,000 years. The stabilized tilt is not time-dependent and is consistent with the field observations (Melzer et al., 2006).

2. A noticeable change in the tilt of the OWC is observed on the east side of the reservoir. This is because the flow of water is locally affected by permeability, layering, geological structure, and other flow restrictions. Figure 4.4 shows a low permeability region in the east side of the reservoir and a change in the available flow area due to the down dipping of the reservoir structure. Other works also reported a correlation between the local tilt of the OWC and the reservoir characteristics (Brown, 2001; Dennis et al., 2000).

3. The OWC tilt can be confirmed using the Hubbert tilt formula:

$$\frac{dz}{dx} = \frac{\rho_w}{\rho_w - \rho_o}\frac{dh_w}{dx} \tag{4.4}$$

where z and h_w are the elevation of the points on the OWC and the water head, respectively. This formula expresses that the tilt of the OWC is equal to the slope of the potentiometric surface times an amplification factor. This amplification factor is the ratio of the water density to the difference between

the water and oil densities. Therefore, dz/dx represents the change in the elevation of the points on the OWC in horizontal direction or the tilt of the OWC. Assuming an oil density of 46 pounds per cubic foot (Honarpour et al., 2010) the amplification factor is calculated to be 3.8. The slope of the potentiometric surface can be approximated from the regional San Andres potentiometric map (McNeal 1965). According to this map, the slope of the potentiometric surface lies within the range of 5 to 10 feet per mile, resulting in a tilt range of 19 to 38 feet per mile which is in good agreement with the simulation results of 30 feet per mile.

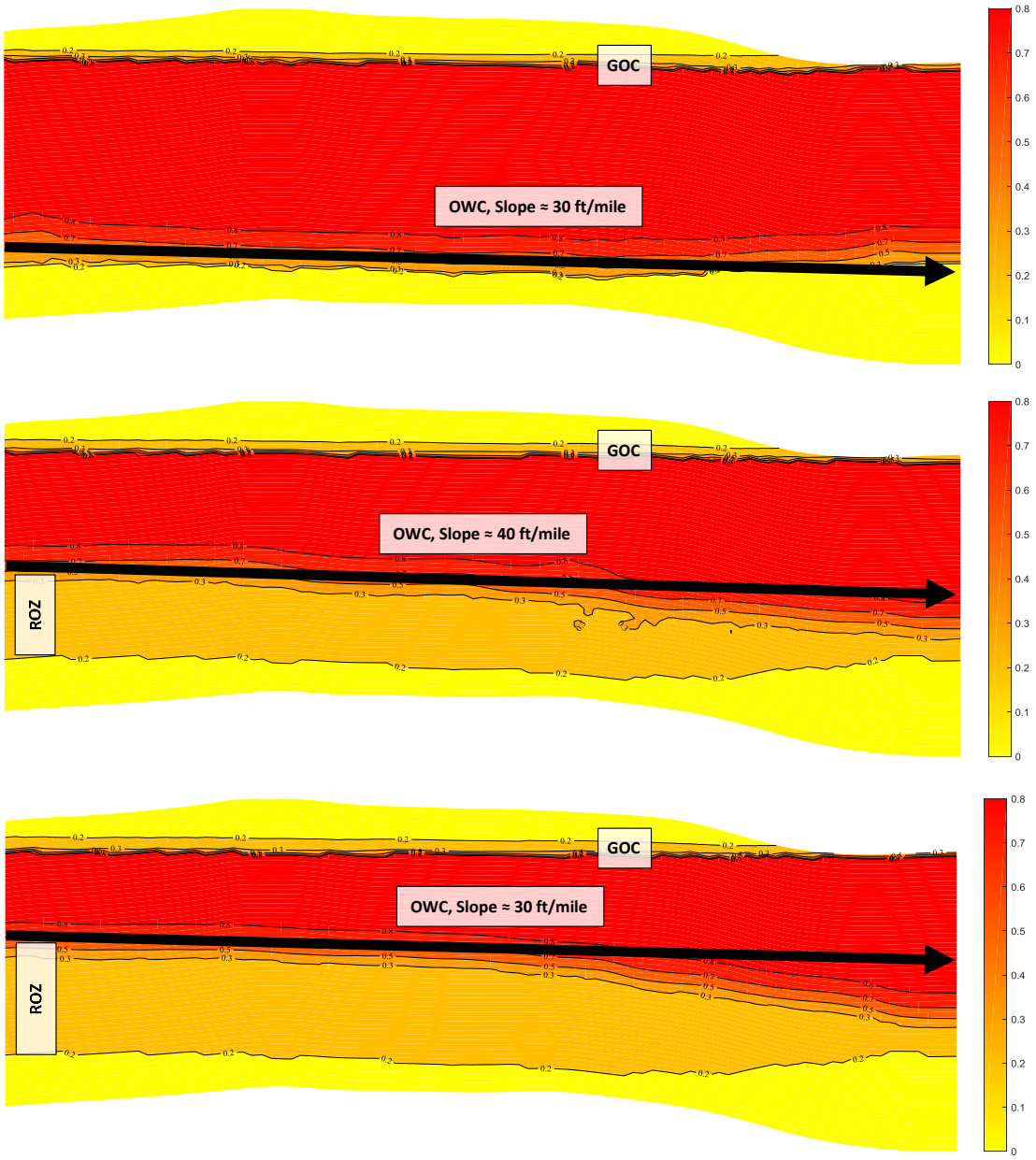

Figure 4.9 Fieldwide oil saturation distribution at 0.03×10^5 (top), 0.50×10^5 (middle), and 1.00×10^5 (bottom) years. Local variations are affected by layering particularly in the low permeable east side of the reservoir; however, the general OWC slope corresponds to both field observations and Hubbert's tilt formula.

The oil saturation profile in the middle of the reservoir is shown in Figure 4.10. This figure shows that the ROZ gross thickness and the MPZ gross thickness correspond to the observed values of 160 feet and 240 feet, respectively (Melzer et al., 2006). Notice the general shape of the oil saturation profile, including an elongated ROZ at oil saturations near residual oil saturation to waterflood. The oil saturation profile and the tilt of the OWC favorably match the field observations (Honarpour et al., 2010; Melzer et al., 2006). This supports the idea that the observed ROZs in the Permian Basin are the results of AHFF.

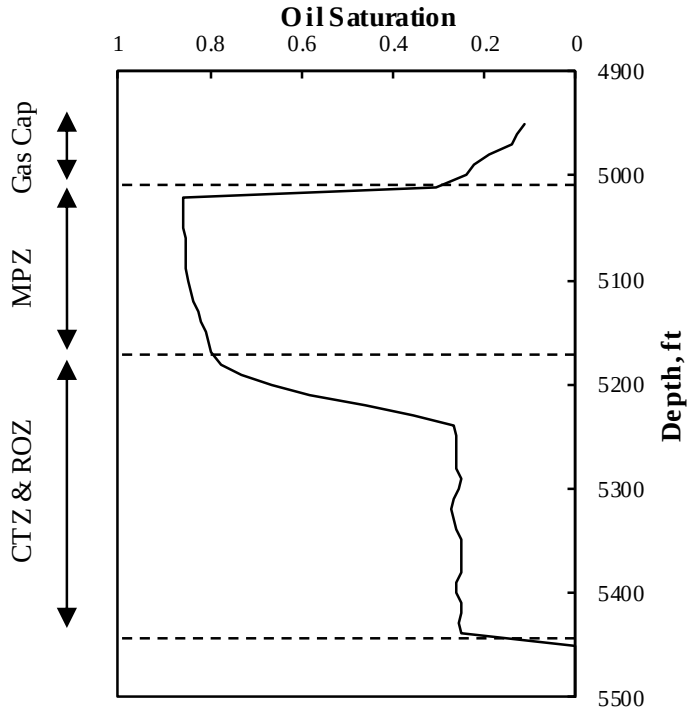

Figure 4.10 Oil saturation profile in the middle of the reservoir at the end of the AHFF process.

One can assess the potential existence of the ROZ in the presence of hydrodynamics effect. To that end, the sensitivity of the saturation profile to key parameters, including vertical to horizontal permeability ratio and the potentiometric gradient should be determined. This is done for several scenarios listed in Table 4.5 and the results are presented in Figure 4.11. Comparison of cases 1 through 3 indicates that the

vertical growth of the ROZ is an exponential function of the vertical to horizontal permeability ratio. In addition, comparison of cases 3 through 5 indicates that the vertical growth of the ROZ is a linear function of the potentiometric gradient.

A review of the effect of the slope of the potentiometric surface and the vertical to horizontal permeability ratio (Kv/Kh) can be instructive in studying and determining the existence of potential ROZs. Figure 4.11 shows the oil saturation profile in the middle section of the reservoir at the end of the AHFF process for various scenarios. The results show that the height of the ROZ is logarithmically proportional to both the vertical to horizontal permeability ratio and the slope of the potentiometric surface. In other words, the progression rate of the ROZ is *not* linearly proportional to these two factors. A linear proportionality is usually the case for Darcy law phenomena; however, the non-linear proportionality observed indicates that the rise of the ROZ is instead governed by capillary imbibition. The reader is encouraged to see Appendix A of this dissertation for further discussion on the derivation of Hubbert's tilt formula and a sensitivity analysis study on the slope of OWC.

Table 4.5 Sensitivity analysis scenarios performed to determine the sensitivity of the saturation profile to key parameters, including vertical to horizontal permeability ratio and the potentiometric gradient.

	Potentiometric Tilt, ft/mile	Kv-Kh Ratio
Run 1	7.5	0.01
Run 2	7.5	0.1
Run 3	7.5	0.5
Run 4	7.5	1.0
Run 5	20	0.5
Run 6	50	0.5

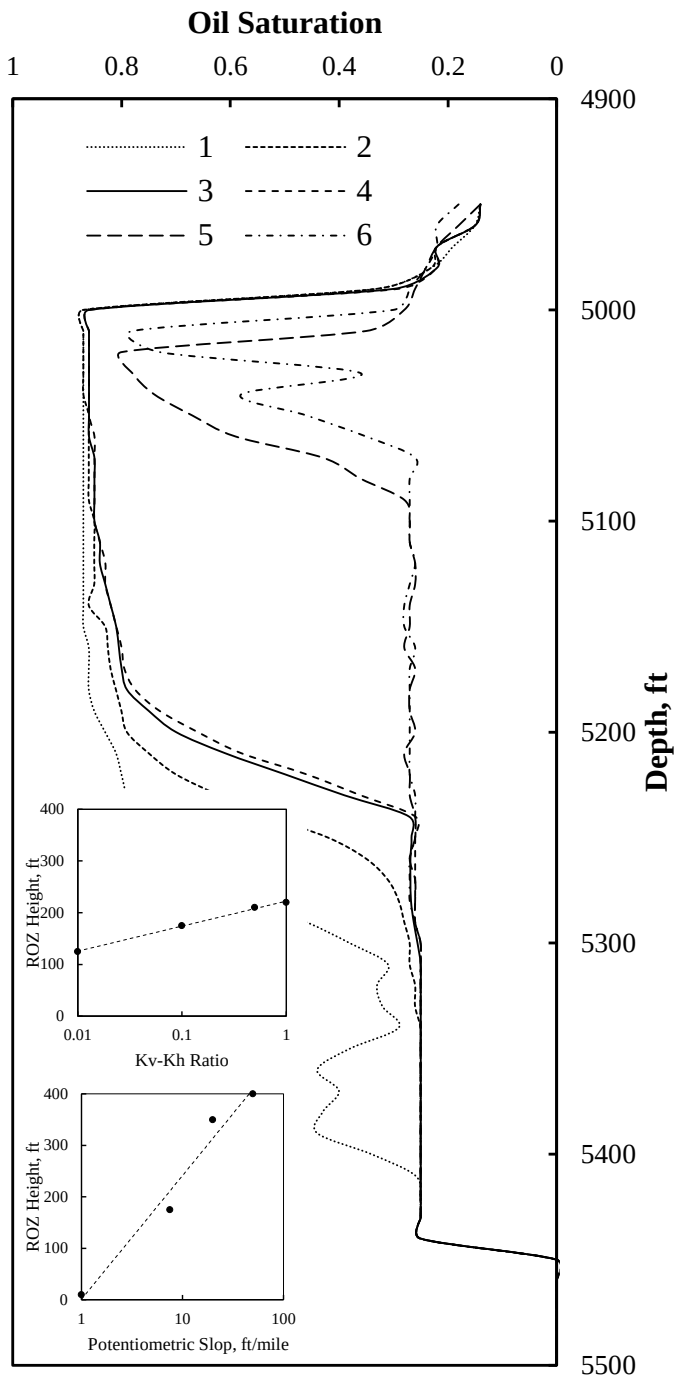

Figure 4.11 Oil saturation profile under various potentiometric slopes (PS) and vertical to horizontal permeability ratios: (1) Kv/Kh = 0.01, PS = 7.5 feet per mile, (2) Kv/Kh = 0.1, PS = 7.5 feet per mile, (3) Kv/Kh = 0.5, PS = 7.5 feet per mile, (4) Kv/Kh = 1.0, PS = 7.5 feet per mile, (5) Kv/Kh = 0.5, PS = 20 feet per mile, (6) Kv/Kh = 0.5, PS = 50 feet per mile.

4.4.2. Primary Recovery and Secondary Waterflood

We define the following framework for the reservoir development. The production stages of the Permian Basin San Andres reservoir comprise 10 years of primary production under gas cap drive and solution gas drive, 40 years of secondary production under waterflood, and 40 years of tertiary production under CO_2-EOR. This adds up to a total reservoir life of 90 years. A line drive injection pattern with a well spacing of 1300 feet is built into the model. Figure 4.12 presents the location of the injectors and the producers. The MPZ waterflooding takes place during the secondary recovery stage.

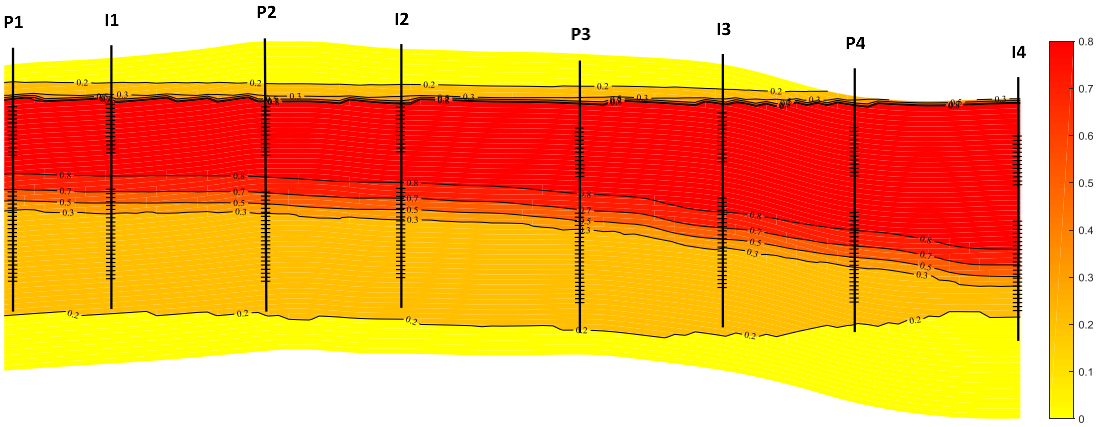

Figure 4.12 Location of the wells with an average 1300 ft well spacing. Only the MPZ is developed during the primary and secondary recovery stages. From west to east, the wells are completed at continuously lower depths to ensure that the injected fluids remain confined to the intended zone and are not affected by the OWC tilt.

Figure 4.13 shows the oil saturation distribution at the end of the waterflood (50 years). The reservoir permeability is relatively low in the east side of the reservoir resulting in a low sweep efficiency in this region. Figure 4.14 shows the reservoir oil production rate and water cut during this stage. By the end of this stage, the water cut exceeds 90% and the MPZ oil recovery factor is approximately 45%.

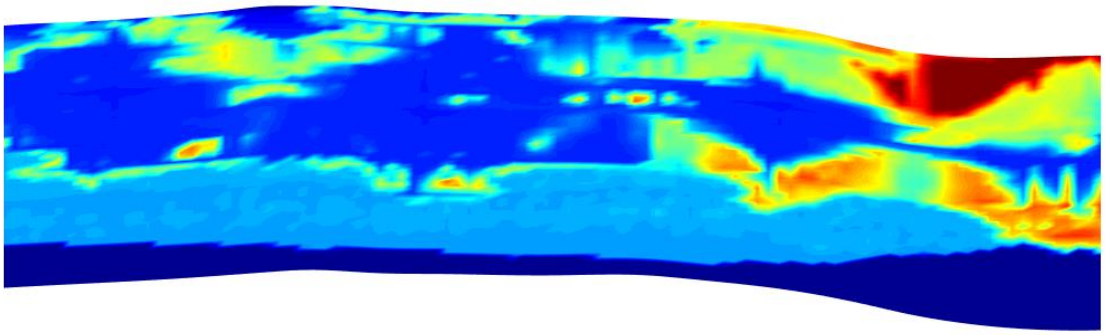

Figure 4.13 Oil saturation distribution at the end of the secondary production stages (50 years).

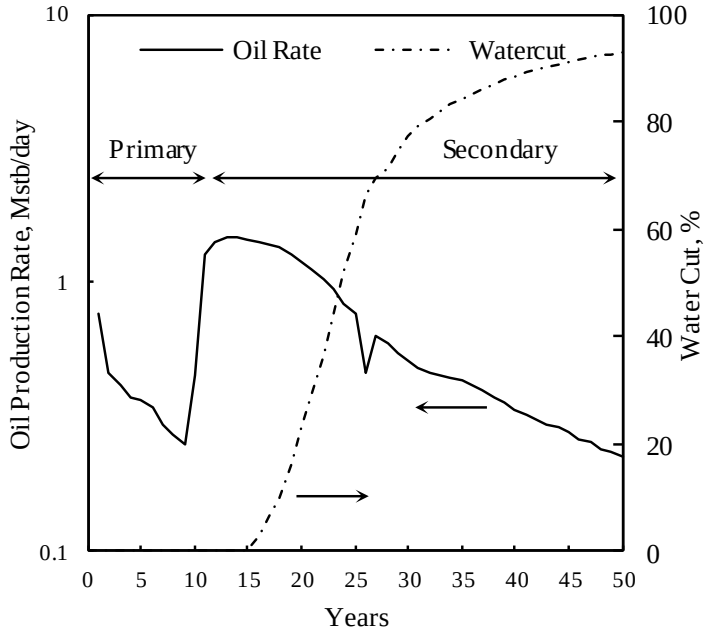

Figure 4.14 Reservoir performance under primary production and secondary water-flood.

4.4.3. CO_2-EOR and Storage Potential of the MPZ-ROZ

We investigate the impact of three decision criteria on the oil production performance and CO_2 storage potential of the MPZ and ROZ. These include: (1) whether or

not to expand the EOR-storage project to the ROZ; (2) the time to expand the EOR-storage project to the ROZ; and (3) the total CO_2 injection volume in the MPZ and ROZ.

Based on these criteria, we may consider several approaches for developing the MPZ and ROZ, each of which puts forward a different implementation timeline, capital investment, and risk propensity. An ongoing MPZ EOR project may be *expanded* into the ROZ by means of deepening the wells. This approach has the several benefits:

1. The development of the MPZ can help with the risk assessment and justify the ROZ expenditures based on the production data and the reservoir response to the MPZ CO_2-EOR.
2. The existing infrastructure and surface facilities are used, which minimizes the upfront investment.
3. The purchase of the additional CO_2 slug may be assessed based on the reservoir response to the MPZ CO_2-EOR.

A more aggressive approach, on the other hand, is the simultaneous MPZ-ROZ development from the beginning. This approach requires a greater upfront investment and involves a higher risk. In addition to the abovementioned variations, the purchased CO_2 feed may vary depending on the CO_2 availability and the operator's investment strategy. The choice of these design variables depends on the operator's development policy and preferences. For the proposed 40 years of EOR-storage, we outline six possible cases based on these design variables:

1. MPZ *only* development with a total CO_2 injection volume of 60 Bscf (approximately 0.5 PV at reservoir conditions).
2. MPZ *only* development with a total CO_2 injection volume of 140 Bscf.
3. MPZ-ROZ *sequential* development with a total CO_2 injection volume of 140 Bscf. Sequential development refers to 20 years of MPZ CO_2-EOR followed by 20 years of MPZ-ROZ CO_2-EOR.

4. MPZ-ROZ *simultaneous* development with a total CO_2 injection volume of 140 Bscf. Simultaneous development refers to 40 years of MPZ-ROZ CO_2-EOR.
5. MPZ-ROZ *sequential* development with a total CO_2 injection volume of 340 Bscf.
6. MPZ-ROZ *simultaneous* development with a total CO_2 injection volume of 340 Bscf.

Figure 4.15 shows the cumulative CO_2 injection for these six cases. We consider three parameters for the assessment of the performance of each case. These are the cumulative oil produced (MMstb), the cumulative CO_2 retained (Bscf), and the net CO_2 utilization (Mscf/stb). The net CO_2 utilization is defined as the surface volume of CO_2 stored in the reservoir for each incremental stock tank barrel of oil produced. The results are shown in Figure 4.16 and Figure 4.17 and are summarized in Table 4.6.

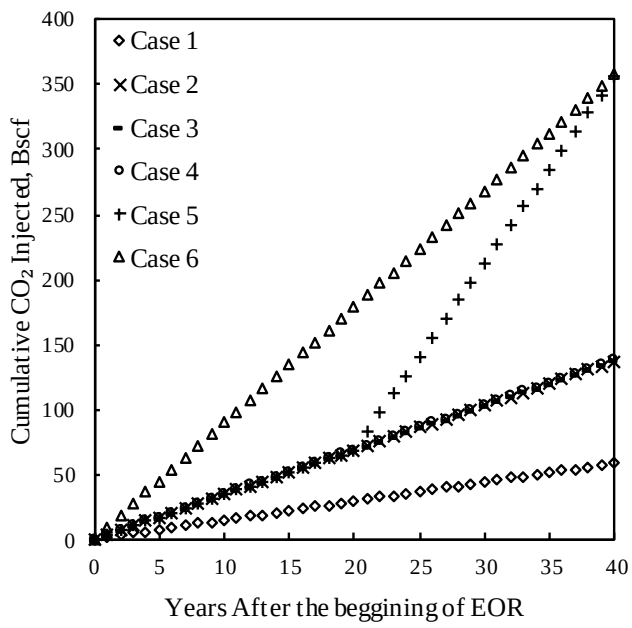

Figure 4.15 Cumulative CO_2 injection for the six scenarios.

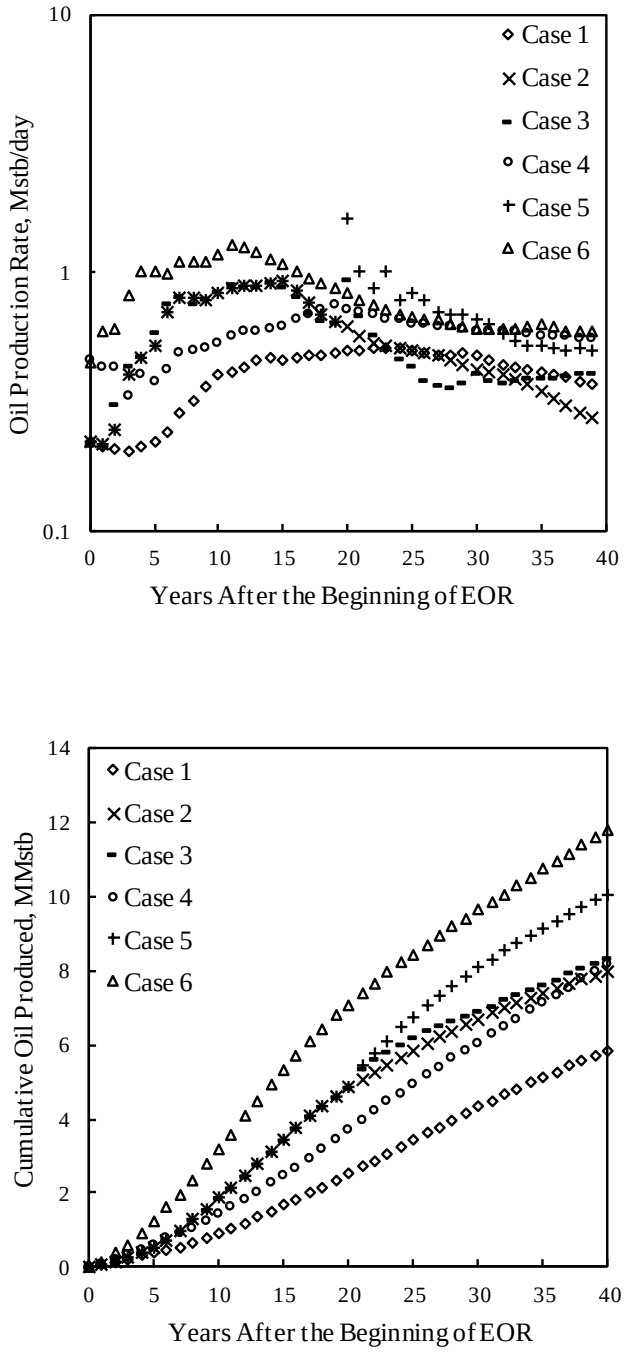

Figure 4.16 Reservoir performance in terms of oil production for the proposed cases (a) oil production rate (top), and (b) cumulative oil production (bottom).

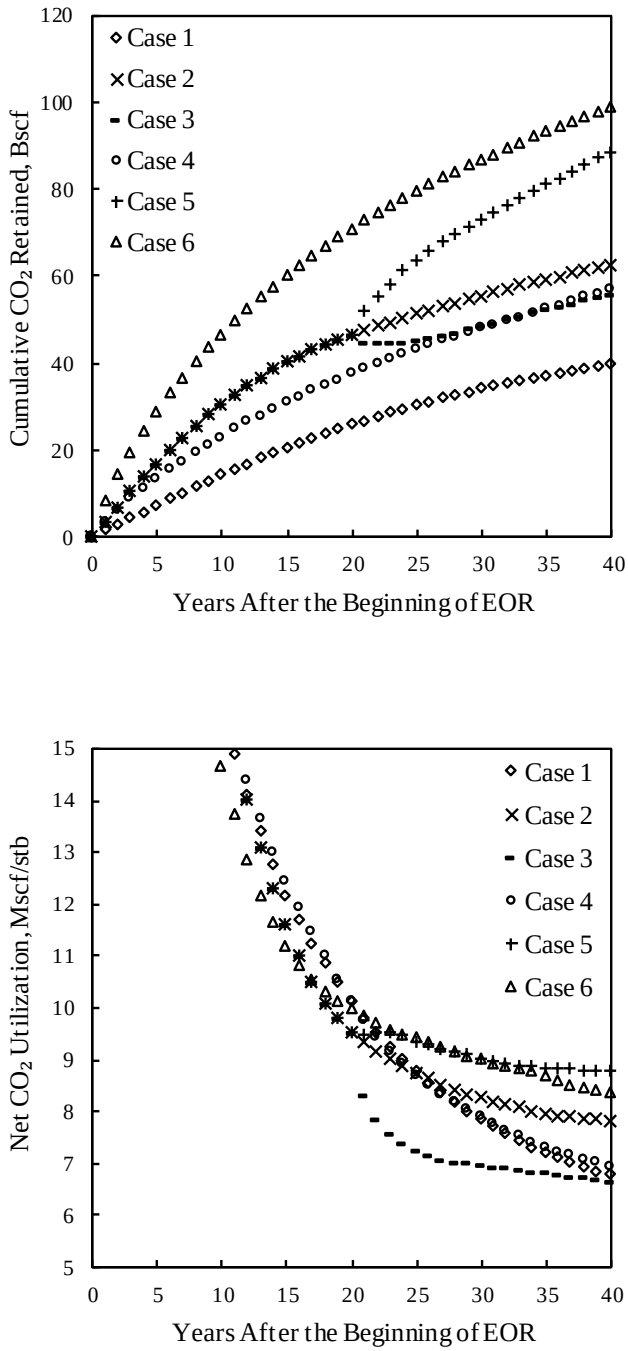

Figure 4.17 Reservoir performance in terms of CO_2 storage for the proposed cases (a) cumulative CO_2 stored (top), and (b) net CO_2 utilization (bottom).

Table 4.6 Development strategy and reservoir performance of cases 1 through 6. The results show that cases 3 and 6 should be prioritized over cases 4 and 5.

	CO_2 **Injected Bscf**	**Development Strategy**	**Oil Produced MMstb**	CO_2 **Stored Bscf**	**Comments**
Case 1:	60	Only MPZ	5.8	40.3	Using high WAG ratios may result in delayed oil production response and reduced CO_2 utilization
Case 2:	140	Only MPZ	8.0	62.5	
Case 3:	140	Sequential MPZ-ROZ	8.4	55.9	In the absence of additional CO_2, the MPZ should be fully developed before the expansion to the ROZ
Case 4:	140	Simultaneous MPZ-ROZ	8.2	56.8	
Case 5:	340	Sequential MPZ-ROZ	10.1	88.5	The operator may purchase additional CO_2 to improve the performance. Under this condition, simultaneous expansion performs better than other strategies
Case 6:	340	Simultaneous MPZ-ROZ	11.9	98.9	

Comparison of Cases 1 & 2: The results show that Case 2 yields a considerably better oil production performance compared to Case 1 (8.0 MMstb vs 5.8 MMstb). Figure 4.17a and Figure 4.17b show that Case 2 stores an additional 22.2 Bscf CO_2 (62.5 Bscf vs 40.3 Bscf) and yields an ultimately higher net CO_2 utilization (7.8 Mscf/stb vs 6.8 Mscf/stb). These results are consistent with other field observations and simulation studies where excessive increase in the WAG ratio considerably delays the peak oil production and decreases the net CO_2 utilization (Agada et al., 2016; Ettehadtavakkol et al., 2014a).

Comparison of Cases 3 & 4: The results show that Case 3 yields a slightly better oil production compared to Case 4 (8.4 MMstb vs 8.2 MMstb), however Case 4 stores an additional 0.7 Bscf CO_2 compared to Case 3 (56.8 Bscf vs 55.9 Bscf) and yields an ultimately higher CO_2 utilization factor (7.0 Mscf/stb vs 6.7 Mscf/stb). These numbers are very close to each other and indicate that the performance of Cases 3 and 4 are very

similar. The CO_2 allocation for Case 4 is 140 Bscf, which is insufficient for simultaneous development of the MPZ and ROZ and results in relatively high WAG ratios. In Case 3, on the other hand, the MPZ peak oil production is reached and considerable volumes of oil is recovered (4.9 MMstb) before the project expands into the ROZ. In other words, the benefits gained by extending the EOR into the ROZ is counteracted by the relatively high WAG ratio implemented in Case 4. Under these conditions, it is favorable to expand the project and utilize the produced CO_2 in the ROZ, where another peak oil production occurs during the second half of the EOR project, without causing any delays in the MPZ oil production response. Therefore, the operator is recommended to prioritize Case 3 over Case 4. In addition, considering the costs of project expansion into the ROZ, Case 2 is preferred over both Case 3 and Case 4. This is because 140 Bscf CO_2 guarantees a satisfactory performance for Case 2, while it results in high WAG ratios for Case 3 and Case 4 which considerably delays their oil production response.

Comparison of Cases 5 & 6: The results show that Case 6 yields a considerably better oil production compared to Case 5 (10.1 MMstb vs 11.9 MMstb). Case 6 also stores an additional 10.4 Bscf CO_2 compared to Case 5 (98.9 Bscf vs 88.5 Bscf). Both Case 5 and Case 6 have superior performances compared to cases 1 through 4 in terms of oil production and CO_2 storage.

Based on these observations, an aggressive project expansion investment (Case 4 and Case 6) is recommended only if there are plans to utilize additional CO_2 supplies (Case 6). In the absence of the required additional CO_2 supplies, it is recommended to prioritize the sequential ROZ expansion over the simultaneous MPZ-ROZ development. Only by prioritizing the investment on CO_2 allocation and using relatively lower WAG ratios, the operator will benefit from maximum oil production and CO_2 storage capacity. These results are summarized in Figure 4.18. The conclusions made here are also applicable to cases where EOR-storage in the MPZ has already begun. In such cases, the project expansion into the ROZ should be delayed until sufficient CO_2 supplies are available. When the required CO_2 supplies are available, immediate project expansion is recommended to maximize the EOR-storage benefits.

CO_2 Allocation / MPZ-ROZ Development	140 Bscf (Moderate)	340 Bscf (Aggressive)
Sequential (Moderate Investment)	Case 3 Oil Produced: 8.4 MMstb CO_2 Stored: 55.9 Bscf	Case 5 Oil Produced 10.1 MMstb CO_2 Stored: 88.5 Bscf
Simultaneous (Aggressive Investment)	Case 4 Oil Produced: 8.2 MMstb CO_2 Stored: 56.8 Bscf	Case 6 Oil Produced: 11.9 MMstb CO_2 Stored: 98.9 Bscf

Figure 4.18 Summary of MPZ-ROZ development cases. The expansion development strategy should be proportional to CO_2 investment strategy. Moderate/moderate or aggressive/aggressive investment scenarios are recommended.

Effect of the Recoverable Oil Volume in the ROZ: The recoverable oil volume is mainly determined by the difference between the residual oil saturation to waterflood and the residual oil saturation to miscible flood. The effect of the ROZ recoverable oil volume on the performance of EOR-storage is investigated by varying the ROZ residual oil saturation to miscible flood from 0.07 to 0.17.

At the end of the 40 years of CO_2-EOR, Figure 4.19a shows the cumulative CO_2 storage as a function of the cumulative oil production for Cases 3 through 6 and for $S_{orm, ROZ}$ = 0.07, 0.12, and 0.17. Also, Case 2 (MPZ *only* development with a total CO_2 injection volume of 140 Bscf) is presented as the *base case* for comparison. The diagonal lines represent the cases with equal net CO_2 utilization (Mscf/stb). At lower ROZ residual oil saturations (higher recoverable oil volumes), the net CO_2 utilization is reduced while the cumulative CO_2 storage remains almost constant. The lower net CO_2 utilization is favorable for operators because it suggests higher oil recovery while maintaining maximum CO_2 storage benefits. The results show how recoverable oil volume affects economic limit of each development strategy. For example, an approximate net CO_2 utilization of 12 Mscf/stb for Case 5 and for $S_{orm, ROZ}$ = 0.17 renders the economic viability of this case questionable.

Effect of ROZ Rock and Fluid Properties: Several studies reported oil degradation in the ROZ as a result of anaerobic sulfate-reducing bacteria introduced to the reservoir from the flow of meteoric water. Oil biodegradation can affect reservoir oil attributes in several ways, including raising the oil viscosity and reducing the oil API gravity both resulting from significant composition difference between MPZ and ROZ oil (Bailey et al., 1973; Honarpour et al., 2010; Ramondetta, 1982; West, 2014). Furthermore, porosity and permeability enhancement as a result of diagenesis in the ROZ is well documented (Lucia, 2000; Saller, 2004). This phenomenon is mainly associated with (1) early-stage dolomitization, resulting from the presence of the magnesium-rich meteoric water, and (2) late-stage sulfate dissolution, also resulting from interaction with the inflowing meteoric water (West, 2014).

The degraded oil composition used for the ROZ is presented in Table 4.2. This is used along with an average enhanced rock porosity of 2-3% in the ROZ to investigate the effects of biodegradation and diagenesis, respectively (Honarpour et al., 2010; Melzer, 2013). The CO_2 storage performance of Case 6 under degradation and diagenesis are compared in Figure 4.19b. Degradation and diagenesis demonstrate opposing effects on CO_2 storage capacity of the reservoir. Degradation significantly reduces the storage capacity, while the digenesis slightly improves the storage capacity. In Case 6, for example, the degradation reduced the storage capacity from 98.9 Bscf down to 75.9 Bscf, and diagenesis improved the storage capacity up to 103.2 Bscf.

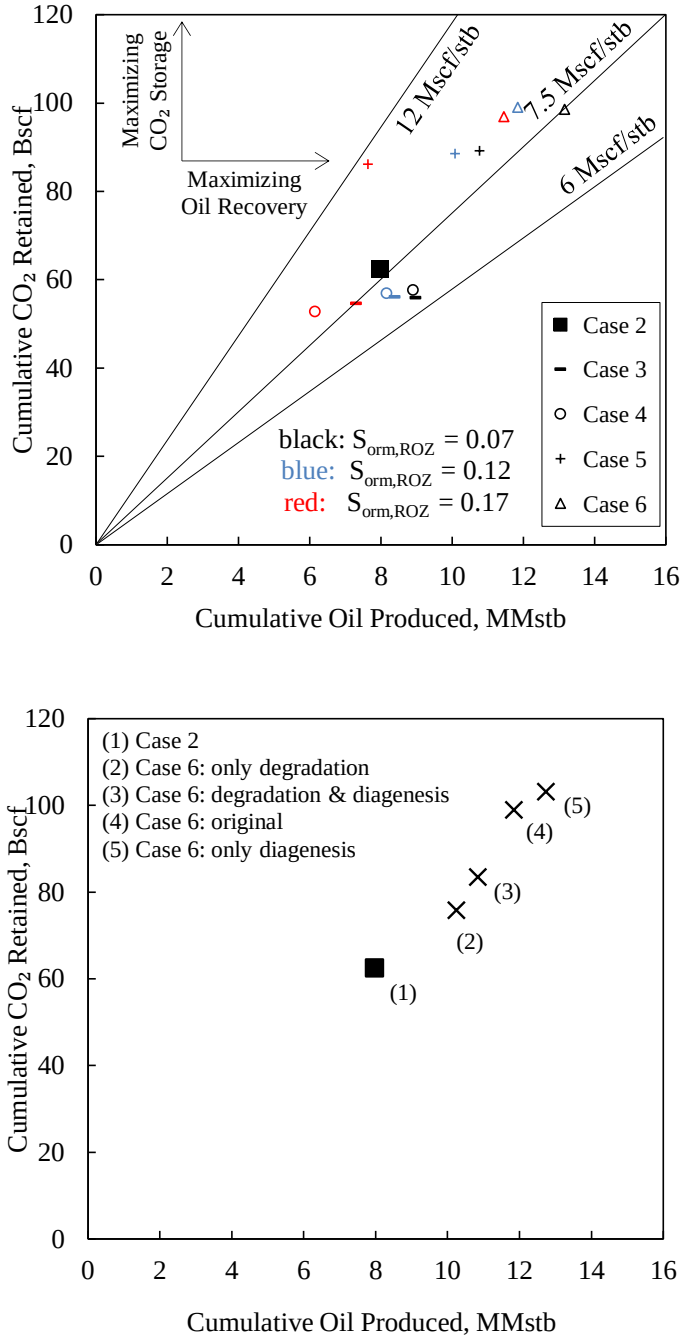

Figure 4.19 CO_2 storage performance plots demonstrating (a) the effect of recoverable oil volume on the performance of all cases and (b) the effects of biodegradation and diagenesis on the performance of Case 6. The diagonal lines represent constant net CO_2 utilizations. The performance of Case 2, i.e. MPZ *only* development with a total CO_2 injection volume of 140 Bscf, is presented for comparison.

4.4.4. CO_2 Storage in the ROZ: Opportunities and Challenges

Geologic storage of CO_2 in the ROZ is a subject of growing interest, and it is important to investigate the various aspects of ROZ storage potential and limitations. This study presents four important aspects as follows.

EOR Storage Beyond the MPZ: The exploitation of the ROZ has several features that make it a unique option for CO_2 storage, particularly in the Permian Basin. The declining oil production rates in many of the mature oil fields in this region provide a strong incentive for the operators to consider such field scale expansions. Also, the existing infrastructure built for the overlaying MPZ, including injection pads, transportation pipelines, and processing plants can be used for the development of the ROZ. This minimizes the surface footprint and eliminates the barrier of public acceptance. Most importantly, the operator's previous experience with the MPZ provides key information on reservoir's injectivity, storage capacity, and CO_2 confinement which can be used to establish assessment and planning of CO_2 storage in the ROZ.

Assessment of ROZ's Storage Performance based on the MPZ's past Performance: It is crucial to accurately estimate CO_2 storage capacity in oil and gas reservoirs. Numerical simulation can be used to provide first-order estimations of field-scale CO_2 storage capacity. For the case of CO_2-EOR, such estimations are obtained based on case-by-case numerical reservoir simulation and through accurate modeling of reservoir behavior during CO_2 flood (Bachu et al., 2007). The results, as presented earlier and summarized in Table 4.6, indicate that CO_2-EOR in the ROZ provides new capacity for additional volumes of CO_2. If the most optimistic scenarios of MPZ and MPZ-ROZ development are compared (Case 2 and Case 6), a 50% increase in the CO_2 storage capacity of the reservoir (62.5 Bscf vs 98.9 Bscf) is accomplished owing to the project expansion to the ROZ. Considering that the available surface area for storage is approximately equal for both the MPZ and ROZ, the CO_2 storage capacity of MPZ and ROZ are 0.4 and 0.15 Bscf per foot of zone thickness, respectively. This shows an almost a 60% decrease in the CO_2 storage capacity of the ROZ. A closer look at the reservoir permeability distribution (Figure 4.4) reveals that there are several high permeability

channels in the ROZ. The presence of these layers results in relatively fast CO_2 breakthrough and low vertical sweep efficiency which in turn reduces the CO_2 storage capacity of the reservoir. This observation has important implications for carbonate reservoirs where the presence of multiscale heterogeneities and permeability sequences result in complicated flow behaviors (Agada et al., 2016; Ettehad, 2014; Yang et al., 2013). This important observation is consistent with the results reported in Melzer (2006) for the Amerada Hess's SSAU CO_2-EOR project. They reported similar conformance consideration associated with CO_2 injection into the ROZ which led to different performance parameters compared to those of the MPZ. Therefore, the EOR-storage potential of the ROZ may strongly differ from that of the MPZ depending on the reservoir characteristics of each zone.

Saltwater Disposal Requirements: Another important consideration associated with CO_2 storage in the ROZ is the excessive water production. Saltwater disposal is performed to mitigate the difference between the water injection and production rates in the EOR-storage process. Disposal of the produced water is a crucial environmental consideration (Koornneef et al., 2012; Vishal and Singh, 2016). The saltwater may be transported to Class II injection wells to in the nearby fields via trucks or pipelines. If the produced water meets the environmental requirements for disposal, it may be directly injected; otherwise, it should be treated at the disposal facility before the injection. All of these processes will impose transportation, remediation, and disposal costs.

An accurate estimate of water production is essential for the saltwater disposal facility development and allocation. The results of the proposed simulation model may be used to quantify the saltwater disposal requirement. Figure 4.20 compares the water injection and production rates of the MPZ-only (Case 2) development with those of the MPZ-ROZ development (Case 6). The initial water production rate for the MPZ-ROZ development (Case 6) is 11.2 Mstb/day, compared to 3 Mstb/day for the MPZ development (Case 2). This reflects the considerable difference between the saltwater disposal requirements in the two scenarios. The excessive water production observed at the beginning is the result of the reservoir water being displaced by the injected CO_2. The

average disposal rate of the MPZ development (Case 2) is 0.45 Mstb/day compared to 1.35 Mstb/day for the MPZ-ROZ development (Case 6), indicating an increase of more than 200%. Therefore, the saltwater disposal planning and allocation is a major design consideration for the CO_2 storage in the ROZ.

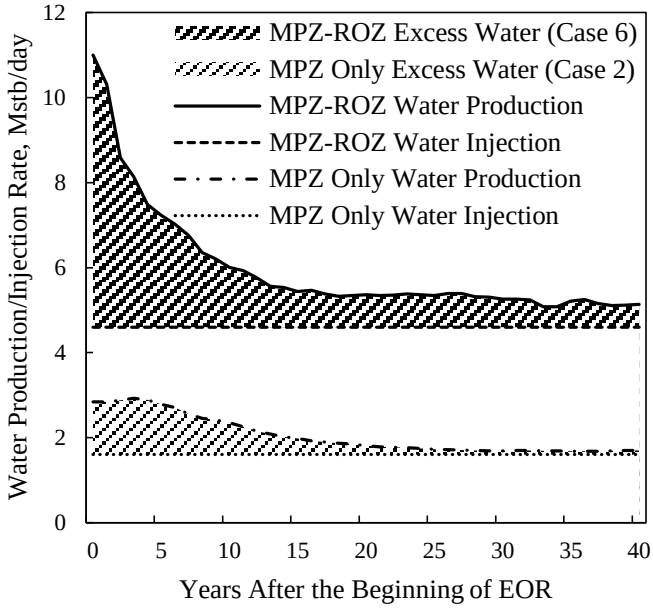

Figure 4.20 Comparison of the water production of the MPZ-only and MPZ-ROZ development scenarios. The difference between the total produced and injected water should be considered for disposal.

Reduced Risk of CO_2 *Leakage:* Many mature oil fields are perforated by a large number of oil wells, including active and abandoned wells. The presence of such wells increases the chance of CO_2 leakage into other formations, shallow water tables, and to the land surface during and after the storage process. This problem occurs if the injected CO_2 plume finds pathways through and around the wellbores of the abandoned wells. This may reduce the efficiency and the sustainability of CO_2 storage in an oil reservoir (Ebigbo et al., 2006; Nordbotten et al., 2005). While this holds true for the conventional CO_2-EOR projects, the majority of the wells in MPZ-ROZ reservoirs are drilled and completed above the OWC to prevent water production (Koperna et al., 2006). Therefore, one important advantage of the CO_2 storage in the ROZ over CO_2 storage in the

MPZ is that the abandoned wells in such reservoirs are rarely completed through the ROZ. This inherent property of the ROZ reduces the risk of CO_2 leakage through the abandoned wells, thus resulting in safer and more sustainable storage of CO_2.

Effect of Oil Price, Carbon Taxation, and CO_2 *Storage Credit:* Several researchers have discussed the economic viability of EOR-storage under variations of oil price and taxation policies (Blunt et al., 1993; Celius and Ingeberg, 1996; Ettehadtavakkol et al., 2014a; Gozalpour et al., 2005). The high oil price provides an incentive for the operators to reduce the economic limit on the field production rate and consequently, increases the life of the EOR-storage project. The CO_2 storage credit will also reduce the net CO_2 cost, and carbon taxation will create a deterrent to uncontrolled discharge of CO_2 into the atmosphere. In general, high oil prices and transparent taxation policies can create a balance between capture and storage costs, thus maximizing the overall benefits of EOR-storage and reducing the operators' investment risk exposure.

EOR-storage in the ROZ may impose relatively high investment risks on such projects. The current low oil price environment is further unfavorable for the oil field operators. Therefore, tax policies in favor of the oil field operators can compensate for the low oil price and facilitates ROZ development. Of the six development strategies presented, and under the current economic conditions, the sequential ROZ development is preferred to operators because it will minimize the risk exposure of the EOR-storage operation in the MPZ-ROZ.

CHAPTER V

CONCLUSIONS AND RECOMMENDATIONS FOR FUTURE WORK

We undertook reservoir characterization, reservoir simulation, and data analytics to investigate various pathways for improving oil production from mature oil fields. This study focused on the fields located in the West Texas Permian Basin. It provided guidelines for optimizing waterflood and CO_2-Enhanced Oil Recovery (CO_2-EOR), maximizing the benefits of well stimulation, and determining the best development strategies for project expansion into Residual Oil Zone (ROZ). Using an approach that combines both proactive and reactive solutions, the oil field operators can mitigate the problem of declining oil recovery from three different angles depending on the characteristics of the reservoir, the investment budget, and the required implementation timeline (Figure 5.1). Conclusions of this study for each method are presented here.

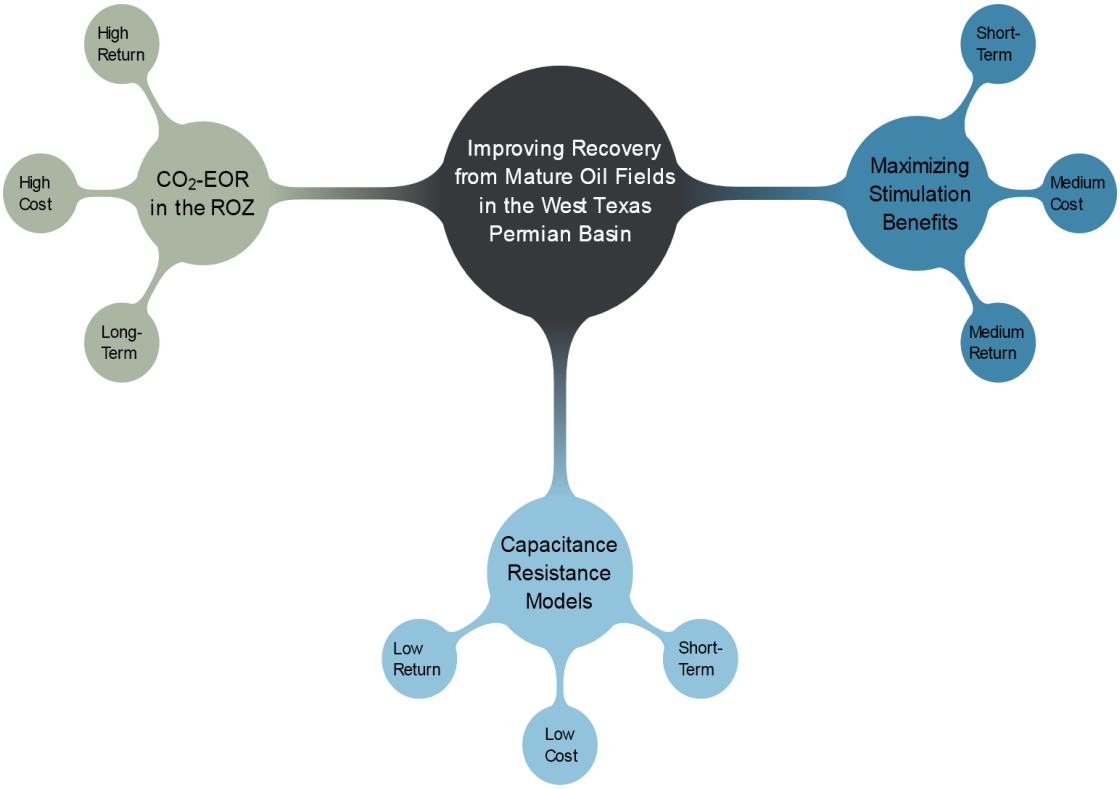

Figure 5.1 Summary of the methodologies investigated in this dissertation.

5.1. Application of Capacitance Resistance Models

We examined practical aspects of the application of Capacitance Resistance Models (CRMs) with an emphasis on overcoming the challenges that are raised in mature oil fields that were not addressed in the earlier studies. This study is the first to address the practical field-scale challenges of CRM implementation as a large-scale problem and how to effectively resolve them. The major contributions and conclusions are as follows:

1. The convexity of CRMP objective function over the feasible solution space is investigated through the implementation of the global optimization algorithm. The results of examination of the CRMP objective function for several problems show that it is convex within its feasible region; therefore, using a local optimization solver is sufficient. Analytical derivation of the proof is a subject of further research.

2. The analytical gradient vector and Hessian matrix of CRMP objective function were derived and supplied to the solver. This results in a reduced solution time because computing the numerical gradient and Hessian matrix is extremely time consuming for the solver. This strategy reduced the solution time down to at least 10 times; this enables the CRMP application to real field-scale problems.

3. Although the absence of flowing bottomhole pressure data might affect the quality of history matching, it was shown that in the absence of such data the connectivities were within a ±20% of the actual values when the flowing bottomhole pressure data are included. The larger connectivities used for further analysis were within an acceptable range of their actual values.

4. Three examples of practical application of CRMP to well management were presented and discussed. Stepwise history matching was shown to be an ef-

fective technique to introduce more reliability to the analysis. The connectivities captured by CRMP was confirmed by comparing CO_2 injection signal and its response in the corresponding producers.

5.2. Maximizing Stimulation Benefits Using Data Analytics

A thorough review of stimulation candidate selection techniques was presented. Several studies suggested that producers with higher oil production rates have higher stimulation potential and should be prioritized for well stimulation. An evidence-based investigation of this idea was lacking and is the subject of this study. We investigated the statistical evidence through (1) analysis of aggregate results of case studies in the literature; (2) analysis of production data from four mature Permian Basin San Andres leases; and (3) analysis of the simulation results of a tuned reservoir model. The major conclusions are:

1. Analysis of pre- and post-stimulation oil production rates of four mature leases in the Slaughter field reveals a positive correlation between pre-stimulation oil production rates and the stimulation incremental oil production. An additional dataset gathered from the literature further confirms the existence of such a relationship. Overall, a total number of 144 producers are analyzed.

2. In preliminary screenings of candidate well selection, the operator is recommended to prioritize wells with higher pre-stimulation oil production rates. This provides a fast and convenient method to eliminate the least prospective wells in terms of stimulation incremental oil production.

3. The method is applied to a field-scale reservoir simulation model as a stimulation candidate selection technique. The top stimulation candidates are those with highest pre-stimulation oil production rates. This ranking method showed an efficiency nearly as good as the perfect information scenario in which the true ranking is known.

5.3. CO_2-EOR in the Residual Oil Zone

We investigated the formation of ROZs under the Altered Hydrodynamic Flow Fields (AHFF) for the Permian Basin San Andres reservoirs. The ROZ carries additional hydrocarbon resource potential and CO_2 storage capacity. The trapped oil in the ROZ is technically recoverable by CO_2 injection. An important synergic advantage of this process is to provide secure underground capacity for CO_2 storage. Based on various decision criteria, such as the investment strategy and the availability of CO_2 resources, the operators may consider several approaches for developing CO_2 storage projects in MPZ-ROZ reservoirs. The performance of each approach in terms of oil production and CO_2 storage is determined for the Permian Basin San Andres reservoir model. Major conclusions follow:

1. AHFF field-scale reservoir simulation model of the Permian Basin San Andres reservoir matches the field observations in terms of the oil saturation profile and the tilt of the OWC. The local variations of these two parameters is associated with the rock quality, layering, and the presence of flow restrictions within the reservoir.

2. The ROZs have a considerable EOR-storage potential. In addition, the operational CO_2 storage capacity is a function of the operators' development and operational strategy.

3. A simultaneous MPZ-ROZ development strategy is superior in terms of oil production and CO_2 storage. This aggressive expansion strategy will be most successful if sufficient CO_2 supplies are utilized. In the absence of additional CO_2 supplies, the operator may fully develop the MPZ EOR-storage first. The ROZ EOR-storage may be initiated after the oil production decline in the MPZ is occurred.

4. The effects of biodegradation and diagenesis on the EOR-storage performance of the ROZ are considerable and should be included in the operational assessments.

5. CO_2 storage in the ROZ has several important considerations, including the storage capacity assessment, excessive saltwater disposal requirement, and reduced risk of CO_2 leakage through the abandoned wells.

5.4. Recommendations for Future Work

In light of the limitations and potentials associated with each method presented in this dissertation, we suggest the following pertinent problems as a continuation of this research:

5.4.1. Future Work for the CRM Study

- CRMs are becoming a standard reservoir engineering and flood optimization tool and an indispensable gadget in reservoir engineers' toolkit. They have shown significant utility in flood optimization, reservoir characterization, and history matching. The constrained nonlinear optimization problem of CRMs requires a commercial solver and may take several hours to converge. It is recommended to develop a state-of-the-art solution approach to the CRM optimization problem for minimizing the solution time and eliminating the need for a commercial solver. This problem can be solved using a primal-dual interior point method to solve the CRM constrained nonlinear optimization problem. The analytically derived gradient vector and Hessian matrix of the CRM objective function could be implemented as an internal part of the solver. An internal scaling scheme could be used to normalize the CRM parameters to reduce the sensitivity of the objective function to perturbations in different model parameters. The results of such study can facilitate the implementation of CRMs in reservoir simulation and flood optimization packages and eliminate the need for commercial solvers.

5.4.2. Future Work for the Candidate Selection Study

- The long-term induced skin or wellbore damage is usually a function of well productivity. The performance of high productivity wells is influenced more strongly by near wellbore effects. Furthermore, a high productivity well may

benefit more from removal of such damage. Therefore, this can intensify the benefit gained from stimulation of wells with higher pre-stimulation oil rate. We recommend the simulation study to be further expanded to include a dynamic relationship between well performance, imposed near-wellbore damage, and skin removal from well stimulation. In addition, the possible effects of well interference due to stimulation of nearby producers were not considered in the analysis of the simulations presented in this dissertation and should be subject of further investigation.

- It is important to note that stimulation of good producers has an inherent risk of losing a good well due to a failed stimulation job. Identification of good intervention candidates and NPV evaluations go hand in hand; therefore, a cost/benefit (NPV) evaluation of such interventions could be further studied.
- Stimulation of waterflood and/or CO_2 injectors is a common field practice for improving well injectivity and flood efficiency. The analysis of field data and field scale simulation could shed some light on whether a similar candidate selection scheme could be beneficial to injection wells.

5.4.3. Future Work for the ROZ Study

- The presented study used a 2-dimensional reservoir simulation model for Seminole San Andres Unit. One positive effect that increased WAG ratio could introduce is the improved areal sweep efficiency which can offset parts of the benefits gained from increased CO_2 volumes in the presented studies. Such effect could not be captured using a 2D model. It is recommended to perform similar analysis using a full-scale 3D reservoir simulation model to honor areal sweep efficiency and its effects.
- The development of ROZs is extensively pursued in the Texas Permian Basin. Several successful ROZ CO_2 Enhanced Oil Recovery (CO_2-EOR) projects indicate enormous resource potential for these emerging oil plays. An-

other approach, called Depressurizing the Upper ROZ (DUROZ), was recently proposed and is currently under extensive investigation. DUROZ refers to the progressive reduction of reservoir pressure through the withdrawal of large volumes of water from a horizontal well in the upper section of ROZ. When reservoir pressure falls below the saturation pressure, gas bubbles liberate from capillary-trapped oil and develop into a continuous gas phase. Consequently, the oil phase may also become mobile beyond waterflood residual oil saturation. In the absence of pre-existing infrastructure and facilities—such as injection pads, transportation pipelines, and processing plants built for CO_2-EOR in the overlaying MPZ—the commerciality of CO_2-EOR for Greenfield ROZs/TZs remains questionable. DUROZ, on the other hand, is particularly applicable to Greenfield ROZs/TZs because it involves neither the surface facility nor the contractual and regulatory requirements attached to CO_2-EOR. Moreover, DUROZ requires minimal capital investment compared to that of EOR, allowing for a higher rate of return. Finally, the operators can benefit from copious horizontal drilling and completion experience in the Permian Basin which provides a competitive advantage for DUROZ (Jamali et al., 2017b). A mechanistic understanding of DUROZ and the factors affecting its viability and performance is lacking from the literature is recommended for further investigation. Depressurization of ROZ core samples could shed some light on the three-phase behavior of such reservoirs below bubble point pressure. Also, for accurate modeling and reservoir performance prediction, one must obtain an accurate estimation of three-phase relative permeabilities under solution gas drive.

BIBLIOGRAPHY

Abdallah, W., Buckley, J.S., Carnegie, A., Edwards, J., Herold, B., Fordham, E., Graue, A., Habashy, T., Seleznev, N., Signer, C., Hussain, H., Montaron, B., Ziauddin, M., 2007. Fundamentals of wettability. Oilfield Review 44–66.

Afolabi, A.F., Opusunju, A.U., Jaspers, H.F., Onyekwere, C., Onyekwere, C.O., Davalos, J.C., 2008. Increasing Production in a Brownfield With Heavy Crude and Fine Problems by Application of New HF-Acid System: Case Histories, in: SPE International Symposium and Exhibition on Formation Damage Control. Society of Petroleum Engineers. doi:10.2118/112558-MS

Agada, S., Geiger, S., Doster, F., 2016. Wettability, hysteresis and fracture–matrix interaction during CO_2 EOR and storage in fractured carbonate reservoirs. International Journal of Greenhouse Gas Control 46, 57–75. doi:10.1016/j.ijggc.2015.12.035

Al-Yousef, A.A., 2006. Investigating Statistical Techniques To Infer Interwell Connectivity From Production and Injection Rate Fluctuations.

Albertoni, A., Lake, L., 2003. Inferring Interwell Connectivity Only From Well-Rate Fluctuations in Waterfloods. SPE Reservoir Evaluation & Engineering 6, 6–16. doi:10.2118/83381-PA

Amaefule, J.O., Altunbay, M., Tiab, D., Kersey, D.G., Keelan, D.K., 2013. Enhanced Reservoir Description: Using Core and Log Data to Identify Hydraulic (Flow) Units and Predict Permeability in Uncored Intervals/Wells, in: SPE Annual Technical Conference and Exhibition. Society of Petroleum Engineers. doi:10.2118/26436-MS

Arps, J.J., 1964. Engineering Concepts Useful in Oil Finding. AAPG Bulletin 48, 157–165.

Athichanagorn, S., Horne, R.N., Kikani, J., 1999. Processing and Interpretation of Long-term Data from Permanent Downhole Pressure Gauges, in: SPE Annual Technical Conference and Exhibition. Society of Petroleum Engineers. doi:10.2118/56419-MS

Babadagli, T., 2007. Development of mature oil fields — A review. Journal of Petroleum Science and Engineering 57, 221–246. doi:10.1016/j.petrol.2006.10.006

Bachu, S., 2003. Screening and ranking of sedimentary basins for sequestration of CO_2 in geological media in response to climate change. Environmental Geology 44, 277–289. doi:10.1007/s00254-003-0762-9

Bachu, S., Bonijoly, D., Bradshaw, J., Burruss, R., Holloway, S., Christensen, N.P., Mathiassen, O.M., 2007. CO_2 storage capacity estimation: Methodology and gaps. International Journal of Greenhouse Gas Control 1, 430–443. doi:10.1016/S1750-5836(07)00086-2

Bailey, N.J.L., Krouse, H.R., Evans, C.R., Rogers, M.A., 1973. Alteration of Crude Oil by Waters and Bacteria; evidence from Geochemical and Isotope Studies. AAPG Bulletin 57, 1276–1290.

Bartko, K.M., Conway, M.W., Krawietz, T.E., Marquez, R.B., Oba, R.G.M., 1992. Field and Laboratory Experience in Closed Fracture Acidizing the Lisburne Field, Prudhoe Bay, Alaska, in: SPE Annual Technical Conference and Exhibition. Society of Petroleum Engineers. doi:10.2118/24855-MS

Behm, E.J., Ebanks Jr., W.J., 1984. Comprehensive geological and reservoir engineering evaluation of the lower San Andres Dolomite reservoir, Mallet Lease, Slaughter field, Hockley County, Texas, in: Proceedings, Permian Basin Oil and Gas Recovery Conference. Society of Petroleum Engineers, pp. 31–42. doi:10.2118/12015-MS

Berg, R., DeMis, W., Mitsdarffer, A., 1994. Hydrodynamic effects on mission canyon (Mississippian) oil accumulations, billings nose area, North Dakota. AAPG Bulletin 78, 501–518.

Blunt, M., Fayers, F.J., Orr, F.M., 1993. Carbon dioxide in enhanced oil recovery. Energy Conversion and Management 34, 1197–1204. doi:10.1016/0196-8904(93)90069-M

Brand, S., 2010. Results from Acid Stimulation in Lloydminster SAGD Applications, in: SPE International Symposium and Exhibiton on Formation Damage Control. Society of Petroleum Engineers. doi:10.2118/126311-MS

Brown, A., 2001. Effects of Hydrodynamics on Cenozoic Oil Migration, Wasson Field Area, Northwestern Shelf of the Permian Basin. West Texas Geological Society 110, 133–142.

Burgos, G.A., Buijse, M.A., Fonseca, E., Milne, A., Brady, M.E., Olvera, R., 2005. Acid Fracturing in Lake Maracaibo: How Continuous Improvements Kept on Raising the Expectation Bar, in: SPE Annual Technical Conference and Exhibition. Society of Petroleum Engineers. doi:10.2118/96531-MS

Celius, H.K., Ingeberg, K., 1996. The Impact of CO_2 Taxation on Oil and Gas Production in Norway, in: SPE Health, Safety and Environment in Oil and Gas Exploration and Production Conference. Society of Petroleum Engineers. doi:10.2118/35961-MS

Chapel, D., Mariz, C., Ernest, J., 1999. Recovery of CO_2 from flue gases: commercial trends, in: Canadian Society of Chemical Engineers Annual Meeting.

Chiarelli, A., 1978. Hydrodynamic framework of eastern Algerian Sahara—influence on hydrocarbon occurrence. AAPG Bulletin 62, 667–685.

Corey, A., 1954. The interrelation between gas and oil relative permeabilities. Producers Monthly 19, 38–41.

Crowley, T., 2000. Causes of climate change over the past 1000 years. Science 289, 270–277. doi:10.1126/science.289.5477.270

Cutler, R.P., Mansure, A.J., 1999. Fluid Dynamics in Sucker Rod Pumps.

Dahlberg, E.C., 1995. Applied Hydrodynamics in Petroleum Exploration. Springer New York, New York, NY. doi:10.1007/978-1-4612-4258-1

Dennis, H., Baillie, J., Holt, T., Wessel-Berg, D., 2000. Hydrodynamic activity and tilted oil-water contacts in the North Sea. Norwegian Petroleum Society Special Publications 9, 171–185. doi:10.1016/S0928-8937(00)80016-8

Ebigbo, A., Class, H., Helmig, R., 2006. CO_2 leakage through an abandoned well: problem-oriented benchmarks. Computational Geosciences 11, 103–115. doi:10.1007/s10596-006-9033-7

Economides, M.J., Nolte, K.G., 2000. Reservoir stimulation, 3rd ed. Wiley, New York.

Eisenberg, L.I., Langston, M.V., Fitzmorris, R.E., 1994. Reservoir Management in a Hydrodynamic Environment, Iagifu-Hedinia Area, Southern Highlands, Papua New Guinea, in: SPE Asia Pacific Oil and Gas Conference. Society of Petroleum Engineers. doi:10.2118/28750-MS

Ely, J.W., Tiner, R., Rothenberg, M., Krupa, A., McDougal, F., Conway, M., Reeves, S., 2000. Restimulation Program Finds Success ICn Enhancing Recoverable Reserve, in: SPE Annual Technical Conference and Exhibition. Society of Petroleum Engineers. doi:10.2118/63241-MS

Estrada, C., Mantilla, C., 2000. Tilted oil water contact in the Cretaceous Caballos Formation, Puerto Colon Field, Putumayo Basin, Colombia, in: SPE Asia Pacific Conference on Integrated Modelling for Asset Management. Society of Petroleum Engineers. doi:10.2118/59429-MS

Ettehad, A., 2014. Storage compliance in coupled CO_2-EOR and storage. Greenhouse Gases: Science and Technology 4, 66–80. doi:10.1002/ghg.1382

Ettehadtavakkol, A., 2013. CO_2 EOR-storage design optimization under uncertainty.

Ettehadtavakkol, A., Lake, L.W., Bryant, S.L., 2014a. CO_2-EOR and storage design optimization. International Journal of Greenhouse Gas Control 25, 79–92. doi:10.1016/j.ijggc.2014.04.006

Ettehadtavakkol, A., Lake, L.W., Bryant, S.L., 2014b. Impact of Storage Tax Credit on Economic Viability of CO_2 Storage with EOR, in: SPE Hydrocarbon Economics and Evaluation Symposium. Society of Petroleum Engineers. doi:10.2118/169838-MS

Ghauri, W.K., 1960. Results of Well Stimulation by Hydraulic Fracturing and High Rate Oil Backflush. Journal of Petroleum Technology 12, 19–27. doi:10.2118/1382-G

Gozalpour, F., Ren, S., Tohidi, B., 2005. CO_2 EOR and storage in oil reservoir. Oil & Gas Science and Technology 60, 537–546.

Gratton, P., LeMay, W., 1969. San Andres oil east of the Pecos. New Mexico Geological Society, Special Publication 3, 37–43.

Hainey, B.W., Troncoso, J.C., 1992. Frac-Pack: An Innovative Stimulation and Sand Control Technique, in: SPE Formation Damage Control Symposium. Society of Petroleum Engineers. doi:10.2118/23777-MS

Harris, O.E., Hendrickson, A.R., Coulter, A.W., 1966. High-Concentration Hydrochloric Acid Aids Stimulation Results in Carbonate Formations. Journal of Petroleum Technology 18, 1291–1296. doi:10.2118/1654-PA

Hashemi, A., Shadizadeh, S., Zoveidavianpoor, M., 2012. A local computerized multi-screening of vast amount of data to select hydraulic fracturing candidates in Iranian carbonate oil fields. International Journal of Computer Applications 39, 37–45.

Hawkins, D.M., 2004. The Problem of Overfitting. Journal of Chemical Information and Computer Sciences 44, 1–12. doi:10.1021/ci0342472

Heffer, K.J., Fox, R.J., McGill, C. a., Koutsabeloulis, N.C., 1997. Novel Techniques Show Links between Reservoir Flow Directionality, Earth Stress, Fault Structure and Geomechanical Changes in Mature Waterfloods. SPE Journal 2, 91–98. doi:10.2118/30711-PA

Herzog, H., Drake, E., Adams, E., 1997. CO_2 capture, reuse, and storage technologies for mitigating global climate change: A White Paper, Energy Laboratory, Massachusetts Institute of Technology.

Hill, B., Hovorka, S., Melzer, S., 2013. Geologic carbon storage through enhanced oil recovery. Energy Procedia 37, 6808–6830. doi:10.1016/j.egypro.2013.06.614

Hiss, W., 1980. Movement of ground water in Permian Guadalupian aquifer systems, southeastern New Mexico and western Texas. New Mexico Geological Society Guidebook, 31st Field Conference, Trans-Pecos Region 289–294.

Honarpour, M.M., Nagarajan, N., Grijalba Cuenca, A., Valle, M., Adesoye, K., 2010. Rock-Fluid Characterization for Miscible CO_2 Injection: Residual Oil Zone, Seminole Field, Permian Basin. Proceedings of SPE Annual Technical Conference and Exhibition. doi:10.2118/133089-MS

Hopkinson, E.C., Fertl, W.H., Oliver, D.W., 1982. The Continuous Carbon/Oxygen Log Basic Concepts and Recent Field Experiences. Journal of Petroleum Technology 34, 2441–2448. doi:10.2118/9613-PA

Hsu, C.-F., Morell, J.I., Falls, A.H., 1997. Field-Scale CO_2-Flood Simulations and Their Impact on the Performance of the Wasson Denver Unit. SPE Reservoir Engineering 12. doi:10.2118/29116-PA

Hubbert, M.K., 1967. Application of Hydrodynamics to Oil Exploration. World Petroleum Congress.

Hubbert, M.K., 1954. Entrapment of Petroleum Under Hydrodynamic Conditions. AAPG Bulletin 38. doi:10.1306/5CEADEE4-16BB-11D7-8645000102C1865D

Jamali, A., Ettehadtavakkol, A., 2017a. Application of capacitance resistance models to determining interwell connectivity of large-scale mature oil fields. Petroleum Exploration and Development 44, 132–138. doi:10.1016/S1876-3804(17)30017-4

Jamali, A., Ettehadtavakkol, A., 2017b. CO_2 storage in Residual Oil Zones: Field-scale modeling and assessment. International Journal of Greenhouse Gas Control 56, 102–115. doi:10.1016/j.ijggc.2016.10.005

Jamali, A., Ettehadtavakkol, A., Fan, D., Moallem, G., 2017a. Positive Correlation Between Historical Oil Production and Well Stimulation Response, in: SPE Western Regional Meeting. Society of Petroleum Engineers. doi:10.2118/185666-MS

Jamali, A., Ettehadtavakkol, A., Watson, M., Zeinuddin, O., 2017b. Depressurizing Permian Basin San Andres Residual Oil Zones: A Feasibility Study, in: SPE Liquids-Rich Basins Conference - North America. Society of Petroleum Engineers. doi:10.2118/187482-MS

Jauhari, U., 2012. Hydrodynamic Trapping, Tilted Contacts and New opportunities in

Mature Onshore Kutei Basin, East Kalimantan, Indonesia. AAPG Search and Discovery.

Jennings, A.R., 1991. Good Wells Make the Best Candidates for Well Stimulation. SPE Production Engineering 6, 371–376. doi:10.2118/19738-PA

Kalfayan, L., 2008. Production enhancement with acid stimulation, 2nd ed. PennWell.

Kartoatmodjo, G.P., Caretta, F., Flew, S.R., Jadid, M. Bin, 2007. Risk-Based Candidate Selection Workflow Improve Acid Stimulation Success Ratio in Mature Field, in: Asia Pacific Oil and Gas Conference and Exhibition. Society of Petroleum Engineers. doi:10.2118/109278-MS

Killough, J.E., 1976. Reservoir Simulation With History-Dependent Saturation Functions. Society of Petroleum Engineers Journal 16, 37–48. doi:10.2118/5106-PA

Killough, J.E., Kossack, C.A., 1987. Fifth Comparative Solution Project: Evaluation of Miscible Flood Simulators, in: SPE Symposium on Reservoir Simulation. Society of Petroleum Engineers. doi:10.2118/16000-MS

Koornneef, J., Ramírez, A., Turkenburg, W., Faaij, A., 2012. The environmental impact and risk assessment of CO_2 capture, transport and storage – An evaluation of the knowledge base. Progress in Energy and Combustion Science 38, 62–86. doi:10.1016/j.pecs.2011.05.002

Koperna, G.J., Melzer, L.S., Kuuskraa, V.A., 2006. Recovery of Oil Resources From the Residual and Transitional Oil Zones of the Permian Basin, in: SPE Annual Technical Conference and Exhibition. Society of Petroleum Engineers. doi:10.2118/102972-MS

Krasey, R., 1988. High Grading Fracture Candidate Selection. Journal of Canadian Petroleum Technology 27. doi:10.2118/88-04-03

Kumar, S., Van Gisbergen, S.J., Harris, J., Murshidi, A., Brady, M.E., Ferdiansyah, E., El-Banbi, A., Al Harthy, S., 2005. Stimulation Challenges and Solutions in Complex Carbonate Reservoirs, in: SPE Middle East Oil and Gas Show and Conference. Society of Petroleum Engineers. doi:10.2118/93413-MS

Lackner, K., 2003. A guide to CO_2 sequestration. Science 300, 1677–1678. doi:10.1126/science.1079033

Lake, L., 2010. Enhanced oil recovery. Society of Petroleum Engineers.

Lasdon, L.S., Waren, A.D., 1983. Large scale nonlinear programming. Computers &

Chemical Engineering 7, 595–604. doi:10.1016/0098-1354(83)80005-2

Lindsay, R., 1998. Meteoric recharge, displacement of oil columns and the development of residual oil intervals in the Permian Basin. West Texas Geological Society 271–274.

Lucia, F.J., 2000. San Andres and Grayburg Imbibition Reservoirs, in: SPE Permian Basin Oil and Gas Recovery Conference. doi:http://dx.doi.org/10.2118/59691-MS

Manrique, E.J., Muci, V.E., Gurfinkel, M.E., 2013. EOR Field Experiences in Carbonate Reservoirs in the United States. SPE Reservoir Evaluation & Engineering 10, 667–686. doi:10.2118/100063-PA

Mature Fields Solution, 2014.

McNeal, R., 1965. Hydrodynamics of the Permian basin. AAPG Special Volumes 308–326.

McNeal, R., 1961. Hydrodynamic entrapment of oil and gas in Bisti field, San Juan County, New Mexico. AAPG Bulletin 45, 315–329.

Meehan, D.N., 1995. Stimulation Results in the Giddings (Austin Chalk) Field. SPE Production & Facilities 10, 96–102. doi:10.2118/24783-PA

Meese, C.A., Mullen, M.E., Barree, R.D., 1994. Offshore Hydraulic Fracturing Technique. Journal of Petroleum Technology 46, 226–229. doi:10.2118/28159-PA

Melzer, L.S., 2016. A Game Changing New Unconventional Play: the Science and Case History Based Economics of Depressuring the Upper Residual Oil Zone, prepared for Research Partnership to Secure Energy for America.

Melzer, L.S., 2013. Residual Oil Zones (ROZs): A Review of ROZ Science and Engineering, in: Enhanced Oil Recovery's Tensleep III Workshop. University of Wyoming.

Melzer, L.S., 2006. Stranded Oil in the Residual Oil Zone, prepared for Advanced International Resources the US Department of Energy.

Melzer, L.S., Koperna, G.J., Kuuskraa, V.A., 2006. The origin and resource potential of residual oil zones, in: Proceedings - SPE Annual Technical Conference and Exhibition.

Metz, B., Davidson, O., Coninck, H. De, Loos, M., Meyer, L., 2005. Carbon dioxide capture and storage. Cambridge University Press.

Mitchell, J., Johns, T., Gregory, J., Tett, S., 1995. Climate response to increasing levels of greenhouse gases and sulphate aerosols. Nature 376, 501–504. doi:doi:10.1038/376501a0

Mohaghegh, S., Platon, V., Ameri, S., 2001. Intelligent systems application in candidate selection and treatment of gas storage wells. Journal of Petroleum Science and Engineering 31, 125–133. doi:10.1016/S0920-4105(01)00125-5

Moore, L.P., Ramakrishnan, H., 2006. Restimulation: Candidate Selection Methodologies and Treatment Optimization, in: SPE Annual Technical Conference and Exhibition. Society of Petroleum Engineers. doi:10.2118/102681-MS

Nguyen, a. P., Kim, J.S., Lake, L.W., Edgar, T.F., 2011. Integrated Capacitance Resistive Model for Reservoir Characterization in Primary and Secondary Recovery, in: SPE Annual Technical Conference and Exhibition. Society of Petroleum Engineers, p. 20. doi:SPE 147344

Nguyen, V.H., Sheppard, A.P., Knackstedt, M.A., Val Pinczewski, W., 2006. The effect of displacement rate on imbibition relative permeability and residual saturation. Journal of Petroleum Science and Engineering 52, 54–70. doi:10.1016/j.petrol.2006.03.020

Nitters, G., Roodhart, L., Jongma, H., Yeager, V., Buijse, M., Fulton, D., Dahl, J., Jantz, E., 2000. Structured Approach to Advanced Candidate Selection and Treatment Design of Stimulation Treatments, in: SPE Annual Technical Conference and Exhibition. Society of Petroleum Engineers. doi:10.2118/63179-MS

Nnanna, E., Ajienka, J., 2005. Critical Success Factors for Well Stimulation, in: Nigeria Annual International Conference and Exhibition. Society of Petroleum Engineers. doi:10.2118/98823-MS

Nnanna, E., Osuagwu, M., Okereke, O., 2009. Important Considerations in Matrix Stimulation Candidate Selection in Niger Delta, in: Nigeria Annual International Conference and Exhibition. Society of Petroleum Engineers. doi:10.2118/128604-MS

Nordbotten, J.M., Celia, M.A., Bachu, S., Dahle, H.K., 2005. Semianalytical Solution for CO_2 Leakage through an Abandoned Well. Environmental Science & Technology 39, 602–611. doi:10.1021/es035338i

Ostistyy, B., Koblov, E., Butsenko, R., 1967. Inclined water-oil contacts in the oil fields of Sakhalin. Geologiya Nefti i Gaza 11, 16–20.

Panda, M.N., Chopra, A.K., 1998. An integrated approach to estimate well interactions, in: SPE India Oil and Gas Conference and …. Society of Petroleum Engineers. doi:10.2118/39563-MS

Pang, S.S.M., Faehrmann, P.A., 1993. Development Planning in a Mature Oil Field, in: SPE Asia Pacific Oil and Gas Conference. Society of Petroleum Engineers. doi:10.2118/25352-MS

Pedersen, K., Christensen, P., Shaikh, J., 2014. Phase behavior of petroleum reservoir fluids. CRC Press.

Peigui Yin, Wo, S., Johnson, M., Jones, N., Murrell, G., Mohrbacher, D., 2012. Residual Oil Zone Potential of Tensleep Sandstone in the Bighorn Basin, Wyoming, in: AAPG Annual Convention and Exhibition. Long Beach, California, USA.

Petit, J., Jouzel, J., Raynaud, D., Barkov, N., 1999. Climate and atmospheric history of the past 420,000 years from the Vostok ice core, Antarctica. Nature 339, 429–436.

Popa, A., Ramos, R., Cover, A.B., Popa, C.G., 2005. Integration of Artificial Intelligence and Lean Sigma for Large Field Production Optimization: Application to Kern River Field, in: SPE Annual Technical Conference and Exhibition. Society of Petroleum Engineers. doi:10.2118/97247-MS

Ramondetta, P.J., 1982. Facies and stratigraphy of the San Andres Formation, Northern and Northwestern Shelves of the Midland Basin, Texas and New Mexico. University of Texas, Bureau of Economic Geology Report of Investigations No. 56.

Reeves, S.R., Bastian, P.A., Spivey, J.P., Flumerfelt, R.W., Mohaghegh, S., Koperna, G.J., 2000. Benchmarking of Restimulation Candidate Selection Techniques in Layered, Tight Gas Sand Formations Using Reservoir Simulation, in: SPE Annual Technical Conference and Exhibition. Society of Petroleum Engineers. doi:10.2118/63096-MS

Reeves, S.R., Hill, D.G., Hopkins, C.W., Conway, M.W., Tiner, R.L., Mohaghegh, S., 1999a. Restimulation Technology for Tight Gas Sand Wells, in: SPE Annual Technical Conference and Exhibition. Society of Petroleum Engineers. doi:10.2118/56482-MS

Reeves, S.R., Hill, D.G., Tiner, R.L., Bastian, P.A., Conway, M.W., Mohaghegh, S., 1999b. Restimulation of Tight Gas Sand Wells in the Rocky Mountain Region, in: SPE Rocky Mountain Regional Meeting. Society of Petroleum Engineers. doi:10.2118/55627-MS

Ren, B., Zhang, L., Huang, H., Ren, S., Chen, G., Zhang, H., 2015. Performance evaluation and mechanisms study of near-miscible CO_2 flooding in a tight oil reservoir of Jilin Oilfield China. Journal of Natural Gas Science and Engineering 27, 1796–1805. doi:10.1016/j.jngse.2015.11.005

Saller, A.H., 2004. Palaeozoic dolomite reservoirs in the Permian Basin, SW USA: stratigraphic distribution, porosity, permeability and production. Geological Society, London, Special Publications 235, 309–323. doi:10.1144/GSL.SP.2004.235.01.13

Sayarpour, M., 2008. Development and Application of Capacitance-Resistive Models to Water/carbon Dioxide Floods. ProQuest.

Sayarpour, M., Kabir, C.S., Lake, L., 2009. Field Applications of Capacitance-Resistance Models in Waterfloods. SPE Reservoir Evaluation & Engineering. doi:10.2118/114983-PA

Sayarpour, M., Zuluaga, E., Kabir, C.S., Lake, L.W., 2009. The use of capacitance-resistance models for rapid estimation of waterflood performance and optimization. Journal of Petroleum Science and Engineering 69, 227–238. doi:10.1016/j.petrol.2009.09.006

Schechter, R., 1992. Oil Well Stimulation.

Selected oil & gas fields in West Texas, 1982. . West Texas Geological Society.

Sencenbaugh, R.N., Lytle, D.M., Birmingham, T.J., Simmons, J.C., Shaefer, M.T., 2001. Restimulating Tight Gas Sand: Case Study of the Codell Formation, in: SPE Rocky Mountain Petroleum Technology Conference. Society of Petroleum Engineers. doi:10.2118/71045-MS

Shelley, R.F., 1999. Artificial Neural Networks Identify Restimulation Candidates in the Red Oak Field, in: SPE Mid-Continent Operations Symposium. Society of Petroleum Engineers. doi:10.2118/52190-MS

Shelley, R.F., Massengill, D.R., Scheuerman, P., McRill, P.E., Hamilton, R., 1998. Granite Wash Completion Optimization with the Aid of Artificial Neural Networks, in: SPE Permian Basin Oil and Gas Recovery Conference. Society of Petroleum Engineers. doi:10.2118/39814-MS

Sinson, C.M., Ogbe, D.O., Dehghani, K., 1988. Optimization of Well Stimulation Strategies in Oil and Gas Fields, in: Petroleum Computer Conference. Society of Petroleum Engineers. doi:10.2118/17792-MS

Strong, A.J., Wright, R.J., Skelly, G.J., 1997. Well Stimulation: A Mature Asset Case

Study, in: SPE Annual Technical Conference and Exhibition. Society of Petroleum Engineers. doi:10.2118/38769-MS

Thomas, S., 2008. Enhanced oil recovery-an overview. Oil & Gas Science and Technology 63, 9–19. doi:10.2516/ogst:2007060

Thomasen, J.B., Jacobsen, N.L., 1994. Dipping Fluid Contacts in the Kraka Field, Danish North Sea, in: SPE Annual Technical Conference and Exhibition. Society of Petroleum Engineers. doi:10.2118/28435-MS

Todd, M.R., Longstaff, W.J., 1972. The Development, Testing, and Application Of a Numerical Simulator for Predicting Miscible Flood Performance. Journal of Petroleum Technology 24, 874–882. doi:10.2118/3484-PA

Towler, B.F., Varma, J., Harris, H.G., 1992. Analysis of hydrodynamic petroleum entrapment in Sage Creek field, Big Horn Basin, Wyoming. Journal of Petroleum Science and Engineering 8, 89–95. doi:10.1016/0920-4105(92)90047-5

Trebbau, G.L., Nunez, G.J., Caira, R.L., Molina, N.Y., Entzeroth, L.C., Schneider, D.R., 1999. Microbial Stimulation of Lake Maracaibo Oil Wells, in: SPE Annual Technical Conference and Exhibition. Society of Petroleum Engineers. doi:10.2118/56503-MS

Treiber, L.E., Owens, W.W., 1972. A Laboratory Evaluation of the Wettability of Fifty Oil-Producing Reservoirs. Society of Petroleum Engineers Journal 12, 531–540. doi:10.2118/3526-PA

Ugbenyen, B.O., Ogbe, D.O., Osisanya, S.O., 2011. Efficient Methodology for Stimulation Candidate Selection and Well Workover Optimization, in: Nigeria Annual International Conference and Exhibition. Society of Petroleum Engineers. doi:10.2118/150760-MS

Ursell, T., 2012. Generate Random Numbers from a 2D Discrete Distribution.

Vishal, V., Singh, T.N. (Eds.), 2016. Geologic Carbon Sequestration. Springer International Publishing, Cham. doi:10.1007/978-3-319-27019-7

Wang, F., Lucia, F., Kerans, C., 1998. Integrated reservoir characterization study of a carbonate ramp reservoir: Seminole San Andres Unit, Gaines County, Texas. SPE Reservoir Evaluation & Engineering 1, 105–113. doi:http://dx.doi.org/10.2118/36515-PA

Ward, R., Kendall, C., Harris, P., 1986. Upper Permian (Guadalupian) facies and their association with hydrocarbons--Permian basin, west Texas and New Mexico. AAPG Bulletin 70, 239–262.

Watson, M.C., 2005. Correlating petrophysical and flood performance in the Levelland slaughter field. Texas Tech University.

Weber, D., Edgar, T.F., Lake, L.W., Lasdon, L.S., Kawas, S., Sayarpour, M., 2009. Improvements in Capacitance-Resistive Modeling and Optimization of Large Scale Reservoirs, in: SPE Western Regional Meeting. Society of Petroleum Engineers, p. 17. doi:SPE 121299

Wells, P.R.A., 1988. Hydrodynamic Trapping in the Cretaceous Nahr Umr Lower Sand of the North Area, Offshore Qatar (includes associated papers 18521 and 18605). Journal of Petroleum Technology 40, 357–361. doi:10.2118/15683-PA

West, L., 2014. Regional analysis of residual oil zone potential in the Permian Basin. University of Texas at Austin.

Whisonant, R.J., Hall, F.R., 1997. Combining Continuous Improvements in Acid Fracturing, Propellant Stimulations, and Polymer Technologies to Increase Production and Develop Additional Reserves in a Mature Oil Field, in: SPE Annual Technical Conference and Exhibition. Society of Petroleum Engineers. doi:10.2118/38789-MS

Xiong, H., Holditch, S.A., 1995. An Investigation Into the Application of Fuzzy Logic to Well Stimulation Treatment Design. SPE Computer Applications 7, 18–24. doi:10.2118/27672-PA

Yang, F., Bai, B., Dunn-Norman, S., Nygaard, R., Eckert, A., 2013. Factors affecting CO_2 storage capacity and efficiency with water withdrawal in shallow saline aquifers. Environmental Earth Sciences 71, 267–275. doi:10.1007/s12665-013-2430-z

Yousef, A., Gentil, P., Jensen, J., Lake, L., 2006. A Capacitance Model To Infer Interwell Connectivity From Production- and Injection-Rate Fluctuations. SPE Reservoir Evaluation & Engineering 9, 630–646. doi:10.2118/95322-PA

Zarei, F., Muradov, K., Davies, D., 2014. Optimal Well Work-over Scheduling: Application of Intelligent Well Control Optimisation Technology to Conventional Wells, in: SPE Intelligent Energy Conference & Exhibition. Society of Petroleum Engineers. doi:10.2118/167818-MS

Zawisza, L., 2006. Hydrodynamic Modelling of the Hydrocarbon Migration and Accumulation in the Lublin Basin, in: SPE Europec/EAGE Annual Conference and Exhibition. Society of Petroleum Engineers. doi:10.2118/100296-MS

Zillur, R., Bartko, K., Al-Qahtani, M.Y., 2002. Hydraulic Fracturing Case Histories in the Carbonate and Sandstone Reservoirs of Khuff and Pre-Khuff Formations,

Ghawar Field, Saudi Arabia, in: SPE Annual Technical Conference and Exhibition. Society of Petroleum Engineers. doi:10.2118/77677-MS

Zoveidavianpoor, M., Arriffin, S., Shadizadeh, S.R., 2012a. A Review on Conventional Candidate-well Selection for Hydraulic Fracturing in Oil and Gas Wells. Internationl Journal of Engineering and Technology 2, 51–60.

Zoveidavianpoor, M., Gharibi, A., 2016. Applications of type-2 fuzzy logic system: handling the uncertainty associated with candidate-well selection for hydraulic fracturing. Neural Computing and Applications 27, 1831–1851. doi:10.1007/s00521-015-1977-x

Zoveidavianpoor, M., Samsuri, A., Shadizadeh, S.R., 2012b. Development of a Fuzzy System Model for Candidate-well Selection for Hydraulic Fracturing in a Carbonate Reservoir, in: SPE Oil and Gas India Conference and Exhibition. Society of Petroleum Engineers. doi:10.2118/153200-MS

APPENDIX A

A. DISCUSSION ON HUBBERT'S TILT FORMULA

In his pioneering work, Hubbert (1954) explains that the anticlinal theory, in which the hydrostatic oil accumulation is explained, cannot justify the many cases of observed titled oil water contact. The oil water contact tends to be horizontal under hydrostatic conditions. Hubbert presented a general formulation valid for both hydrostatic and hydrodynamic conditions and backed it up with both experimental work and numerous field observations.

5.1. Potentiometric Surface

The principle argumentation builds upon the formulations burrowed from the groundwater hydrology literature as follows. Groundwater potential at any given point is defined as a function of elevation and pressure,

$$\Phi = g(z - z_0) + \frac{p - p_0}{\rho} \tag{A.1}$$

This is essentially the energy required to transport a unit mass of this fluid from some arbitrarily chosen standard position to the state of the point in question. Upon choosing zero elevation and 1 atmosphere pressure for the reference point, the potential simplifies to,

$$\Phi = gz + \frac{p}{\rho} \tag{A.2}$$

The kinetic energy of the underground flow is neglected since it has a slow motion. We can now equate this formula to the height that water will raise in a manometer, h,

$$\Phi = gh \tag{A.3}$$

In principle, the sum of energy stored in the fluid due to its pressure and due to its elevation can be expressed using h, the total head. This value can be measured through a given stratum by drilling multiple wells.

Using the total head measured in various points on the upper surface of a given stratum, a *potentiometric surface* can be constructed. A horizontal potentiometric surface represents constant potential throughout the stratum and therefore the water will be at rest. Otherwise, if this surface is slopping, the water will be in motion. We now have a unique way of measuring the potential across any point in any given stratum. If the values of potential across the space is known, the force exerted on water can be calculated (Figure A.1).

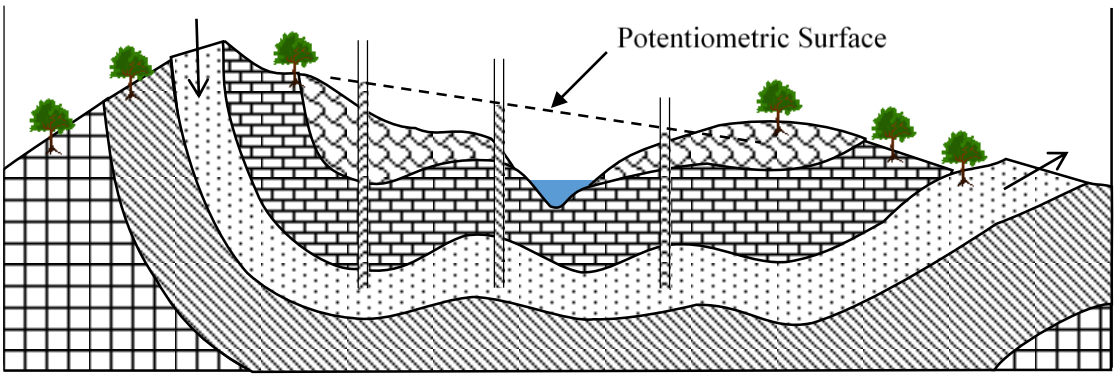

Figure A.1 The concept of lateral pressure gradient or potentiometric surface. Regional flow of water through sand from higher to lower outcrop results in continuous drop in potential. This figure is adopted from Hubbert (1954).

To formulate the forces upon the system, the gravitational forces and the forces exerted from changes in potential can be broken into their components. As in Darcy's equation, the forces exerted on the body of fluid are proportional to the pressure gradient (Figure A.2). Here, we consider potential gradient. Now, consider a family of surfaces along which Φ is constant. Let the potentials of two such surfaces be Φ and $\Phi + \Delta\Phi$ and their normal distance of separation to be Δn. The unknown value E is the force required to move the unit mass of the fluid between these two surfaces,

$$E = -\frac{\Delta\Phi}{\Delta n} = -\,grad\,\Phi = -\mathrm{g}\,\mathrm{grad}\,\mathrm{h} = \mathrm{g} - \frac{\mathrm{grad\ p}}{\rho} \qquad \text{(A.4)}$$

The force intensity vector E is the sum of the tow independent forces, gravity, and the negative gradient of the pressure divided by the fluid density. Unless in static conditions, these two forces are non-parallel and therefore, the resultant E will be parallel with neither of them.

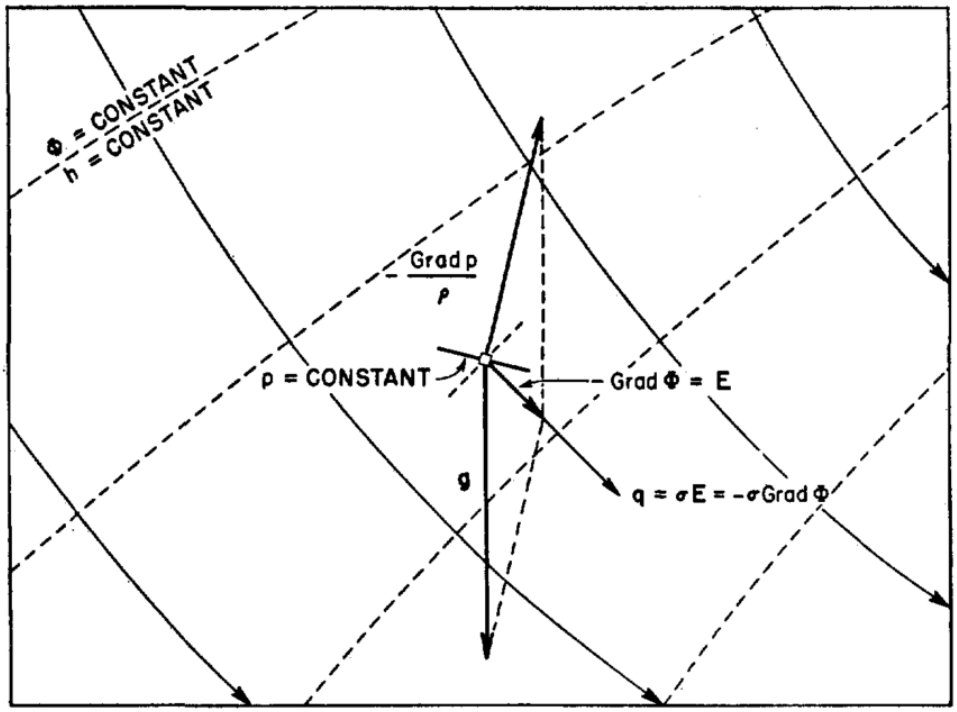

Figure A.2 Force intensity vector and the physical interpretation of Darcy's law. Adopted from Hubbert (1954).

The equipotential surfaces are used to represent the potential field, where the lines of force are orthogonal to these surfaces. We know that the flow lines are perpendicular to the equipotential surfaces, therefore no equipotential surface can close upon itself; otherwise the conservation of matter is violated. In a stratum with downward flow, we expect to see continuous flow lines along the bedding. This will help better envision the movement of the fluids and the process of migration and entrapment of hydrocarbons.

So far, we have been concerned with the flow of water. Moving on to cases where water and hydrocarbon flow together and for the sake of simplicity, we ignore the effect of capillary forces. Also, we consider water and oil to have a constant density. We write the potential and the force intensity vector for oil and water as follow,

$$\Phi_o = gz + \frac{p}{\rho_o} \tag{A.5}$$

$$E_o = -grad\ \Phi_o = g - \frac{grad\ p}{\rho_o} \tag{A.6}$$

$$\Phi_w = gz + \frac{p}{\rho_w} \tag{A.7}$$

$$E_w = -grad\ \Phi_w = g - \frac{grad\ p}{\rho_w} \tag{A.8}$$

Solving for oil potential and force intensity in terms of those of water,

$$\Phi_o = \frac{\rho_w}{\rho_o}\Phi_w - \frac{\rho_w - \rho_o}{\rho_o} gz \tag{A.9}$$

$$E_o = g + \frac{\rho_w}{\rho_o}(E_w - g) \tag{A.10}$$

These two equations can be now used to map the family of oil equipotential surfaces as well as the corresponding lines of forces. Figure A.3a shows the forces exerted on water, oil and gas in hydrodynamic environment based on the above equation. Based on the force vectors a secondary fluid such as oil or gas can be expressed using the two vectors E_w and g. As shown in this figure the impelling force on oil or gas is making a smaller angle with the vertical axis compared with that of water. This is a representation of buoyancy effect, driving upward the less dense fluids in presence of a denser fluid. Considering the equipotential surfaces for oil and gas to be perpendicular to their intensity vectors, one can envision how these surfaces can be oriented in the space. The lighter fluid will tend to move upwards in the direction of the force lines until it hits the impermeable barrier. Then it will move in the direction of decrease in fluid potential. In Figure A.4 the stratum has a dip of δ. Depending on the direction and magnitude of E_w and the density difference between the fluids, oil and gas will migrate upward at different angles with respect to the vertical plane. If the tilt of force intensity on each of the hydrocarbons is greater/smaller than δ, that fluid will tend to migrate upward/downward after hitting the shale barrier.

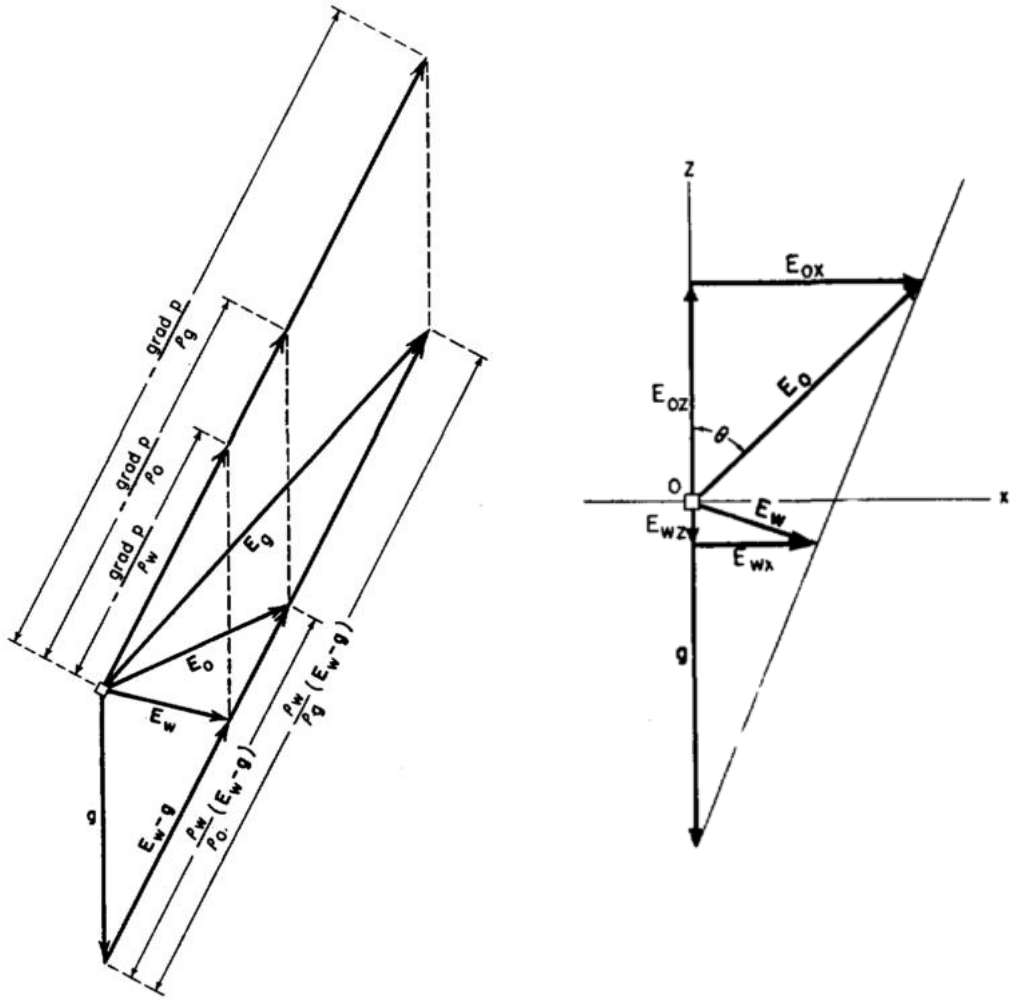

Figure A.3 (a) Impelling forces on water, oil and gas in hydrodynamic environment (left) and (b) vector analysis (right). Adopted from Hubbert (1954).

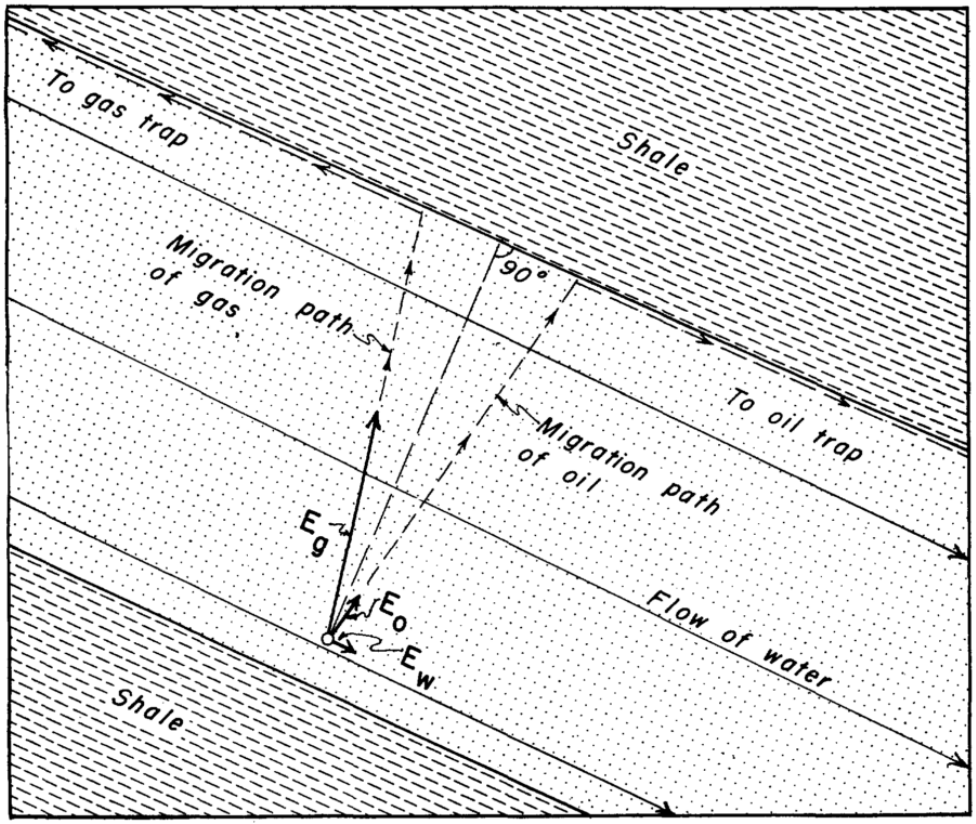

Figure A.4 Divergent migration of oil and gas in hydrodynamic environment. Adopted from Hubbert (1954).

Furthermore, we can now compute the slope of equipotential surfaces by performing vector analysis (Figure A.3b),

$$\tan(\theta) = -\frac{E_{ox}}{E_{oz}} = -\frac{\left[g+\frac{\rho_w}{\rho_o}(E_w-g)\right]_x}{\left[g+\frac{\rho_w}{\rho_o}(E_w-g)\right]_z} = \frac{\frac{\partial h_w}{\partial x}}{\frac{\rho_w-\rho_o}{\rho_w}-\frac{\partial h_w}{\partial z}} \tag{A.11}$$

The tilt of the oil water contact is itself an equipotential surface. This tilt has a critical value when it's equal to the negative of the dip. At this point, the force lines of oil and water are mutually perpendicular. For tilts greater than/less than this amount, the oil migration will be downdip/updip, respectively. In order to calculate this critical value, we note that because the vectors E_o and E_w are perpendicular. After performing vector analysis and by replacing $\frac{\partial h_w}{\partial z}$ and $\frac{\partial h_w}{\partial x}$ by appropriate values, one can obtain the following equation for computing the critical angle,

$$\tan\theta_c = \frac{\rho_w}{\rho_w - \rho_o}\frac{dh_w}{dx} \tag{A.12}$$

where dh_w/dx is the slope of the water potentiometric surface. This condition also prevails when water is flowing underneath an accumulation of petroleum where the oil-water interface is an equipotential surface parallel to the water flow lines. Therefore, by using this equation, the tilt of the oil-water interface can be computed if the slope of the potentiometric surface is known.

5.2. Parameters Affecting the Tilt of Oil Water Contact During Hydrodynamic Flushing

Hubbert's formula does not include the effects of reservoir heterogeneity, capillary pressure, and vertical to horizontal permeability ratio. In this section, we investigate the sensitivity of OWC tilt to these parameters and compare the results to the values predicted from Hubbert's tilt formula. Table A1 summarizes the scenarios investigated for this sensitivity analysis.

Table A.1 List of sensitivity analysis scenarios performed on the effects of heterogeneity, capillary pressure, vertical to horizontal permeability ratio, and potentiometric gradient.

	Potentiometric Tilt, ft/mile	Kv-Kh Ratio	Capillary Pressure	Heterogeneity
Case 1	7.5	0.1	Yes	Yes
Case 2	5.0	0.1	Yes	No
Case 3	7.5	0.1	No	No
Case 4	7.5	0.5	No	No
Case 5	7.5	1.0	No	No
Case 6	12.5	0.1	No	No
Case 7	25	0.1	No	No

Figure A.5 compares the slope of the OWC calculated from Hubbert's tilt formula with the results of the simulation model for the case studies presented in Table A.1. The effects of vertical to horizontal permeability ratio and heterogeneity are small, as evident from the proximity of the points associated with Case 1, Case 3, Case 4, and Case 5. The inclusion of capillary pressure in Case 2 resulted in lower pressure gradients (a less steep potentiometric surface) for the same injection rates imposed by the hydrodynamic flushing; however, the predictions of Hubbert's tilt formula is only slightly affected by that. Overall, the simulated slope for the cases with capillary effects are slightly larger than the value predicted by Hubbert's tilt formula. Finally, the most influential factor on the slop of the OWC is the potentiometric gradient as illustrated by the performance of Case 6 and Case 7. These observations correspond very well with Hubbert's assumptions and confirms the accuracy of his formula, when compared to the results of the general continuity equation for two-phase flow.

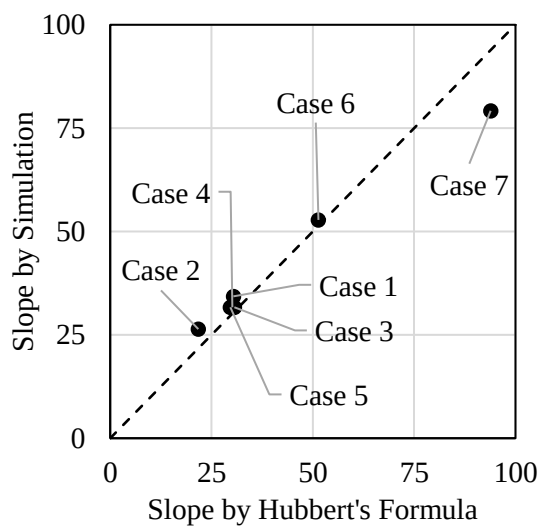

Figure A.5 Theoretical vs simulated OWC tilts for the case studies presented in Table A.1.

VITA

Permanent Address:

Bob L. Herd Department of Petroleum Engineering

807 Boston Ave

Lubbock TX 79406

Email Address:

alijamali@live.com

Education:

Ph.D., Petroleum Engineering

Texas Tech University

Lubbock TX 79406

M.Sc., Petroleum Engineering

Texas Tech University

Lubbock TX 79406

B.Sc., Petroleum Engineering

Sharif University of Technology

Tehran, Iran